

2012

Relationships among Fine Sediment Settling and Suspension, Bed Erodibility, and Particle Type in the York River Estuary, Virginia

Kelsey A. Fall

College of William and Mary - Virginia Institute of Marine Science

Follow this and additional works at: <https://scholarworks.wm.edu/etd>



Part of the [Geomorphology Commons](#), and the [Oceanography Commons](#)

Recommended Citation

Fall, Kelsey A., "Relationships among Fine Sediment Settling and Suspension, Bed Erodibility, and Particle Type in the York River Estuary, Virginia" (2012). *Dissertations, Theses, and Masters Projects*. Paper 1539617918.

<https://dx.doi.org/doi:10.25773/v5-hfz9-5r79>

This Thesis is brought to you for free and open access by the Theses, Dissertations, & Master Projects at W&M ScholarWorks. It has been accepted for inclusion in Dissertations, Theses, and Masters Projects by an authorized administrator of W&M ScholarWorks. For more information, please contact scholarworks@wm.edu.

Relationships Among Fine Sediment Settling and Suspension, Bed
Erodibility, and Particle Type in the York River Estuary, Virginia

A Thesis

Presented to

The Faculty of the School of Marine Science

The College of William and Mary

In partial fulfillment

of the requirements for the degree of

Master of Science

by

Kelsey A. Fall

2012

Approval Sheet

This thesis is submitted in partial fulfillment of the

Requirements for the degree of

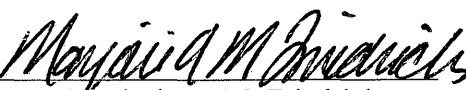
Master of Science

December 2012


Kelsey A. Fall

Academic Committee Members


Dr. Carl T. Friedrichs
Advisor


Dr. Marjorie A. M. Friedrichs
Co-Advisor


Dr. Courtney K. Harris

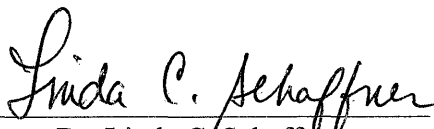

Dr. Linda C. Schaffner

Table of Contents

Acknowledgments	v
List of Tables	vi
List of Figures.....	vii
Abstract.....	ix
Chapter 1: Introduction	2
Chapter 2: Controls on Particle Settling Velocity and Bed Erodibility in the Presence of Muddy Flocs and Pellets as Inferred by ADVs, York River Estuary, Virginia, USA	9
Abstract.....	10
2.1 Introduction.....	10
2.2 Methods.....	11
2.2.1 Environmental Setting	13
2.2.2. ADV Observations	13
2.3 Results	15
2.3.1 Classification of Two Regimes	18
2.3.2 Phase-Averaged Velocity, Bed Stress, Sediment Concentration, and Drag Coefficient for Two Regimes	18
2.3.3 Phase-Averaged Erosion and Deposition for Two Regimes	19
2.3.4 Phase-Averaged Settling Velocity for Two Regimes.....	20
2.3.5: Influence of Stress History on Bed Erodibility for Two Regimes	22
2.4 Discussion	23
2.4.1 Regime 1: Easily Suspended Flocculated Mud	23
2.4.2 Regime 2: Less easily suspended, biologically formed pellets	24
2.4.3 Sediment suspension and settling during each regime: Interpreting water column composition	26
2.4.4 Settling Velocity of Flocs and Pellets	27
2.4.5 Evidence of the bed behaving both cohesively and non-cohesively	30
2.5 Conclusions.....	31
Chapter 3: The 2007 Clay Bank Region Sediment Regime Shift: Modeling Study Utilizing the York 3-D Hydrodynamic Cohesive Bed Model.....	35
Abstract.....	36
3.1 Introduction.....	36
3.2 Acoustic Doppler Velocimeter (ADV) Observations from the York River Estuary ...	37
3.3 York River 3-D Hydrodynamic Cohesive Bed Model	38
3.4 Model Modifications	40
3.5 Performance Assessment of Simulation-1, Simulation-2 and Simulation-3	43

3.6 Comparison of Model-2 Results to ADV Observations.....	46
3.6.1 Model Performance Over Individual Tidal Cycles	46
3.6.2 Variability in Bed Erodibility and Settling Velocity	49
3.7 Evaluation of York River 3-D Cohesive Hydrodynamic ROMS Model Performance	50
3.8 Summary of Model-ADV Comparison	53
Chapter 4: Conclusions and Future Work.....	54
Appendix: York River Hydrodynamic Cohesive Bed Model Code.....	Error! Bookmark not defined.
Literature Cited	123
VITA	134

Acknowledgments

To my major advisors, Dr. Carl T. Friedrichs and Dr. Marjorie A. M. Friedrichs for their encouragement, support, and guidance throughout the course of this project. To my committee members, Dr. Courtney K. Harris for all her patience and help with the York ROMS model, and Dr. Linda C. Schaffner for her insight and interest in my work. To the many individuals who set up and help maintain the MUDBED observing system that made this project possible. Notably Grace Cartwright, Tim Gass, and Wayne Reisner. To Adam Miller and Julia Moriarty for all their technical assistance with the York ROMS model. To my family and friends for all their love, support, and encouragement.

Funding for this work was provided by National Science Foundation Grants OCE-0536573 and OCE-1061781.

List of Tables

Table	Page
Table 3.1: Summary of the difference between model simulations.....	58
Table 3.2: Normalized and non-normalized root mean square error (RMSE) between ADV observed and modeled current speed, concentration, and bed stress RMSE values for Simulation-1 and Simulation-2 are compared in Table 3.2A and RMSE values comparing Regime 2 and Regime 2 during Simulation-2 are shown in 3.2B.	59

List of Figures

Figure	Page
Figure 2.1: Map of York River Estuary, Southeastern VA from Cartwright et al., 2009. The location of the MUDBED Intermediate site is in green. X-radiographs for the upper estuary (a.), middle estuary (b.) and lower estuary (c.) are courtesy of L. Schaffner.....	60
Figure 2.2: Long-term ADV measured bulk settling velocity for the MUDBED Intermediate (green) and Biological (blue) sites courtesy of G. Cartwright. The purple box indicates the time period of this study (June-August 2007).	61
Figure 2.3: Long-term estimates of bed erodibility measured by the ADV (line) and with the Dual Core Gust Microcosm (symbols) for the MUDBED Intermediate (green) and Biological (blue) sites courtesy of G. Cartwright and P. Dickhudt. The purple box indicates the time period of this study (June-August 2007).	62
Figure 2.4: MUDBED bottom tripod with mounted 5mHz Sontek ADV Ocean Probe. Photo courtesy of G. Cartwright.	63
Figure 2.5: Total suspended solids determined by pump samples collected on the July 18, 2007 calibration cruise (Cartwright et al., 2009) versus acoustic backscatter measured by the ADV mounted on the MUDBED benthic tripod (black X's). The red line indicates the calibration relationship from Cartwright et al., 2009 ($C=e^{0.034x-0.87}$) used to calculate suspended sediment concentration from ADV acoustic backscatter.	64
Figure 2.6: Instantaneous (blue line) and daily averaged (red line) ADV measurements of bulk settling velocity (a), bed erodibility (b), bed stress (c), suspended sediment concentration (d), and drag coefficient (e) from the summer of 2007. The transition between Regime 1 (blue box) and Regime 2 (green box) is marked by an increase in settling velocity and decrease in erodibility.....	65
Figure 2.7: ADV measured current speed (a), bed stress (c), suspended sediment concentration (c), and drag coefficient (d) for the top 20% of tidal cycles with the strongest bed stresses for Regime 1 (blue) and Regime 2 (green). Error bars denote +/- 1 standard error.	66
Figure 2.8: Hysteresis plots of C vs. τ_b for the top 20 % of tidal cycles with the strongest τ_b for Regime 1 (a) and Regime 2 (b).	67
Figure 2.9: Bulk settling velocity (a) and the settling component of the settling velocity (b) during the increasing tidal velocity phase for the top 20% of tidal cycles with the highest bed stresses. Error bars denote +/- 1 standard error.	68

Figure	Page
Figure 2.10: Daily averaged erodibility versus 25 hour averaged bed stress (a) and versus 120 averaged hour bed stress (b). Daily averaged erodibility during Regime 1 (blue) is better correlated to 120 hour averaged bed stress, while during Regime 2 daily averaged erodibility more strongly correlated to 25 hour averaged bed stress.	69
Figure 3.1: Map of York River estuary, Southeastern VA from Cartwright et al., 2009. The location of the MUDBED Intermediate Site is in green. X-radiographs for the upper (a), middle (b), and lower (c) estuary are courtesy of L. Schaffner.....	71
Figure 3.2: Instantaneous (blue line) and daily averaged (red line) ADV measurements of bulk settling velocity (a), bed erodibility (b), bed stress (c), suspended sediment concentration (d), and drag coefficient (e) from the summer of 2007. The two regimes defined in Chapter 2 are marked out in blue (Regime 1) and green (Regime 2).....	72
Figure 3.3: The York River Estuary Cohesive Bed Hydrodynamic ROMS Model grid (Rinehimer, 2008). Each square represents five model grid cells. The black circle represents the relative location of the MUDBED Intermediate Site.....	73
Figure 3.4: Tidally averaged ADV measurements (black line) and results from Simulation-1 (blue line) of current speed (a), bed stress (b), and suspended sediment concentration (c) from the summer of 2007. The two sediment Regimes are in the blue (Regime 1) and green (Regime 2) box.....	74
Figure 3.5: Tidally averaged hydraulic roughness (Z_o) during the observation period at the Intermediate site, estimated by the ADV assuming the law of the wall. Observations show a mean $Z_o=0.004$ centimeters above the bed.	75
Figure 3.6: Tidally averaged ADV measurements (blue line), Simulation-1 (black line), and Simulation-2 (red line) of current speed (a), bed stress (b), and suspended sediment concentration (c) from the summer of 2007. The two sediment Regimes are within the blue box (Regime 1) and green box (Regime 2).....	76
Figure 3.8: Current speed (a), bed stress (b) and suspended sediment concentration (c) for a two week period determined by Simulation-2 (black) and Simulation -3 (red). Model results were very similar between the two simulations.	78
Figure 3.9: Comparison of tidal analysis of current speed (a), bed stress (b), and concentration (c) between ADV observations collected during Regime 1 (blue) and Regime 2 (green) and Simulation-2 results during Regime 1 (black) and Regime 2 (red).79	79

Figure 3.10: Hysteresis plots of concentration versus bed stress measured by the ADV (solid line) and estimated by Simulation-2 (dashed line) for the top 20% of tidal cycles with the strongest bed stress for Regime 1 (a) and Regime 2 (b). Note the similar bed stresses during both regimes estimated by Simulation-2.....80

Figure 3.11: Bed erodibility estimated by Simulation-2 (a) and by the ADV (b). Arrow trend lines indicate that both methods show bed erodibility decreasing throughout the study period.....81

Figure 3.12: Tidally averaged bulk settling velocity (W_s) estimated by Simulation-2 (red) and by the ADV (blue). The black line corresponds to $W_s = 1$ mm/s.82

Figure 3.13: 25-hour averaged bed erodibility versus either 25 hour or 120-hour bed stress. Daily-averaged erodibility is correlated to either 25-hour average erodibility (Regime 2, green) or 120-hour averaged erodibility (Regime 1, blue).83

Abstract

In order to understand the processes controlling the temporal variability in settling velocity (W_s) and bed erodibility (ϵ), in the middle reaches of the York River estuary, VA, the relationships between the hydrodynamics and particle types were investigated with a near-bed Acoustic Doppler Velocimeter (ADV) and the York River 3-D Hydrodynamic Cohesive Bed Model.

ADV observations of the flow characteristics that occurred over a strong temporal transition period indicated that W_s and ϵ were characterized by two distinct regimes with contrasting sediment and water column characteristics: (i) a physically-dominated regime (Regime 1) which was a period dominated by flocculated muds (flocs), and (ii) a biologically-influenced regime (Regime 2) which was a period dominated by biologically formed pellets mixed with flocs. During Regime 1, W_s averaged about 0.5 mm/s, and ϵ averaged about 3 kg/m²/Pa. In contrast, during Regime 2 average W_s increased to 1.5 mm/s, and average ϵ dropped to 1 kg/m²/Pa. The change between these two regimes and the transition in W_s and ϵ were linked with the arrival and departure of a seasonal density front.

Comparison between ADV observations and the results from the York River 3-D Hydrodynamic Cohesive Bed Model suggested that the current model version was not conducive to examining the temporal variability in settling velocity associated with the transition of the distinct sediment regimes. The existing model version estimated realistic values for current speed and concentration and resolved the daily variation associated with in current speed, bed stress, concentration, and settling velocity. However, model estimates of bed stress, current speed, settling velocity, and erodibility did not suggest the presence of two distinct sediment regimes. The model did a poor job of predicting peak bed stresses and settling velocities. Both were over estimated by a factor of 2 throughout most of the study period. Possible modifications to create a version that is able to simulate the bed stresses and sediment properties (i.e. erodibility and settling velocity) during each regime with more accuracy are: (1) define finer sediment classes in the model that are more representative of the water column and not just the seabed, (2) use a consolidation time scale of 5 days rather than 24 hours to allow more sediment to be suspended at lower bed stresses, (3) further reduce hydraulic roughness, and (4) turn on sediment induced stratification.

Relationships among fine sediment settling and suspension, bed erodibility, and particle type in the York River Estuary, Virginia

Chapter 1
Introduction

Introduction

Understanding fine sediment dynamics in coastal environments is economically and ecologically important. Cohesive sediments accumulate in navigational channels and harbors, necessitating frequent costly and destructive dredging (Mackenzi, 2007; Winterwerp and Kesteren, 2005; Miller et al., 2002). Heavy sediment deposition inhibits macrobenthic activity through burial of organisms or burial of favored hard bottom habitats (Mackenzi 2007; Miller et al., 2002; Schaffner et al., 2001). Sediments in suspension reduce light availability for primary producers by decreasing water clarity (Reay, 2009). This can result in degradation of entire ecosystems. For example, the historical decline in abundance of submerged aquatic vegetation (SAV) in the York River and Chesapeake Bay estuaries is associated with excess suspended sediments and linked to the loss of essential habitats for many marine and freshwater species (Moore, 2009; Reay, 2009; Waycott et al. 2009; Orth and Moore, 1984). Cohesive sediments also promote the transport of toxic materials (i.e. nutrients and pathogens), which can severely deteriorate water quality (Reay, 2009; Drake et al, 2002). Historically, the decline of water quality in coastal areas has contributed to a decrease in abundance of many economically important fisheries, such as finfishes, oysters, and other shellfish (Reay, 2009; Kemp et al., 2005).

Bed erodibility and settling velocity are key parameters influencing fine sediment dynamics in coastal and estuarine environments (Sanford, 1997).

Bed erodibility controls how much sediment is suspended, and settling velocity determines how far that sediment is transported (Friedrichs et al, 2008).

Here we define erodibility as the asymptotic relationship between a steady, externally imposed stress and total eroded mass. Because total eroded mass is realized once net erosion has caused the critical shear stress of the sediment surface to reach the applied bed stress, erodibility is essentially a characteristic of the bed rather than the flow (Dickhudt et al., 2009; Friedrichs et al., 2008). Erodiability is generally measured in situ using benthic annular flumes, such as Sea Carousels and Mini flumes, (Amos et al. 2010; Amos et al., 2004; Maa and Sanford, 1998) or in the lab on recently collected cores using a dual core Gust erosion microcosm system (Dickhudt et al., 2010; Dickhudt et al., 2009). However these techniques are unable to collect high-resolution time series, are labor intensive and disruptive to the seabed, and use of different benthic flumes can produce different erodibility estimates for the same area (Amos et al., 2010; Friedrichs et al., 2008; Sanford, 2005).

Particle settling velocity is a function of particle diameter and density, which can be difficult to measure in situ for natural estuarine muds (Fugate and Friedrichs, 2003). The settling velocity of an individual sediment mineral grain with a known density and size can be reasonably estimated via Stokes' law, which takes into account gravity acting on the particle and the opposing fluid resistance (Cartwright et al., 2011; Dyer and Manning, 1999). Natural muds however have a tendency to form aggregates with varying degrees of compaction and porosity, so their settling velocities are harder to estimate because settling velocity cannot be accurately

determined based on particle size alone (Winterwerp and van Kesteren, 2004; Fugate and Friedrichs, 2003; Drake et al., 2002; Dyer 1984).

Within estuaries both erodibility and settling velocity are highly variable in time and space (Cartwright et al., 2011; Amos et al., 2010; Dickhudt et al., 2009; Friedrichs et al., 2008; Anderson, 2001) and are influenced by many different physical and biological forcings. Previous work has shown that many factors influence bed erodibility and settling velocity in fine sediment environments including: grain size, water content, organic content, temperature, degree of flocculation, degree of bed consolidation, degree of stratification and mixing of the overlying water column, depositional and erosional history of the bed, and biological activity such as bioturbation, biostabilization, and resilient fecal pellet production (Kraatz et al., 2012; Cartwright et al., 2011; Dickhudt et al., 2009; Stevens et al., 2007; Fugate and Friedrichs, 2003; Scully and Friedrichs, 2003; Drake et al., 2002; Maa and Kim, 2002; Anderson et al., 2001; Dyer and Manning, 1999; Maa et al., 1998).

Hydrodynamics and particle composition are important factors in determining fine sediment settling velocity and bed erodibility, yet the relationship between key physical parameters and particle types has not been sufficiently documented. This project focused on examining the temporal and spatial variability in settling velocity and bed erodibility in the York River estuary, VA, to gain insight on the complex, temporally-varying relationships among the hydrodynamics in the water column (current speed and settling), bed properties (stresses and erodibility), and particle types (flocculated muds versus pelletized muds).

Hydrodynamics and sediment dynamics in the York River estuary have been the focus of previous studies as part of the NSF and CoOP funded Multidisciplinary Benthic Exchange Dynamics (MUDBED) project (Friedrichs et al., 2008). A well-pronounced temporal transition in settling velocity and bed erodibility is observed seasonally in the middle reaches of the estuary (Cartwright et al., 2009; Dickhudt et al., 2009; Friedrichs et al., 2008). Recent field studies have attributed this temporal variability to the seasonally-varying concentration of resilient fecal pellets or aggregates in the upper seabed (Kraatz et al., 2012; Dickhudt et al., 2009; Friedrichs et al., 2008). This project used observations collected by an Acoustic Doppler Velocimeter (ADV) and the 3-D York River Hydrodynamic Cohesive Bed Model (Rinehimer, 2008) and examined the relationships between the hydrodynamics of the water column and suspended sediment characteristics during a temporal transition in bed erodibility and particle settling velocity.

Near-bed ADVs have been maintained in the York River estuary as part of the MUDBED project since 2006 to provide insight inherently complex, temporally varying relationships among hydrodynamics, bed properties and particle types. Unlike most in-situ measurements, ADVs do not disrupt the seabed and can provide continual, long-term hydrodynamic data despite extensive biofouling (Cartwright et al., 2009; Friedrichs et al., 2008; Fugate and Friedrichs, 2002). ADVs provide measurements of burst-averaged bottom stress (τ_b , via Reynolds averaging of turbulent velocity), suspended sediment concentration (C , via acoustic backscatter

calibrated by pump samples), sediment settling velocity (W_s , via a balance between upward Reynolds flux and gravitational settling) and bed erodibility (ϵ , by estimating the depth-integrated concentration (C) as a function τ_b) (Cartwright et al., 2009; Fugate and Friedrichs, 2002).

Chapter 2 presents observations collected by a 5MHz Sontek ADVOcean Probe that was deployed mid-estuary at the MUDBED Intermediate site from June to August 2007. This time period was chosen because it was the strongest transition period captured by the ADV that coincided with the collection of sediment cores for bed property analysis. The ADV measured 3-dimensional water velocity and acoustic backscatter at roughly 35 centimeters above the bed in the log-layer. ADV output was used to estimate bed stress, suspended sediment concentration, sediment settling velocity and bed erodibility. A full description of the instrument set-up can be found in Cartwright et al. (2009). In this study, ADV observations were analyzed over individual tidal phases in order to gain a better understanding of the processes controlling the temporal variability in settling velocity and bed erodibility, and to examine patterns in suspension and deposition in the area.

In Chapter 3, the York River 3-D Hydrodynamic Cohesive Bed Model (Rinehimer, 2008) was run for the same time period that the ADV was collecting measurements to examine the flow and sediment characteristics that occurred over a transition period. The York River 3-D Hydrodynamic Cohesive Bed Model is based on the Regional Ocean Model System (ROMS; Shchepetkin and McWilliams, 1998, 2005) that uses various finite difference techniques to solve the Reynolds averaged

Navier-Stokes equation (Warner et al., 2008). The York River model implemented the Community Sediment Transport Modeling System (CSTMS) cohesive bed sub-model that accounts for the depth and temporal variability of critical shear stress (τ_c). This chapter used the York River 3-D Hydrodynamic Cohesive Bed Model (Rinehimer, 2008) to further evaluate the processes controlling temporal variability in bed erodibility and settling velocity and examined how well the model simulated these two distinct regimes identified by the ADV observations described in Chapter 2.

Chapter 2

Controls on Particle Settling Velocity and Bed Erodibility in the Presence of Muddy Floccs and Pellets as Inferred by ADVs, York River Estuary, Virginia, USA

Abstract

A pronounced transition period in settling velocity (W_s) and bed erodibility (ϵ) is observed seasonally in the middle reaches of the York River estuary, VA. In order to understand the processes controlling the temporal variability in W_s and ϵ , water column hydrodynamics and bed stresses during a strong transition period were studied using a near-bed Acoustic Doppler Velocimeter (ADV). W_s and ϵ appeared to be characterized by two distinct regimes with contrasting sediment and water column characteristics: (i) A physically dominated regime (Regime 1): a period dominated by flocculated muds (flocs) and (ii) A biologically-influenced regime (Regime 2): a period dominated by a mixture of biologically formed pellets plus flocs. During the floc-dominated Regime 1, W_s averaged about 0.5 mm/s, ϵ averaged about 3 kg/m²/Pa, and stress for initiation of erosion (τ_{cINT}) was only 0.02 Pa. During the pellet-influenced Regime 2, average W_s increased to 1.5 mm/s, average ϵ dropped to 1 kg/m²/Pa, and τ_{cINT} increased to 0.05 Pa. Over a given tidal cycle, as bed stress (τ_b) decreased, the pellet component of the suspended sediment concentration (C) decreased relatively quickly, but the floc component of C did not decrease until τ_b was less than 0.08 Pa. This suggested that over individual tidal cycles, cohesion of flocs to the seabed is inhibited when τ_b exceeded about 0.08 Pa. Averaged over 25 hours, floc ϵ on a given day was positively correlated to the magnitude of τ_b observed over the previous 5 days, providing an in situ estimate of a consolidation-relaxation time-scale for homogeneous estuarine mud. In contrast, ϵ during periods strongly influenced by pellets was inversely correlated to τ_b with a

zero time lag, which is more consistent with bed armoring. This suggested that under pellet-influenced conditions a muddy bed might behave relatively more like a non-cohesive bed.

2.1 Introduction

Erosion and deposition represent a continuous dynamic relationship between the fluid forces applied to the bed and the physical condition of the seafloor (Sanford, 2008). Particle settling velocity and bed erodibility are key factors influencing fine sediment erosion and deposition in coastal and estuarine environments, yet they are poorly constrained parameters in many fine sediment transport studies (Harris et al., 2005; Yang and Hamrick, 2003). Erodeability controls the amount of sediment that is suspended while settling velocity determines how far sediment is transported before it is deposited (Friedrichs et al., 2008). Both vary in space and time, and are directly influenced by many different physical and biological factors (Kraatz et al., 2012; Rodriguez-Calderón, 2010; Dickhudt et al., 2009; Stevens et al., 2007; Amos et al., 2004; Fugate and Friedrichs, 2003; Anderson and Pejrup, 2002; Anderson, 2001; Maa and Kim, 2002; Dyer and Manning, 1999; Maa et al., 1998).

Particle packaging is one of the major factors influencing fine sediment settling velocity and bed erodibility. Flocculated muds (flocs) and biologically packaged pellets or aggregates are the main constituents being suspended and transported in most muddy estuaries (Friedrichs et al., 2008; Kdelvang and Austen, 1997) and recently, variability of settling velocity and bed erodibility in some

settings has been attributed to the presence of resilient fecal pellets or aggregates. (Kraatz et al., 2012; Cartwright et al., 2011; Cartwright et al., 2009; Dickhudt et al., 2009; Friedrichs et al., 2008; Drake et al., 2002; Anderson and Pejrup, 2001). Muddy flocs form when suspended clay/silt particles are brought close enough together by moderate turbulence and/or the turbulence associated with settling, that they adhere to one another because of the attraction between the electrostatic charges on their individual surfaces (Cartwright et al., 2011; Fugate and Friedrichs, 2003; Dyer and Manning, 1999; Kdelvang and Austen, 1997). Estuaries contain a range of sizes of flocs, and due to their open structure the density of a given floc is not size dependent, which makes predicting settling velocities based only disaggregated grain size very difficult (Cartwright et al., 2011; Dyer and Manning 1999). Pellets or aggregates are also composed of clays and silts, but are formed through the compaction that occurs when mud is ingested and processed through deposit and benthic feeding organisms (Cartwright et al., 2011; Drake et al., 2002; Schaffner et al., 2001; Kdelvang and Austen, 1997). The density of pellets increases with pellet size and exceeds the density of flocs (Cartwright et al., 2011; Drake et al., 2002).

The difficulty in obtaining in-situ measurements of settling velocity and bed erodibility further adds to the complexity of determining the relationship between these key parameters and particle types. Commonly used field techniques such as in-situ benthic flumes (Amos et al., 2004; Maa and Sanford, 1998), in-situ settling tubes (Dyer et al., 1996), or dual core Gust erosion microcosm erodibility experiments (Kraatz et al., 2012; Dickhudt et al., 2009; Dickhudt et al., 2010) are labor intensive, disruptive to the seabed and unsuitable for collecting highly

resolved (Friedrichs et al. 2008). Also, these techniques produce a large amount of uncertainty with regards to the accuracy of their data (Friedrichs et al., 2008; Sanford, 2006; Dyer et al., 1996). For example, different benthic flumes can produce a range of erosion estimates for the same location (Amos et al., 2010) and methods that isolate particles in settling tubes (i.e. Owen Tube) can alter the turbulence and disrupt aggregates during sampling, resulting in an under prediction of settling velocities (Maa and Kwon, 2007; Fugate and Friedrichs, 2002; Dyer et al., 1996). Also, video settling systems can be biased towards larger, more optically responsive particles (Cartwright et al., 2011; Friedrichs et al., 2008). New field applications utilizing turbulence resolving Acoustic Doppler Velocimeters (ADV) have provided promising insight into fine sediment settling and erodibility (Cartwright et al., 2011; Ha and Maa, 2010; Cartwright et al., 2009; Friedrichs et al., 2008; Anderson et al., 2007; Fugate and Friedrichs, 2003). ADVs do not disrupt the seabed, and they can provide continual, long-term observations despite extensive biofouling (Cartwright et al., 2009; Friedrichs et al., 2008; Fugate and Friedrichs, 2002). This study used a near-bed ADV to better constrain inherently complex, temporally-varying relationships among near bed hydrodynamics and particle types.

2.2 Methods

2.2.1 Environmental Setting

The York River (Figure 2.1) is a partially mixed sub-estuary of the Chesapeake Bay located in southeastern Virginia that extends 50 kilometers from West Point down to the Goodwin Islands (Friedrichs, 2009). The York is

characterized by a main (~5-20 meters deep) and secondary (~5 meters deep) channels dominated by mud, bordered by well-developed sandy shoals (~2 meters deep) (Dellepenna et al., 2003; Friedrichs, 2009). Even though the York estuary is considered microtidal, tidal currents can reach ~ 1m/s at the water surface and dominate sediment suspension in the York (Schaffner et al., 2001).

A distinct physical-biological gradient (Figure 2.1) is found along the York estuary (Schaffner et al., 2001), making it an ideal place to study the relationship between biology and overlaying hydrodynamics. In the upper York, and seasonally near the MUDBED Intermediate site, physical disturbances reduce macrobenthic activity and sediment layering is preserved (x-radiograph A and B in Figure 2.1). Biological abundance increases towards the river mouth, so in the lower York, near Gloucester Point or the MUDBED Biological Site, bioturbation destroys physical layering (x-radiograph C in Figure 2.1) (Cartwright et al., 2011; Cartwright et al., 2009; Dickhudt et al. 2009; Friedrichs, 2009).

Long-term ADV data (Cartwright et al, 2009) and Gust microcosm experiments (Dickhudt, 2009) revealed temporal variability in sediment settling velocity (Figure 2.2 green line) and bed erodibility (Figure 2.3 green line) at the Intermediate Site, but little variability in either at the Biological Site (Figure 2.2 and 2.3, blue line). Typically from spring to summer, a transition period occurs at the Intermediate Site, and measurements of settling velocity and bed erodibility become similar to those observed year round at the Biological Site. Previous studies suggested that the periodic presence and exposure of resilient fecal pellets on the surface of the seabed at the Intermediate Site is responsible for the variation

observed (Kraatz et al, 2012; Cartwright et al, 2011; Rodriguez-Calderón, 2010; Dickhudt, 2009). This study focuses on ADV data collected during the distinct transition period observed between June and August 2007 at the Intermediate Site (Box in Figure 2.2 and 2.3) in order to gain a better understanding of the processes controlling the variation in settling velocity and bed erodibility.

2.2.2. ADV Observations

Sontek ADVOcean Probes have been maintained more-or-less continually at the MUDBED Intermediate Site since 2006. Occasional time gaps in observations at the site are associated with necessary maintenance due to instrument battery life and memory space. The MUDBED ADVs are attached to bottom-mounted tripods and measure 3-dimensional water velocity and acoustic backscatter at roughly 35 centimeters above the bed in the log-layer (Figure 2.4). A full description of the instrument set-up can be found in Cartwright et al. (2009). This project used data collected by a 5MHz ADV deployed from June to August 2007. As described below, ADV data was used to estimate:

1. Burst-averaged bottom stress (τ_b)
2. Suspended sediment concentration (c)
3. Bulk sediment settling velocity (W_{SBULK})
4. Bed erodibility (ϵ)
5. Drag Coefficient (C_d)

Burst averaged bottom stress in Pascals (τ_b) was calculated by estimating the Reynolds Flux from the measured velocity:

$$\tau_b = \rho \langle u'w' \rangle \quad (1)$$

where ρ is water density (assumed to be 1025 kg/m^3), $\langle u'w' \rangle$ is the Reynolds stress, u' is the turbulent velocity deviation from the burst averaged horizontal velocity, and w' is the turbulent velocity deviation from the burst averaged vertical velocity (Cartwright et al., 2009; Fugate and Friedrichs, 2003; Fugate and Friedrichs, 2002). The overbar indicates that the product of the velocities was time-averaged over the duration of the burst.

The backscatter associated with the acoustic returns can be used to estimate local suspended sediment concentration, c , at the height of the ADV sensor when properly calibrated (Cartwright et al., 2009; Fugate and Friedrichs, 2003; Fugate and Friedrichs, 2002). Figure 10 in Cartwright et al., 2009 showed the results of in-situ calibrations of ADV backscatter for total suspended solids based on ADV backscatter and filter pump samples that were collected at both MUDBED sites from 2007-2008. The calibrations were done using an identical model 5MHz Sontek ADV Ocean Probe attached to a profiler that collected measurements and water samples throughout the water column within 100 meters of the bottom-mounted tripod. Comparing ADV backscatter from the tripod ADV used in this study with profiler pump samples collected near the tripod on the calibration cruise during this study period (Figure 2.5) verified that the calibration relationship presented in Cartwright et al., 2009 accurately estimated c :

$$c = e^{(0.034x-0.87)} \quad (2).$$

In equation 2, c is suspended sediment concentration in mg/L at the height of the ADV, and x is burst averaged acoustic backscatter in counts. Removing a wash load

concentration (c_{WASH}) or the background concentration of particles too small to settle out from the water column (Cartwright et al., 2009), from c provided the concentration of particles that are assumed to be capable of depositing onto the seabed (C_{SET}) in mg/L:

$$C_{SET} = C - C_{WASH} \quad (3)$$

C_{WASH} was assumed to be equal to the concentration suspended when current velocity and bed stresses reached their lowest magnitudes over individual tidal phases.

Estimates for bulk sediment settling velocity (W_{sBULK}) were made by assuming a balance between settling due to gravity and upward transport due to Reynolds flux:

$$\langle c \rangle W_{sBULK} = \langle c'w' \rangle \quad (4)$$

where w was vertical water velocity, primes indicated within burst fluctuations, and $\langle \rangle$ indicated a burst average (Dyer, 1984; Fugate and Friedrichs, 2002; Friedrichs et al., 2008; Cartwright et al., 2011).

Finally, the proportionality between eroded mass (depth integrated sediment settling concentration (C_{SET})) and bottom stress (τ_b) provided a measure of the depth-limited bed erodibility (ϵ) (Cartwright et al., 2009; Friedrichs et al., 2008):

$$\epsilon = C_{SET} / \tau_b \quad (5).$$

C_{SET} in kg/m² was calculated by assuming the Rouse Sediment Profile:

$$W_s C_{SET} = A_z \frac{dC_{SET}}{dz} \quad (6)$$

and integrating C_{SET} over the height of the water column (Cartwright et al., 2009;

Fugate and Friedrichs, 2002; Dyer, 1984). In Equation 6, W_s is the settling velocity in mm/s, c_{SET} is concentration at the height of the ADV in kg/m³, and A_z is parabolic eddy viscosity (Dyer, 1986):

$$A_z = \kappa u_* z (1-z)/h \quad (7).$$

In Equation 7, κ is Von Karman's constant (~ 0.408), u_* is shear velocity, z is height above the bed, and h is water column height (5 meters).

ADV measurements were used to calculate an elevation specific drag coefficient to help assess the possible influence of stratification in damping turbulence and thus reducing frictional drag:

$$C_d = \langle u'w' \rangle / (u^2) \quad (8)$$

where u is the burst-averaged horizontal velocity at the height of the ADV.

2.3 Results

2.3.1 Classification of Two Regimes

ADV data collected in the summer of 2007 showed the clearest transition period in settling velocity (Figure 2.2) and bed erodibility (Figure 2.3) observed at the MUDBED Intermediate site (Figure 2.1) between 2006 to 2009. Initial analysis of the ADV data collected during this period revealed two distinct regimes with different hydrodynamic and sediment characteristics: (1) Regime 1, at the beginning of deployment (Figure 2.6-blue box) and (2) Regime 2, beginning mid July (Figure 2.6- green box). The transition from Regime 1 to Regime 2 was marked by an increase in bulk settling velocity from ~ 0.5 mm/s to ~ 1 mm/s (Figure 2.6a), a decrease in bed erodibility from ~ 3 kg/m²/Pa to ~ 1 kg/m²/Pa (Figure 2.6b), and

an in bed stress amplitude from ~ 0.15 Pa to > 0.2 Pa (Figure 2.6c). Suspended sediment concentrations were higher during Regime 1 than Regime 2 (Figure 2.6d). Lower than normal drag coefficients (C_d) were estimated for both regimes ($C_d \sim 0.001$), with a somewhat higher and more variable C_d observed during Regime 2 (Figure 2.6e).

2.3.2 Phase-Averaged Current Speed, Bed Stress, Sediment Concentration, and Drag Coefficient for Two Regimes

The top 20% of tidal current speed “cycles” with the strongest observed bed stresses in each regime were used for tidal phase analysis. Individual tidal cycles were defined using the observed tidal pattern in the current speed (U), such that an individual ebb or individual flood formed a full cycle, with the beginning and end of each cycle corresponding to the times of minimum observed U . Observations over the tidal cycles were then interpolated to a common interval in tidal phase to produce tidal average values of current speed (U , Figure 2.7a), bed stress magnitude (τ_b , Figure 2.7b), suspended sediment concentration (c , Figure 2.7c) and drag coefficient (C_d , Figure 2.7d), with no distinction made between floods and ebbs. Tidal analysis highlighted the similarities and differences in U , τ_b , c , and C_d between the two regimes. During both regimes, U peaked between 40 and 45 cm/s. Both τ_b and c were strongly correlated with U . As U increased through the tidal cycle, τ_b increased and more sediment was suspended. A wash load concentration (c_{WASH}) or the concentration observed when U and τ_b approached zero (i.e. slack tide) of 20-40 mg/L was present in both regimes.

Despite similar current velocities, the magnitudes of τ_b and c throughout the

tidal phase were different between Regime 1 (Figure 2.7b and c, blue line) and Regime 2 (Figure 2.7b and c, green line). About 40% more sediment was suspended during Regime 1, even though lower bed stresses occurred (peak τ_b for Regime 1 \approx 0.15 Pa and peak τ_b for Regime 2 \approx 0.22 Pa). Oddly for Regime 1, even as U and τ_b began to decrease, c remained high (Figure 2.7b and c, blue line). c did not begin to decrease until τ_b fell below 0.08 Pa.

Both regimes have relatively low C_d , however the drag coefficients observed during Regime 2 were almost double that observed during Regime 1 (Figure 2.7d). During Regime 1, the C_d significantly decreased as c increased and then remained constant ($C_d \approx 0.0007$) throughout the tidal phase even as c peaks. When c began to decrease, the C_d increased back to the value observed at the beginning of the tidal phase. C_d did not follow the same pattern during Regime 2, and appeared to be fairly constant ($C_d \approx 0.0011$) throughout the entire tidal phase.

2.3.3 Phase-Averaged Erosion and Deposition for Two Regimes

Hysteresis plots of c versus τ_b presented patterns of erosion and deposition, and suggested differences in the general composition of the seabed during Regime 1 (Figure 2.8a) and Regime 2 (Figure 2.8b). Even though more sediment was suspended during Regime 1 than Regime 2, both have similar patterns of initial erosion and suspension. Once τ_b increased past a certain threshold, \sim 0.02 Pa during Regime 1 and \sim 0.05 Pa during Regime 2, c increased until τ_b peaked (Figure 2.8a and b).

Figure 2.8 highlighted the differences in deposition between Regime 1 and Regime 2. During Regime 1, c remained high (\sim 160 mg/L) until τ_b decreased to

~ 0.08 Pa. Unlike the deposition patterned observed during Regime 1, c observed during Regime 2 gradually decreased with τ_b until τ_b fell below ~ 0.08 Pa. After τ_b decreased past 0.08 Pa, c decreased more quickly back to 20 mg/L.

The depositional patterns in Figure 2.8 were used to infer what particles were in suspension at the height of the ADV (~35 cmab). Three distinct particle groups were inferred to be present during the study period. They are defined in this paper as: (1) wash load (red box), (2) flocculated muds or flocs (blue box), and (3) pelletized mud or pellets/fine sand (green box).

The deposition pattern shown in Figure 2.8 was used to roughly estimate the proportions of the different particles types in suspension. An average total concentration of about 160 mg/L was suspended during Regime 1. Figure 2.8a showed that once τ_b dropped below 0.08 Pa, c decreased continuously to 40 mg/L as τ_b approached 0. This suggested the presence of 40 mg/L of a washload concentration and 120 mg/L of flocs, translating into roughly 20% and 80%. A lower average total concentration of about 100 mg/L was suspended during Regime 2, and as τ_b decreased, c gradually decreased for τ_b greater than 0.08 Pa (Figure 2.8b). The decline in c accelerates for τ_b less than 0.08 Pa suggesting a transition to floc deposition. The initial decrease in c was thought to be the deposition of resilient pellets, which would not be able to be kept in suspension at lower τ_b (Cartwright et al., 2011; Fugate and Friedrichs, 2003). Regime 2 consisted of 20 mg/L of a washload concentration, 50 mg/L of flocs, and 30 mg/L of pellets, translating to roughly 20%, 50%, and 30%.

2.3.4 Phase-Averaged Settling Velocity for Two Regimes

Tidal analysis of bulk sediment settling velocity (W_{SBULK}) during the accelerating phase of U emphasized how it differs between Regime 1 and Regime 2 (Figure 2.9). Observed W_{SBULK} is similar for both regimes at the beginning of the tidal phase (Figure 2.9a). Midway through the increasing tidal phase, W_{SBULK} during Regime 2 increased to 1.2 mm/s (Figure 2.9a, green line), almost double the W_{SBULK} during Regime 1 (Figure 2.9a, blue line). Recall that higher τ_b occurred during Regime 2, which allowed faster settling pellets to be suspended. The increased W_{SBULK} is associated with the influence of faster settling resilient fecal pellets on W_{SBULK} .

Figure 2.8 partitioned total c into pelletized, flocculated and wash load components. The wash load component was assumed to never settle ($W_{SWASH} \approx 0$), and was removed from W_{SBULK} . This allowed the settling velocity of the other “depositing” components, either flocs or pellets, (W_{SDEP}) to be determined:

$$W_{SDEP} = (c / (c - c_{WASH})) * W_{SBULK} \quad (9).$$

During Regime 1, W_{SDEP} was composed solely of flocs (Figure 2.8a), therefore W_{SDEP} is equal to the settling velocity of flocs (W_{SFLOCS}). Removing the c_{WASH} from W_{SBULK} suggested that the flocs were settling at about 0.85 mm/s (Figure 2.9b blue line). During Regime 2, W_{SDEP} consisted of both flocs and pellets (Figure 2.8b). This resulted in a larger spread of W_{SDEP} during Regime 2, with a $W_{SDEP} \approx 1.5$ mm/s at the peak τ_b (Figure 9b green line). Previous work in the York, also found W_{SDEP} be around 1.5 mm/s during periods influenced by pellets (Cartwright et al., 2011; Friedrichs et al., 2008). The approximate fractions of flocs (F_F) and pellets (F_P) are

presented in Figure 2.8b. The W_{SFLOCS} from Figure 2.9b (~ 0.85 mm/s) and the peak W_{SDEP} during Regime 2 (~ 1.43 mm/s) were used to calculate the settling velocity of pellets ($W_{SPELLETS}$):

$$W_{SDEP} = F_F W_{SFLOCS} + F_P W_{SPELLETS} \quad (10)$$

Assumed at peak c: $f_F = 5/8$, $f_P = 3/8$

Equation 12 estimated the pellets to be settling at roughly 2.4 mm/s.

2.3.5: Influence of Stress History on Bed Erodibility for Two Regimes

The data also revealed distinct relationships between bed erodibility ($\epsilon = C_{SET}/\tau_b$) and bed stress during the two different regimes (Figure 2.10). During Regime 1 (blue symbols), daily averaged ϵ was most strongly correlated to the 5-day averaged τ_b , ($R = 0.74$) so that ϵ increased proportional to the average τ_b observed over the last 5 days. Conversely, daily-averaged ϵ observed during Regime 2 (green dots) is most strongly correlated to daily-averaged τ_b ($R = -0.78$) during this period, and decreases as daily-averaged τ_b increases.

2.4 Discussion

A pronounced seasonal transition period in bulk settling velocity and bed erodibility (Figure 2.2 and 2.3, green line) is observed in the middle reaches of the York River estuary near Clay Bank, VA (Cartwright et al., 2009; Dickhudt et al., 2008; Friedrichs et al., 2008; Maa and Kim, 2002). Data presented here suggested that bulk settling velocity and erodibility are characterized by two distinct regimes with contrasting sediment characteristics, (i) Regime 1 and (ii) Regime 2. The transition between regimes that occurred in the middle of July 2007 was focused on

for this study and was marked by an increase in bed stress, a decrease in suspended sediment concentration, and an increase in the value of the drag coefficient (Figure 2.6).

Over seasonal and spring/neap tidal time scales, the bed composition in the middle reaches of the York River estuary tends to alternate between dominance by muddy floccs or presence of resilient pellets mixed with floccs (Kraatz et al., 2012; Dickhudt, 2008). Cartwright et al. 2011 presented evidence for the simultaneous presence of both particle types suspended 1 meter above the bed. Our results suggested that Regime 1 represents periods dominated by easily suspended, flocculated muds while Regime 2 represents periods strongly influenced by less easily suspended, biologically formed pellets or aggregates mixed together with floccs.

2.4.1 Regime 1: Easily Suspended Flocculated Mud

Observations from Friedrichs et al. (2008), Dickhudt et al. (2009) and Cartwright et al. (2011) in the York suggested that floccs are associated with slower settling velocities, higher values for erodibility and higher suspended sediment concentrations. During Regime 1, lower average bulk settling velocity ($W_{SBULK} \sim 0.5$ mm/s) and higher average bed erodibility ($\epsilon \sim 3$ kg/m²/Pa) were observed (Figure 2.6). Also, despite lower bed stresses ($\tau_b \sim 0.15- 0.2$ Pa) sediment concentrations were higher (Figure 2.7), implying the presence of more easily erodible sediment on the seabed surface. Dickhudt et al., (2009) measured erodibility with a Gust microcosm on cores collected at the Intermediate Site, near the ADV tripod monthly from April 2006 to October 2007. When subjected to $\tau_b = 0.4$ Pa, more than twice

the amount of sediment ($\sim 2 \text{ kg/m}^2$) was eroded from the cores collected during Regime 1 than cores collected during Regime 2 ($\sim 0.5 \text{ kg/m}^2$). These results also strongly suggested that the surface of the bed was dominated by more easily erodible flocs at this time period.

The results from Dickhudt et al., 2009 combined with previous work in the York suggests that more erodible sediment is typically observed at Clay Bank during the spring and winter in response to high river discharge promoting sediment convergence by a seasonal density front (Cartwright et al., 2009; Friedrichs et al., 2008; Lin and Kuo, 2001). During Regime 1, according to the United States Geological Society discharge from the Pamunkey River, one of the York's tributaries, (Figure 2.11, solid black line) was higher (USGS, <http://waterdata.usgs.gov/nwis>) and monitoring by the Chesapeake Bay National Estuarine Research Reserve indicated that bottom salinity was lower (CBNEERS, <http://www2.vims.edu/vecos>). Surface and bottom measurements of salinity from two sites from the Virginia Estuarine and Coastal Observing System (VECOS) long term monitoring stations about 10 kilometers upstream and downstream from the Intermediate Site measured a change in salinity (ΔS) of about 3 ppt during Regime 1 (<http://www2.vims.edu/vecos>). Also, ADV measurements found that the average drag coefficient during Regime 1 was low, about 0.0005 (Figure 2.7e) and previous work by Scully and Friedrichs (2007) found that drag coefficients were negatively correlated with the degree of salinity stratification. These results imply that the dominance of flocs during Regime 1 was associated with trapping of fine material at the seasonal density front.

Over individual tidal cycles, the drag coefficient appeared to decrease as sediment concentration peaked (Figure 2.7d), and despite having similar current speeds, bed stresses were roughly half of those measured during Regime 2 (Figure 2.7a and b). Thus sediment-induced stratification may also have dampened the near bed turbulence (Scully and Friedrichs, 2003; Kim and Friedrichs, 2000). Typically, sediment-induced stratification requires near bed sediment concentrations to be on the order of at least hundreds of mg/L (Winterwerp, 2006). Sediment concentrations over individual tidal cycles during Regime 1 peaked at about 150 mg/L (Figure 2.7c). However, Friedrichs et al. (2000) found that turbulence damping in the York may be due to a combination of both salinity stratification and sediment-induced stratification. Both these processes may be responsible for preventing more resilient particles from being suspended during this time. Future work measuring concentration and salinity profiles is needed to better examine sediment induced stratification in the York.

2.4.2 Regime 2: Less easily suspended, biologically formed pellets

The transition from Regime 1 to Regime 2 was marked by an increase in bulk settling velocity as bed stress increased and by a significant decrease in bed erodibility (Figure 2.6). An increase in bulk settling velocity with stress is consistent with the resuspension of denser pellets (Cartwright et al., 2011), and erodibility in the York has been seen to decrease with the presence of pellets in the top few centimeters of the seabed (Kraatz et al., 2012; Dickhudt et al., 2009).

During Regime 2, river discharge decreased, near bottom salinity increased, ΔS decreased to 1 ppt (Figure 2.11), and the drag coefficient increased (Figure 2.6e

and 2.7d). This suggests that the water column was becoming less stratified and more well mixed with the retreat of the seasonal density front (Dickhudt et al. 2009; Friedrichs et al., 2008; Scully and Friedrichs, 2003). Even though similar current velocities occurred during Regime 1 and Regime 2, turbulence was no longer being dampened by stratification during Regime 2, so higher stresses were observed (Figure 2.6c and 2.7b). During the summer, biological particle packaging into pellets at the bed is expected to increase, due to increased biological abundance, but the pellets on the bed cannot be suspended into the water column if they are not exposed. The ADV data suggested that the suspension of pellets during Regime 2 is associated with the seasonal departure of the density front causing the dispersal of the recently trapped flocs, and exposing the pellets on the surface of the bed.

2.4.3 Sediment suspension and settling during each regime: Interpreting water column composition

By definition, sediment suspension occurs when bed stress exceeds a certain critical stress (τ_c) or threshold (Sanford and Maa, 2001; Sanford and Halka, 1993). Figure 2.8 showed that significant suspension beyond the wash load did not occur in either Regime until bed stresses increased past a certain initiation stress (Regime 1: $\tau_{cINIT} \approx 0.02$ Pa and Regime 2: $\tau_{cINIT} \approx 0.05$ Pa). Critical initiation stresses at Clay Bank generally have large temporal variation due to the seasonally varying patterns of sediment transport convergence and divergence, which favors different degrees of sediment consolidation and strong variability in the overall particle aggregation state (Dickhudt, 2008; Maa and Kim, 2002). The difference in initiation stress between the two regimes was expected because of the difference in dominant

particle type and sediment trapping versus dispersal between the two regimes. The critical stresses of initiation determined by the ADV were within the range that has been observed previously at Clay Bank ($\tau_{cINIT} = 0.01-0.1$ Pa) by Gust microcosm experiments (Dickhudt, 2008) and by an in situ annular flume (Maa and Kim, 2002).

Once bed stress increased past a critical stress for initiation of suspension, concentration continually increased for both Regime 1 and Regime 2 (Figure 2.8). This is consistent with depth-limited erosion. Cohesive bed theory implies that flocs, pellets and fine sand will not be sorted during erosion and that a given bed stress will be capable of removing all sediment above the depth z where $\tau_c(z) = \tau_b$ (Rinehimer, 2008; Sanford and Maa, 2001).

Using the hysteresis plots in Figure 2.8 and three simple assumptions, the particle composition of the water column within a meter of the seabed was characterized. The main particles found in suspension at Clay Bank are interpreted to be (i) pellets, (ii) flocs, and (iii) a wash load concentration of smaller particles that never settle to the bed (Cartwright et al., 2011; Cartwright et al., 2009). Due to higher densities, pellets settle out of the water column more quickly than flocs (Cartwright et al., 2011; Friedrichs et al., 2008). As stress initially decreases, therefore, pellets would be expected to deposit first. Thus the pellet component of the total concentration was assumed to be equal to the amount of sediment lost as bed stresses initially decreased. To estimate the fraction of flocs, washload concentration was removed and the concentration that was left over was assumed to be flocs. The data suggested that Regime 1 is solely composed of flocs (80%) plus wash load sediment (20%). Pellets do not appear to be present during Regime 1,

because there was not any drop in concentration when τ_b first started to decrease. The hysteresis plot suggested pellets accounted for $\sim 30\%$ of the suspended material in Regime 2, roughly consistent with the percentage of fecal pellets observed in the top few centimeters of the seabed. Laboratory analysis of cores suggest that seasonally resilient fecal pellets can seasonally make up roughly 25-35% of the top few centimeters of sea bed near the Intermediate Site (Kraatz et al., 2012; Rodriguez-Calderón, 2010).

Once bed stress peaked and began to decrease during a given tidal cycle, the pelletized sediment component in Regime 2 decreased relatively quickly (Figure 2.8b), because the lower stresses were incapable of keeping the denser particles in suspension (Cartwright et al., 2011; Fugate and Friedrichs, 2003). However, the floc concentration in both regimes remained high and rapidly decreased only after bed stresses dropped below about 0.08 Pa. Under floc-dominated conditions as turbulence decreases, other studies have found that floc size increases because flocs will adhere to one another, thus decreasing mass concentration (Cartwright et al., 2011; Fugate and Friedrichs, 2003). As bed stress decreases, concentration should then immediately decrease if flocs are adhering to one another or rapidly settling to the bed. This is not observed in the study. The observations presented in Cartwright et al. (2011) and Fugate and Friedrichs (2003) were either made at a different location or made during times of stronger bed stresses. Fugate and Friedrichs (2003) focused on the main channel, and Cartwright et al. (2011) observed stresses greater than 0.3 Pa. The results here suggest that over individual tidal cycles, at low observed bed stresses ($\tau_b \sim 0.15$ Pa) net deposition of flocs to the surface of the

seabed was inhibited when bed stresses exceed about 0.08 Pa. We interpreted this as a τ_{cDEP} of flocs of 0.08, but recall the data here show concentration at 35 centimeters above the bed. The lack of change in c as τ_b decreases may not necessarily mean particles are not being deposited. It could be a result of continuous erosion and deposition maintaining sediment at the height of the ADV even as sediment is being deposited (Ha and Maa, 2009; Sanford and Chang, 1997). Also, note that the change in c over time responds to sediment settling above and upstream the ADV height, which could result in a lag between a decrease in c with a decrease τ_b . Concentration measurements at different depths are needed to clarify the depositional patterns.

2.4.4 Settling Velocity of Flocs and Pellets

The ADV provided estimates for the bulk settling velocity, which takes into account all particle sizes present in suspension (Dyer, 1984; Fugate and Friedrichs, 2002; Friedrichs et al., 2008; Ha and Maa, 2010; Cartwright et al., 2009). Filtering out the non-settling component from the bulk settling velocity provided estimates of the settling velocity of flocs and pellets. During the floc-dominated Regime 1, flocs were settling about 0.85 mm/s. (Figure 2.9b, blue line). Flocs have a spectrum of sizes, and a large range of settling velocities has been reported for estuaries. Dyer and Manning (1999) showed that flocs from the Elbe and Tamar estuaries have settling velocities ranging from 0.001 mm/s to 100 mm/s, and that flocs with the same settling velocities could be completely different sizes due to differences in density. Previous work in the York suggested the settling velocity for

flocs is expected to be between 0.1 to 1 mm/s (Cartwright et al., 2011; Cartwright et al., 2009; Dickhudt et al., 2009; Friedrichs et al., 2008).

In the observations presented here, the settling velocity of flocs remained fairly constant even as bed stress changed over individual tidal phases during Regime 1 (Figure 2.9b, blue line), implying that floc size was limited by settling-induced turbulence rather than turbulence associated with bed stress. If the turbulence associated with bed stress was the limiting factor, floc settling velocity would decrease as increasing bed stresses tore flocs apart (Cartwright et al., 2011; Fugate and Friedrichs, 2003).

The increase in the settling velocity during Regime 2 supports the idea that the suspended concentration is composed of both flocs and pellets (Figure 2.9b, green line). Settling velocity increased as bed stress increased, because heavier pellets were being suspended by larger stresses. Previous studies estimate the settling velocity for the depositing component of suspended sediment in the presence of both flocs and pellets in the York to be between 1 and 1.5 mm/s (Cartwright et al., 2009; Dickhudt et al., 2009; Friedrichs et al., 2008). This is consistent with the value observed here to be the combined settling velocity of both flocs and pellets ($W_{sDEP} \approx 1.5$ mm/s). Based on the estimates of the proportions of flocs and pellets in the water column the calculations presented here suggest that the pellet component is settling at about 2 m/s (Figure 2.8b).

2.4.5 Evidence of the bed behaving both cohesively and non-cohesively

Sediments in the York River estuary are predominately mud so it generally is assumed to act as a cohesive environment (Dickhudt et al., 2009;

Friedrichs et al., 2009; Rinehimer et al., 2008; Friedrichs et al., 2008). However, the seabed of the York is not solely composed of purely cohesive, non-pelletized sediment. Analysis of bottom sediment samples reveals sands, resilient fecal pellets, and bed aggregates can be present at varying proportions (Kraatz et al., 2012; Rodriguez-Calderón, 2010; Dickhudt, 2009). This study's results showed that the erodibility of the bed was altered due to the presence of these less cohesive materials (Figure 2.3, green line and Figure 2.6b).

Erodibility of cohesive sediments is influenced by the degree of the consolidation of the bed (Kraatz et al., 2012; Dickhudt et al., 2010; Rinehimer, 2008). The more time the bed has to consolidate without being disturbed by erosion, the harder it becomes to erode (Rinehimer, 2008; Sanford, 2008; Sanford and Maa, 2001; Parchure and Mehta, 1985). Consolidation proceeds quickly at first and then slows with time. Gust microcosm erosion experiments (Kraatz et al., 2012) suggested that a typical consolidation time for cohesive sediment near Clay Bank is about 5 days. Consistent with the microcosm experiments of Kraatz et al., the strongest correlation between bed erodibility inferred from ADV data during the floc-dominated Regime 1 and bed stress was likewise found when average erodibility on a given day was plotted against the magnitude of bed stress observed over the previous 5 days (Figure 2.10, blue). This is consistent with cohesive bed evolution dominated by the consolidation of flocs and provides further evidence that the consolidation time scale for cohesive estuarine mud in systems like the York is often about 5 days.

In contrast, 25 hour averaged erodibility during the pellet-dominated Regime 2 was inversely correlated to 25 hour averaged bed stress (Figure 2.10, green). Erodibility decreased as bed stress increased, suggesting that the pellet component may be armoring the bed. Bed armoring is often observed occurring on non-cohesive beds (Rinehimer, 2008; Warner et al., 2008; Harris and Wiberg, 1997), which implies that during Regime 2 the bed behaved more non-cohesively.

2.5 Conclusions

Analysis of data collected at the MUDBED Intermediate site during the summer of 2007 highlights two distinct regimes with contrasting sediment characteristics. Regime 1 represents periods dominated by easily suspended, flocculated muds, while Regime 2 represents periods strongly influenced by less easily suspended, biologically formed pellets mixed together with flocs. Dominance by flocs during Regime 1 is associated with extensive trapping of flocs at a seasonally present density front; while the strong influence of pellets during Regime 2 reappeared with the seasonal departure of the density front and dispersal of the recently trapped flocs. Bottom drag coefficients derived from ADV measurements were observed to be significantly lower during Regime 1 than Regime 2, consistent with the presence of a salinity-induced density front during Regime 1, possibly enhanced by sediment-induced stratification.

During the floc-dominated Regime 1, erodibility (ϵ) averaged about 3 kg/m²/Pa and τ_b for initiation of erosion (τ_{cINT}) was only 0.02 Pa. During the pellet influenced Regime 2, ϵ dropped \sim 1 kg/m²/Pa, and τ_{cINT} increased to 0.05 Pa. During

the floc-dominated Regime 1, a remarkably stable value of $W_s = 0.85$ mm/s for the non-washload component of c was observed, consistent with floc size limitation by settling-induced turbulence rather than turbulence associated with τ_b . In contrast, during the pellet-influenced Regime 2, W_s for the non-washload component increased with greater τ_b , consistent with suspension of heavier pellets at higher τ_b and a limited supply of flocs due to bed armoring by pellets. Based on an estimate of 20% washload, 50% flocs and 30% pellets at peak τ_b during Regime 2, the settling velocity of the pellet component was estimated to be about 2.4 mm/s.

Once τ_b had peaked and then started to decrease during a given tidal cycle, the pellet component of c seemed to clear relatively quickly. But floc c did not rapidly decrease during either regime until τ_b dropped below about 0.08 Pa. This may suggest that over individual tidal cycles, cohesion of settling flocs to the surface of the seabed is inhibited for τ_b larger than ~ 0.08 Pa. Averaged over 25 hours, floc erodibility on a given day was positively correlated to the magnitude of τ_b observed over the previous 5 days, providing an in situ estimate of a consolidation-relaxation time-scale for cohesive estuarine mud. In contrast, erodibility during periods strongly influenced by pellets was inversely correlated to τ_b with a zero time lag, which was more consistent with bed armoring.

Chapter 3

The 2007 Clay Bank Region Sediment Regime Shift: Modeling Study Utilizing the York 3-D Hydrodynamic Cohesive Bed Model

Abstract

Sediment in the middle reaches of the York River estuary regularly experiences pronounced temporal transitions in settling velocity and bed erodibility. Analysis of data collected with a 5MHz Sontek ADVOcean Probe during a strong transition period indicated that the variability in settling velocity and bed erodibility was characterized by two distinct regimes with contrasting sediment and hydrodynamic characteristics: (i) Regime 1, a period dominated by flocculated muds (flocs) and (ii) Regime 2, a period dominated by biologically formed pellets mixed with flocs. This study used the York River 3-D Hydrodynamic Cohesive Bed Model (Rinehimer, 2008) to further evaluate the processes controlling bed erodibility and settling velocity by examining how well the model simulated these two distinct regimes. Comparison between model and ADV observations collected during the 2007 Clay Bank regime shift revealed that under the current set-up the model does not resolve the temporal variability in settling velocity associated with the transition of these two Regimes, nor suggest the presence of the two distinct sediment regimes. The model did estimate realistic values for current speed and concentration (normalized RMSE 0.71 and 0.96), and resolved the tidal variation in current speed, bed stress, concentration, and settling velocity. Although erodibility was underestimated, the model did also find that Regime 1 was more erodible than Regime 2. The model did a poor job of reproducing observed bed stresses and settling velocities. Throughout most of the study period, both were over-estimated by a factor of 2. The following model modifications are suggested to create a version that is able to simulate the bed stresses and sediment properties (i.e. erodibility and settling velocity) during each

regime with more accuracy: (1) Define finer sediment classes in the model that are a more representative of the water column and not just the seabed, (2) use a consolidation time scale of 5 days rather than 24 hours to allow more sediment to be suspended at lower bed stresses, (3) continue to lower hydraulic roughness, and (4) turn on sediment induced stratification.

3.1 Introduction

Fine sediment transport in coastal and estuarine environments has significant physical, biological and chemical ramifications. Mobilized sediments reduce water clarity, transport toxic materials, pathogens and nutrients, and fill navigational channels (Reay, 2009; Winterwerp and Kesteren, 2004). Bed erodibility and settling velocity are important parameters controlling cohesive sediment transport (Friedrichs et al., 2008). Both vary in space and time and are influenced by many physical and biological factors, making them two of the most poorly constrained key parameters in fine sediment transport studies (Friedrichs et al., 2008; Harris et al., 2005). Many studies have examined the physical and biological influences on bed erodibility and settling velocity (Kraatz et al., 2012; Amos et al., 2010; Rodriguez-Calderón, 2010; Dickhudt et al., 2009; Stevens et al., 2007; Amos et al., 2004; Fugate and Friedrichs, 2003; Anderson and Pejrup, 2002; Anderson, 2001; Dyer and Manning, 1999; Maa et al., 1998), but the processes controlling their spatial and temporal variability have received less attention.

Observations have recognized that both bed erodibility and settling velocity strongly vary spatially and temporally in the York River estuary (Figure 3.1), especially in the middle reaches of the estuary between West Point and Gloucester Point (Cartwright et al., 2009; Dickhudt et al., 2009; Friedrichs et al., 2008). Recently the

temporal variability in settling velocity and bed erodibility has been attributed to the presence of resilient fecal pellets or aggregates, convergence or divergence of sediment flux, asymmetries between spring and neap tidal cycles, and seasonally-varying degrees of salinity stratification (Kraatz et al., 2012; Cartwright et al., 2011; Cartwright et al., 2009; Dickhudt et al., 2009; Friedrichs et al., 2008; Scully et al., 2005). These are all time dependent processes with spatial variability in the York, so even though in-situ measurements were able to identify them, a multi-dimensional model would be beneficial in further evaluating and understanding these complex processes.

Previously, a 3-D sediment transport model of the York River based on the Regional Ocean Model System (ROMS; Shchepetkin and McWilliams, 1998, 2005) was used to examine erodibility in the York (Rinehimer, 2008). The York River 3-D Cohesive Bed Model was able to simulate temporal and spatial variations in tidally averaged erodibility and suspended sediment concentration, but the results were not analyzed to examine the flow conditions or sediment properties of settling velocity and erodibility during a temporal transition period (Rinehimer, 2008). The objective of this study was to further evaluate the processes controlling bed erodibility and settling velocity by examining how well the York River 3-D Hydrodynamic Cohesive Bed Model predicted sediment and bed properties and flow characteristics over a transition period.

3.2 Acoustic Doppler Velocimeter (ADV) Observations from the York River Estuary

Temporal variability in settling velocity and bed erodibility in the middle of the York River estuary have been the focus of several studies as part of the NSF and CoOP funded Multidisciplinary Benthic Exchange Dynamics (MUDBED) project (Friedrichs et

al., 2008). A well-pronounced temporal transition period in settling velocity and bed erodibility has been observed seasonally at the MUDBED Intermediate Site near Clay Bank since 2006 (Cartwright et al., 2009; Dickhudt et al, 2009; Friedrichs et al, 2008). Analysis of observations collected with a Sontek Acoustic Doppler Velocimeter during a strong transition period (June 12, 2007 to August 24, 2007) indicated that the variability in settling velocity and bed erodibility was characterized by two distinct regimes with contrasting sediment and hydrodynamic characteristics. The transition from Regime 1 to Regime 2 was marked by a two-fold increase in bed stresses, a decrease in suspended sediment concentration, an increase in bulk settling velocity, and a decrease in bed erodibility (Figure 3.2). A full description of these regimes can be found in Chapter 2.

3.3 York River 3-D Hydrodynamic Cohesive Bed Model

Rinehimer (2008) created and implemented a 3-D sediment transport model of the York River using the Regional Ocean Model System (ROMS; Shchepetkin and McWilliams, 1998, 2005) to examine temporal and spatial variability in erodibility and suspended sediment concentration. ROMS is a community, primitive equation model that uses various discretization techniques to solve the hydrostatic Reynolds averaged Navier-Stokes equation on a curvilinear orthogonal grid with vertically stretched terrain-following coordinates (Haidvogel et al., 2008; Shchepetkin and McWilliams, 1998, 2005). ROMS provides the user with options for different advection schemes, sub-models and boundary conditions.

Rinehimer's (2008) York River model used a 3-D curvilinear grid with ~120 meter across channel resolution and ~170 meter along channel resolution (Figure 3.3). The grid consisted of 92 cross channel cells, 334 along channel cells, and 40 vertical cells

(20 that extend up the water column and 20 that go into the seabed). The model implemented the Community Sediment Transport Modeling System's (CSTMS) cohesive bed sub-model to account for the depth and temporal variability of critical shear stress (τ_c) (Rinehimer et al, 2008; Sanford et al., 2008; Warner et al., 2008). The bed model utilized two sediment types defined by distinct settling velocities ($W_s = 0.8$ and 0.1 mm/s). Additionally, the model included forcing by tides and freshwater discharge from the Mattaponi and Pamunkey Rivers. A complete description of the model is included in Rinehimer (2008).

3.4 Model Modifications

Rinehimer's (2008) model represented the first 200 days of 2007, but did not include wind as a forcing, and only accounted for two sediment sizes. Previous field studies in the York indicated that winds significantly influence sediment dynamics (Scully et al., 2005), and the seabed and water column contain multiple particles sizes (Cartwright et al, 2011; Rodriguez-Calderón, 2010; Dickhudt 2008). In order to generate more informative results, the model was modified to include wind forcing and six sediment sizes ($W_s = 3.2, 1.6, 0.8, 0.4, 0.2, 0.1$ mm/s), whose settling velocities spanned the range previously observed in the area (Cartwright et al., 2011; Cartwright et al., 2009; Friedrichs et al., 2008). The model simulation time was also extended 44 days to encompass the transition period observed by the ADV. The objectives of this modeling exercise were to examine the controls on the temporal transition in bed erodibility and settling velocity at the Intermediate Site and to evaluate the model's ability to reasonably reproduce the patterns documented by the ADV observations. For that reason we

analyzed the model results from the time period when the ADV was collecting data (June 12, 2007-August 24, 2007).

Model performance was assessed based on how well the calculations of bed stress, current speed, and suspended sediment concentration matched the observed values visually through graphs and by calculating the total normalized root mean square error and root mean square error (normalized RMSE and RMSE, Joliff, et al., 2008). RMSE for the various model simulations can be found in Table 3.2 A and B. The model consisted of 354 along channel grid cells, 92 across channel grid cells and 20 vertical grid cells (Figure 3.3). Results from grid cells along channel grid cells 199-201 and across channel grid cells 51-53 were averaged together and to approximately represent the MUDBED Intermediate Site (Figure 3.3, black dot). These grid cells were chosen because (1) they are within the area that the ADV tripod was deployed and Dickhudt (2008) collected his sediment cores for analysis, and (2) the water depth of these model cells was similar to depth of the observations (~5-6 meters). Model estimates of both current speed and suspended sediment concentration were interpolated to the height of the ADV measurements (~35 cmab) prior to comparison.

The initial model run (Simulation-1) did a poor job simulating bed stresses (normalized RMSE= 2.83) and concentration (normalized RMSE=1.06) (Table 3.2 A). In fact, bed stresses were over estimated by a factor of 2 (Figure 3.4 b). Even though the RMSE of current speeds was less than 1 (normalized RMSE=0.87), peak current speeds were still underestimated by about 20 cm/s (Figure 3.4 a). Modifications were made in subsequent models in attempts to better match available observations. In total, three model simulations were completed:

1. Simulation-1: This is the Rinehimer (2008) model simulation with the addition of wind and additional grain sizes. All of the other parameters that were used in Rinehimer (2008) were kept the same.
2. Simulation-2: This is the same simulation as Simulation-1, except that hydraulic roughness (Z_o) was decreased in an attempt to lower modeled bed stresses.
3. Simulation-3: This is the same simulation as Simulation-2, except that a more erodible equilibrium critical stress profile was used in an attempt to increase suspended sediment concentration.

The differences between these simulations are summarized in Table 3.1.

Bed erodibility from the model was estimated using the same method that was used to estimate erodibility from ADV data, i.e. bed erodibility (ϵ in $\text{kg}/\text{m}^2/\text{Pa}$) was defined as the ratio of depth-integrated concentration (C in kg/m^2) to bed stress (τ_b in Pa) averaged among the selected grid cells (Cartwright et al, 2009; Friedrichs et al, 2008):

$$\epsilon = C/\tau_b \quad (1).$$

Note that this definition differs from the definition used by Rinehimer (2008) and Dickhudt (2008). They defined ϵ as amount of sediment eroded at a given bed stress and both looked at the amount of sediment eroded in kg/m^2 at a bed stress of 0.2 Pa.

In all three simulations, six sediment classes were defined, each with distinct settling velocities: 3.2 mm/s, 1.6 mm/s, 0.8 mm/s, 0.4 mm/s, 0.2 mm/s and 0.1 mm/s. The proportion of each size class in every vertical layer was tracked at every model time step. By definition, bulk settling velocity takes into account all particles present at the ADV sample height (Dyer et al., 1984); therefore the sum of the proportion by weight of each

size class multiplied by their respective settling velocity provided estimates for bulk settling velocity. Calculations of bed erodibility and settling velocity, as well as tidal phase analysis, are presented only for the results from Simulation-2, the model simulation that best resolved observed current speed, bed stress and concentration.

3.5 Performance Assessment of Simulation-1, Simulation-2 and Simulation-3

As stated above, Simulation- 1 over-estimated bed stresses and underestimated current speed (Figure 3.4). The York model used a logarithmic profile (uv_logdrag), when relating bed stress to current velocity in the bottom boundary layer (Rinehimer, 2008; Warner et al., 2005). The logarithmic formulation assumes the von Kármán-Prandtl or law of the wall equation:

$$\bar{U} = \frac{u_*}{\kappa} \ln\left(\frac{Z}{Z_o}\right) \quad (2)$$

where \bar{U} is a current speed at a height Z in meters above the bed, u_* is friction velocity, κ is the von Kármán constant (~ 0.408), and Z_o is hydraulic roughness (WikiROMS; Kim et al., 2000). Z_o is a parameter that represents a small distance above the seabed where theoretically the velocity profile intersects the y-axis or goes to zero. When a logarithmic profile is assumed, C_d depends on a user defined hydraulic roughness (Z_o):

$$C_d = \left(\frac{u_*}{\bar{u}}\right)^2 = \left(\frac{\kappa^2}{(\log(\frac{Z}{Z_o}))^2}\right) \quad (3).$$

Bed stress (τ_b) is related to friction velocity (u_*) by:

$$\tau_b = \rho u_*^2 \quad (4)$$

where ρ is the density of water (Kim et al., 2000). Both bed stress and friction velocity are dependent on Z_o , therefore decreasing Z_o should result in a decrease in bed stress.

The original model of Rinehimer (2008) defined $Z_o=0.1$ centimeters above the bed (cmab). Observations suggest mean $Z_o= 0.004$ cmab during the study period, however (Figure 3.5). Simulation-2 lowered Z_o from 0.1 cmab to 0.005 cmab, a value more consistent with the observed Z_o and similar to values used in some other sediment transport models (Wiberg et al, 1994; Harris and Wiberg, 1997). The results of Simulation-1 and Simulation-2 are compared to each other and to ADV observations graphically in Figure 3.6 and statistically in Table 3.2 A, which shows the RMSE and the RMSE that was normalized over the standard deviation. Using a lower Z_o improved the simulations of current speed, decreasing the normalized RMSE from 0.81 to 0.71, and the RMSE from 10.35 cm/s to 8.24 cm/s. Modeled estimates of concentration were slightly improved as well, with normalized RMSE <1 . Even though modeled τ_b did decrease, and the normalized RMSE improved from 2.83 to 1.96 (Table 3.2a), the reduction in Z_o did not create a large enough decrease in τ_b . The normalized RMSE for concentrations improved with Simulation-2 (normalized RMSE=0.96), but the simulation did worse at capturing peak observed concentrations (Figure 3.6c). Unfortunately the slight decrease in τ_b resulted in a decrease in peak model concentration.

The next test was aimed to increase concentration despite lower τ_b by changing the erodibility of the seabed. Erosion of the bed occurs when bed stress (τ_b) exceeds the critical stress (τ_c) of the bed surface. In cohesive environments τ_c varies with time and depth in the bed (Rinehimer et al., 2008; Sanford, 2008). Rinehimer et al. (2008) developed the cohesive sediment bed sub-model of ROMS to account for the change in τ_c

with depth and to add time-dependence to τ_c . The cohesive bed model includes a user defined, empirically derived critical stress equilibrium reference profile (τ_{ceq}), which is prescribed in the model in the form of a power-law (Rinehimer et al., 2008; Sanford, 2008). An instantaneous τ_c profile is determined at each time step and is nudged towards τ_{ceq} through a relaxation step (eqn. 2.6 in Rinehimer et al., 2008) that accounts for consolidation after deposition and swelling after erosion (Rinehimer et al., 2008; Sanford, 2008).

Rinehimer (2008) used data from the Dickhudt (2008) Gust Microcosm experiments in choosing τ_{ceq} (Figure 3.7). Figure 3.7 shows the profiles and power laws derived from Gust experiments done on cores collected in April 2007 and in September 2007. Simulation-1 and Simulation-2 assumed the power law defined for September as the equilibrium profile. However, the observations that the model was trying to simulate were collected during the late spring/early summer when higher erodibility was observed (Dickhudt, 2008). A third model simulation (Simulation-3) was completed using the τ_{ceq} profile derived from the April cores and the lower $Z_o = 0.005$ cmab.

Little difference was seen between the results of Simulation-2 and Simulation-3 (Figure 3.8). During Simulation-3 only the τ_{ceq} profile was changed, not the initial τ_c profile. The use of the same initial τ_c profile or error in altering the code for a different τ_{ceq} profile may be why results from Simulation-3 were so similar to Simulation-2. Because Simulation-2 and Simulation-3 were practically identical, Simulation-3 was not quantitatively compared to ADV observations.

3.6 Comparison of Model-2 Results to ADV Observations

The objective of this study was to examine the hydrodynamics and sediment properties of settling velocity and bed erodibility in the middle reaches of the York River estuary, specifically evaluating how well the York River 3-D Cohesive Hydrodynamic ROMS model (Rinehimer, 2008) simulated the flow and particle characteristics during a temporal transition in bed erodibility and settling velocity. Analysis of Simulation-2 results over the 80 day observational period revealed that the model successfully reproduced observed current speeds and the tidal variation in current speeds, bed stress, and concentration (Figure 3.6). However, it was not able to adequately reproduce peak bed stress, concentration, settling velocity, or bed erodibility. Visually, it appeared that the model did slightly better simulating bed stresses and concentrations during Regime 2 (Figure 3.6). Tidal analysis was used to look more closely at the Simulation-2's ability to resolve the distinct regimes seen by the ADV.

3.6.1 Model Performance Over Individual Tidal Cycles

Tidal analysis on results from Simulation-2 was done by first identifying the top 20% of tidal cycles within in each Regime in the ADV data with the strongest observed bed stresses. The top 20% of modeled tidal cycles with the strongest bed stresses were then defined by selecting tidal cycles in the model that occurred at the same time as the tidal cycles selected from observations. Current speed, bed stress, and concentration were each averaged to show how each generally behaved over individual tidal phases (Figure 3.9). Normalized and un-normalized RMSE from the results of the tidal analysis from Simulation-2 for each parameter during each Regime 1 and Regime 2 are presented in

Table 3.2 B. Figure 3.9 shows that the model reproduced realistic patterns over individual tidal cycles. Modeled current speed, bed stress, and concentration followed the same pattern as the observations over individual tidal phases. Both model and observed bed stresses and concentration increased with current speed (Figure 3.9). Overall, the model was most successful at predicting current speeds, especially during Regime 2 when a normalized RMSE decreased from 1.17 (Regime 1) to 0.25 (Regime 2) and RMSE decreased from 16.35 cm/s (Regime 1) to 3.01 cm/s (Regime 2) (Table 3.2 B).

The tidal phase analysis highlighted the difference in model performance between Regime 1 and Regime 2. The model significantly underestimated concentration during Regime 1, with RMSE \approx 50 mg/L (Figure 3.9c). Modeled concentrations during Regime 2 are lower than those observed, but compared to Regime 1, the model does a much better job. The normalized RMSE decreases below 1 and modeled concentrations are within less than 20 mg/L of observations (Table 3.2 B). Simulation-2 captured the differences in concentration between the two regimes (Figure 3.9c), supporting the idea presented in Chapter 2 that during Regime 1, more easily suspended material is available. Also, similar to observations, modeled concentrations do initially decrease as modeled bed stress began to decrease (Figure 3.9b and c). Both the model and observations suggested that sediment is not being deposited until bed stresses decrease past a certain value.

Tidal analysis further emphasized that the model was poorest at reproducing observed bed stress. Bed stresses over individual tidal phases were almost 2 times higher than observed bed stress, especially during Regime 1. The model failed to capture the significant difference in bed stresses the ADV observed between Regime 1 and 2, and

modeled bed stresses were practically identical during Regime 1 and Regime 2 (Figure 3.9b). According to normalized RMSE a value, the model was better at predicting bed stress during Regime 2 (normalized RMSE = 0.92) than Regime 1 (normalized RMSE = 2.38).

Hysteresis plots of modeled bed stress versus modeled concentration further highlighted the differences between modeled bed stress and observed bed stress (Figure 3.10). Current speed in the model during Regime 1 and Regime 2 was very similar (Figure 3.9a). Current speed measured by the ADV was also similar for both Regimes (Figure 3.9a), but bed stresses estimated by the ADV data were different between the two, and the model did not show that (Figure 3.9b, and 3.10). Observed peak bed stress during Regime 1 and Regime 2 were about 0.15 Pa and 0.25 Pa. Peak modeled bed stresses during both Regime and Regime 2 were similar and higher, ~0.3 Pa.

Despite the larger variation in bed stress between the model and observations, the model results showed an overall pattern of erosion similar to that observed by the ADV (Figure 3.10). Both the model and observations suggested everything begins to be eroded together once bed stresses reached 0.02-0.03 Pa. During Regime 2, observations showed that as bed stress decreased, concentration initially decreased continuously until bed stresses reached 0.08 Pa. Once bed stresses fell below 0.08 Pa concentration decreased at a faster rate, which suggested the presence of resilient fecal pellet and flocculated muds (Figure 3.10). The model does not clearly suggest this. The model results showed that for both Regime 1 and Regime 2, once bed stresses fall below ~0.2-0.25 Pa, concentrations continually decrease. The two groups of settling material highlighted in Chapter 2 are not clearly resolved in the model.

3.6.2 Variability in Bed Erodibility and Settling Velocity

Comparing ADV estimated bed erodibility to model estimated erodibility revealed that the model underestimated erodibility (Figure 3.11). ADV observations range from 4 kg/m²/s (Regime 1) to less than 1 kg/m²/s (Regime 2), and the modeled estimates barely peaked at 1 kg/m²/s (Figure 3.11a). Recall in this study bed erodibility (ε in kg/m²/Pa) was defined as the ratio between depth-integrated concentration and bed stress ($\varepsilon = C/\tau_b$), so considering that the model overestimated bed stresses, it was expected that erodibility would be lower. The model erodibility does show a decreasing trend towards the end of the study period, similar to the observations. This suggests that the model did simulate the temporal trend in erodibility, and that if model bed stresses were lower it could more quantitatively estimate erodibility.

The model simulated tidal variability in settling velocity, but did not resolve the temporal variability associated with the transition from Regime 1 to Regime 2 (Figure 3.12). ADV observations show peak settling velocity increasing from less than 1 to greater than 1 around July 22, 2007 (Figure 3.12). The model estimated peaked settling velocities greater than 1 throughout the entire study period (Figure 3.12). The model overestimated settling velocity and predicted settling velocities greater than 2 mm/s for the majority of the time. The York model estimates settling velocity by multiplying the sum of the proportion by weight of each size class by their respective settling velocities. In the York Model, settling velocities are defined by the user as model input to define sediment size classes. Overestimates in settling velocity suggested that the sediment size

distribution at the time period was being dominated by coarser particles with faster settling velocities.

3.7 Evaluation of York River 3-D Cohesive Hydrodynamic ROMS Model Performance

ADV analysis concluded the temporal transition in settling velocity and bed erodibility observed in the summer of 2007 was attributed to the transition between two distinct regimes with contrasting sediment characteristics: (i) Regime 1, a period dominated by flocculated muds (flocs) and (ii) Regime 2, a period dominated by biologically formed pellets mixed with flocs. Comparison between model and ADV observations collected during the 2007 Clay Bank regime shift revealed that under the current set-up, the model predicts temporal variability associated to the transition between Regime 1 and Regime 2 in erodibility, but not in settling velocity. The model estimated realistic values for current speed and concentration and simulated tidal variability in current speed, bed stress, concentration, and settling velocity. Also, although erodibility was underestimated, the model did suggest Regime 1 was more erodible than Regime 2. Compared to the other parameters, the model did poorest at reproducing observed bed stress and settling velocity. Throughout most of the study period, bed stresses and settling velocities were over-estimated by a factor of 2.

Recall, the model estimated settling velocity by taking the sum of the proportion by weight of each size class multiplied by their respective settling velocities. The settling velocity estimates from the model imply that during the time period of the study, the area was dominated by faster settling particles. Analysis of model grain size distribution throughout the entire estuary for the entire 244 days indicated the slower settling

sediments (finer particles) were being advected from the study area prior to this study period. In order to decrease settling velocity, the model needs to keep the finer settling particles (0.8 mm/s and less) in the area. However, this may be difficult to do with high bed stresses. Also, observations indicated that flocculated muds dominated Regime 1 and pellets mixed with flocs dominated Regime 2. Even though the York ROMS sediment model is capable of accounting for different sediment sizes, they are defined with specific settling velocities that do not change throughout the model run. The model does not account for varying particle sizes and settling velocity associated with flocculation and floc break up (Cartwright et al., 2011; Dyer and Manning, 1999), which could be another reason why the model does not reproduce observed settling velocity well.

Even though the model did better at predicting sediment concentration compared to bed stress and settling velocity, concentration was still underestimated, and concentration was found to be sensitive to bed stress in a manner somewhat inconsistent with observations. The slight change in bed stresses from Simulation-1 to Simulation-2 decreased concentration by at least 50 mg/L (Figure 3.6c), and even with significantly higher bed stresses, the model underestimated the suspended sediment concentration by about 40 mg/L (Table 3.2 A) The model seabed may be a factor limiting the model predictive skill of concentration and settling velocity for this period. The results suggested that the characteristics (grain distribution and erodibility) of the present version of the model bed were not a good representation of the seabed during Regime 1. It appeared the model bed needed to be more erodible, especially since modeled concentration was high sensitive to bed stresses, and bed stresses need to be lowered to obtain accuracy. Unfortunately, this was not achieved by changing the τ_{ceq} profile.

The York model used the cohesive sediment bed model (Rinehimer et al. 2008). Cohesive sediment erodibility is also influenced by the degree of bed consolidation (Kraatz et al., 2012; Dickhudt et al., 2010; Rinehimer, 2008; Sanford, 2008). The York model accounts for consolidation by assuming the effects can be approximated by a first-order relaxation equation depending on a user defined consolidation time scale (T_c) (Rinehimer, 2008; Sanford, 2008). Larger consolidation time scales slow consolidation and increase suspended sediment concentration (Rinehimer, 2008). All the models runs used a consolidation time of 24 hours. Recent observations at the Intermediate Site (Figure 3.13) indicated that a T_c of 1 day was appropriate for Regime 2, but suggested a $T_c = 5$ days may be a better approximation during Regime 1 (Kraatz et al., 2012). These observations suggest a longer T_c such as 5 days may need to be used to increase concentration at lower bed stresses.

The reasons above suggest why the model is underestimating concentration, but do not account for why bed stresses are over predicted by a factor of 2. The responses of model stresses to changes in hydraulic roughness length were tested. However, lowering Z_o only resulted in a slight decrease in bed stress.

ADV data (chapter 2) suggest that the lower bed stresses observed during Regime 1 are likely due to a combination of sediment and salinity induced stratification (Scully and Friedrichs, 2003; Kim and Friedrichs, 2000). Although the model is capable of accounting for sediment induced stratification, the feature was not implemented in any of the model simulations. Turning on sediment-induced stratification in the model could result in lower bed stresses during Regime 1.

3.8 Summary of Model-ADV Comparison

The current set-up of the York River 3-D Hydrodynamic Cohesive Bed Model is not conducive to examining the temporal variability in settling velocity associated with the transition between the distinct sediment regimes. The current model version estimated realistic values for current speed and concentration (normalized RMSE 0.71 and 0.96), and resolved the tidal variation in current speed, bed stress, concentration, and settling velocity. Bed erodibility was underestimated the model but the model did suggest Regime 1 was more erodible than Regime 2, which was clearly shown in ADV observations from Chapter 2 and by Dickhudt's (2008) gust microcosm experiments. The model did a poor job of reproducing observed peak bed stresses and settling velocity. Both were over estimated by a factor of 2 throughout most of the study period.

The following model modifications are suggested to create a version that is better able to simulate the bed stresses and sediment properties (i.e. erodibility and settling velocity) during each regime with more accuracy: (1) Define finer sediment classes in the model that are a more representative of the water column and not just the seabed, (2) use a consolidation time scale of 5 days rather than 24 hours to allow more sediment to be suspended at lower bed stresses, (3) continue to lower hydraulic roughness, and (4) turn on sediment induced stratification.

Chapter 4
Conclusions and Future Work

Conclusions and Future Work

This thesis used observations collected by a near-bed Acoustic Doppler Velocimeter (ADV) and a 3-D sediment transport model based on the Regional Oceanography Modeling System (ROMS) to investigate the relationships between the hydrodynamics and particle types in the York River estuary, VA. The ADV measured hydrodynamics over a distinct temporal transition period in the middle of the York, and in Chapter 2 these data were used to examine the processes controlling the temporal variability in settling velocity (W_s) and bed erodibility (ϵ). Results of the ADV analysis were then used in Chapter 3 to evaluate how well a 3-D sediment transport model of the York River was able to simulate the hydrodynamics during a transition period. In Chapter 2, the ADV analysis concluded that the temporal variability in bed erodibility and settling velocity was due to the transition between two distinct regimes with contrasting sediment characteristics.

Regime 1 was observed at the beginning of the study, and is characterized by an easily erodible seabed ($\epsilon \sim 3 \text{ kg/m}^2/\text{Pa}$) dominated by flocculated muds settling at roughly 0.85 mm/s. Low ADV-derived bottom drag coefficients and high sediment concentrations ($C \sim 100 \text{ mg/L}$), despite low bed stresses ($\tau_b \sim 0.1 \text{ Pa}$), suggest the dominance of flocs during this regime is associated with the extensive trapping of fine sediment at a seasonally present density front, possibly enhanced by sediment-induced stratification. Because observations were only taken from one height above the bed, however, the influence of sediment stratification in the York was not fully resolved. Future work plans include the deployment of vertically stacked ADVs in conjunction with vertically stacked conductivity-temperature sensors, and a surface wind anemometer

to better determine the combined influence of salinity and sediment induced stratification on the sediment dynamics.

During Regime 2, observed in the second half of the study period, erodibility decreased ($\varepsilon \sim 1 \text{ kg/m}^2/\text{Pa}$) and settling velocity increased, indicating the region was influenced by less easily suspended, faster settling biologically formed pellets ($W_s \sim 2.4 \text{ mm/s}$) mixed together with the slower settling flocs ($W_s \sim 0.85 \text{ mm/s}$). Higher ADV derived drag coefficients suggest that this regime appears with the seasonal departure of the density front and dispersal of recently trapped flocs.

The ADV observations also provided an in situ estimate of a consolidation-relaxation time-scale for homogeneous estuarine mud. Averaged over 25 hours, erodibility on a given day during Regime 1 was most positively correlated to the magnitude of τ_b observed over the previous 5 days, suggesting a bed consolidation time scale of 5 days. In contrast, erodibility during Regime 2 was inversely correlated to τ_b with a zero time lag, which is more consistent with bed armoring.

Comparison of ADV observations and results from the York River 3-D Hydrodynamic Cohesive Bed Model (Rinehimer, 2008) presented in Chapter 3 suggested the current model was not conducive to examining the temporal variability in settling velocity associated with the transition of the distinct sediment regimes. The model version estimated realistic values for current speed and concentration and resolved tidal variability in current speed, bed stress, concentration, and settling velocity. However, the model did a poor job of reproducing observed peak bed stresses and settling velocity. Both were over estimated by a factor of 2 throughout most of the study period. Possible model modifications to create a version better able to simulate observed bed stresses and

sediment properties (i.e. erodibility and settling velocity) during each regime are: (1) define finer sediment classes in the model that are a more representative of the water column and not just the seabed, (2) use a consolidation time scale of 5 days rather than 24 hours to allow more sediment to be suspended at lower bed stresses, (3) continue to lower hydraulic roughness, and (4) turn on sediment induced stratification.

More observations of the sediment in the bed and water column are needed to determine what sediment classes should be used in the model to adequately represent the water column in the middle reaches of the York. The ADV was only able to identify the three main particle groups in suspension (wash load, flocs and pellets) and provide estimates on the mean settling velocity in each group. In order to identify individual particles with more constrained settling velocities, a high definition particle-settling camera will be deployed at the site.

Table 3.1: Summary of the difference between model simulations.

Model	Hydraulic Roughness (Z_o)	Critical Stress Equilibrium Profile	Notes
Simulation-1	0.1 cmab	September, 2007	Original model run
Simulation-2	0.005 cmab	September, 2007	Decrease bed stresses
Simulation-3	0.005 cmab	April, 2007	Increase concentration

Table 3.2: Normalized and non-normalized root mean square error (RMSE) between ADV observed and modeled current speed, concentration, and bed stress RMSE values for Simulation-1 and Simulation-2 are compared in Table 3.2A and RMSE values comparing Regime 1 and Regime 2 during Simulation-2 are shown in 3.2B.

A.

	Simulation-1	Simulation-2
Current Speed	0.87 (10.35 cm/s)	0.71 (8.24 cm/s)
Concentration	1.06 (49.45 mg/L)	0.96 (39.63 mg/L)
Bed Stress	2.83 (0.16 Pa)	1.96 (0.12 Pa)

B.

	Regime 1	Regime 2
Current Speed	1.17 (16.35 cm/s)	0.25 (3.01 cm/s)
Concentration	1.07 (50.67 mg/L)	0.65 (18.39 mg/L)
Bed Stress	2.38 (0.11 Pa)	0.92 (0.07 Pa)

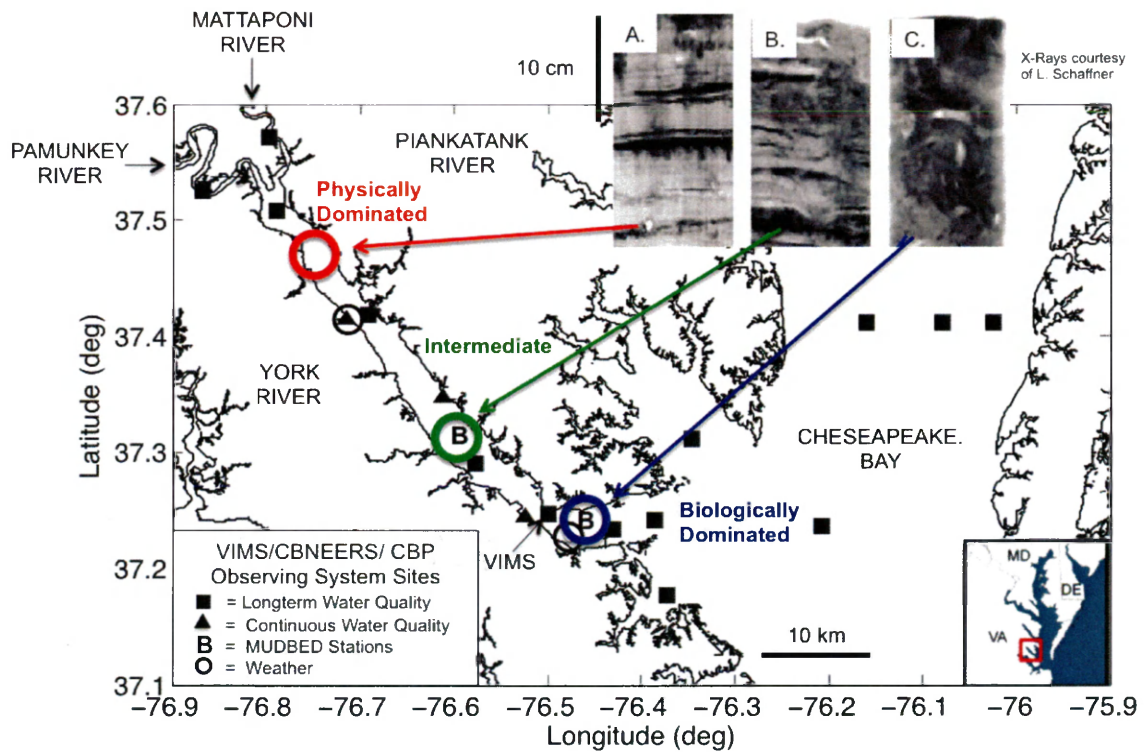


Figure 2.1: Map of York River Estuary, southeastern VA from Cartwright et al., 2009. The location of the MUDBED Intermediate site is in green. X-radiographs for the upper estuary (a.), middle estuary (b.) and lower estuary (c.) are courtesy of L. Schaffner.

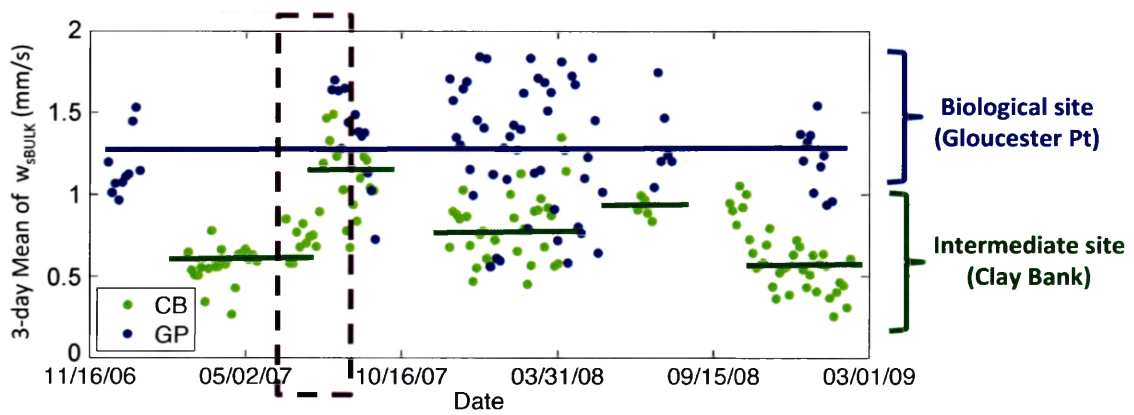


Figure 2.2: Long-term ADV measured bulk settling velocity for the MUDBED Intermediate (green) and Biological (blue) sites courtesy of G. Cartwright. The purple box indicates the time period of this study (June-August 2007).

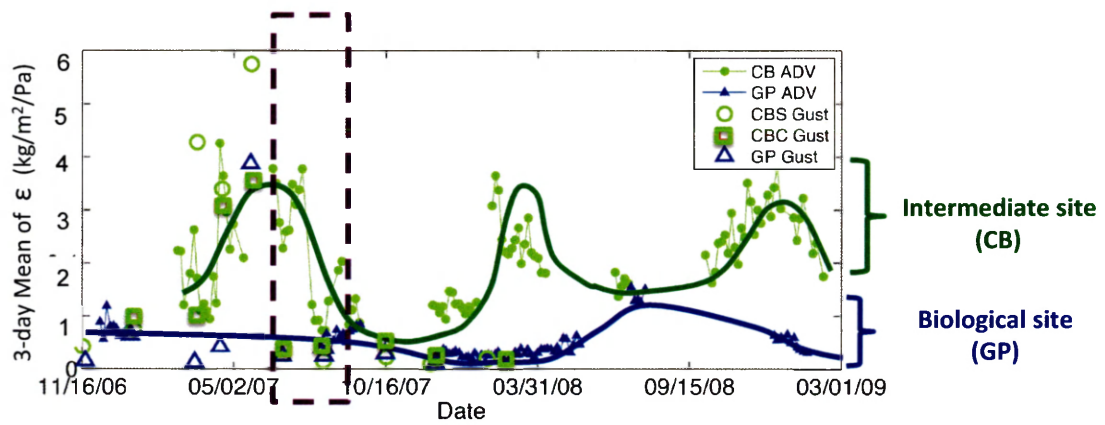


Figure 2.3: Long-term estimates of bed erodibility measured by the ADV (line) and with the Dual Core Gust Microcosm (symbols) for the MUDBED Intermediate (green) and Biological (blue) sites courtesy of G. Cartwright and P. Dickhudt. The purple box indicates the time period of this study (June-August 2007).

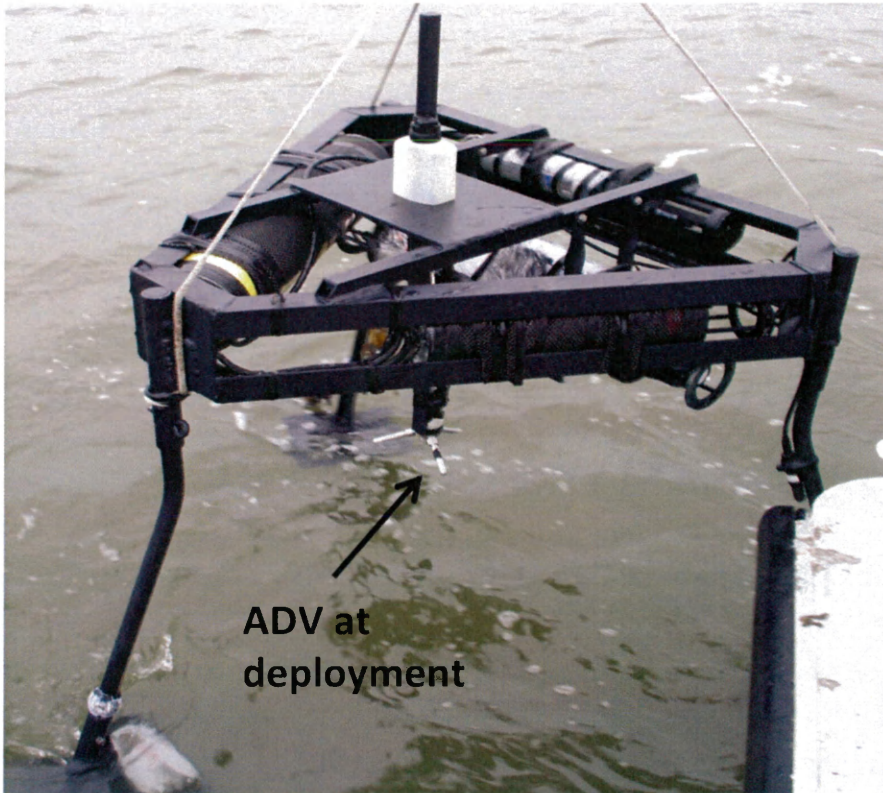


Figure 2.4: MUDBED bottom tripod with mounted 5MHz Sontek ADVOcean Probe. Photo courtesy of G. Cartwright.

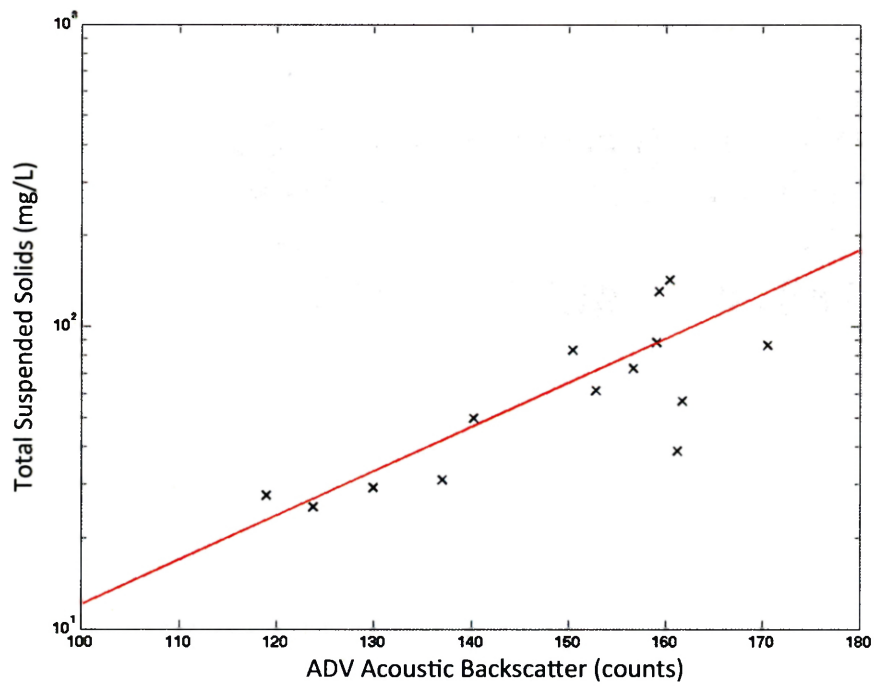


Figure 2.5: Total suspended solids determined by pump samples collected on the July 18, 2007 calibration cruise (Cartwright et al., 2009) versus acoustic backscatter at corresponding times as the pump samples were taken by the ADV on the Tripod (black X's). The red line indicates the calibration relationship from Cartwright et al., 2008 ($c = e^{(0.034x - 0.87)}$) used to calculate suspended sediment concentration from acoustic backscatter.

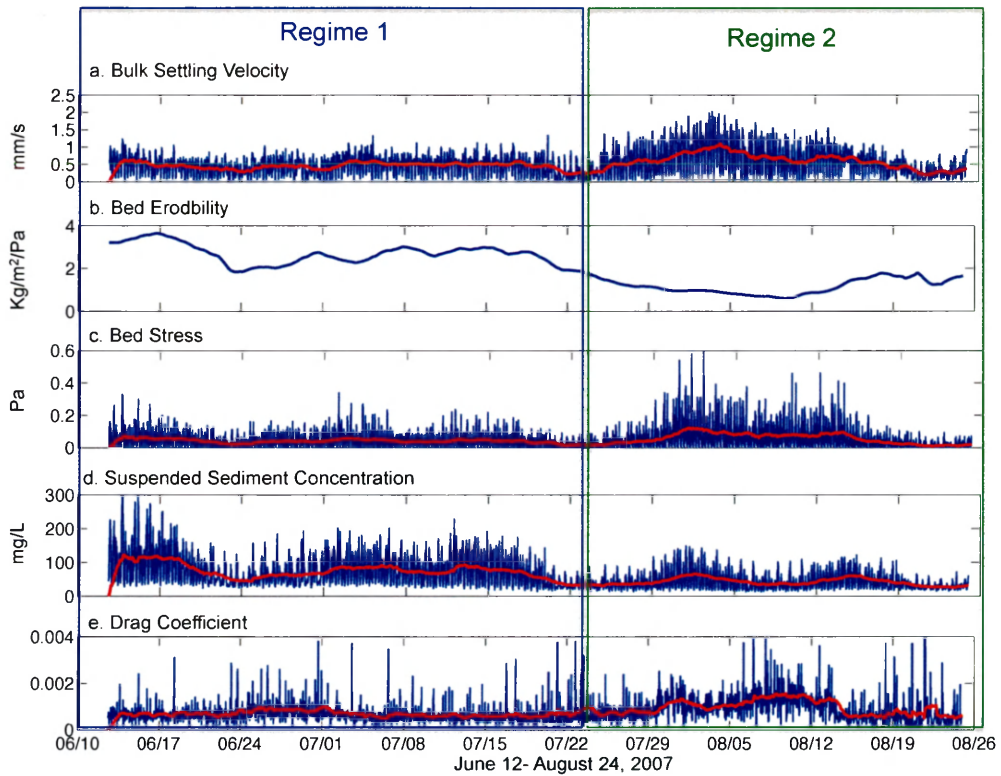


Figure 2.6: Instantaneous (blue line) and daily averaged (red line) ADV measurements of bulk settling velocity (a), bed erodibility (b), bed stress (c), suspended sediment concentration (d), and drag coefficient (e) from the summer of 2007. The transition between Regime 1 (blue box) and Regime 2 (green box) is marked by an increase in settling velocity and decrease in erodibility.

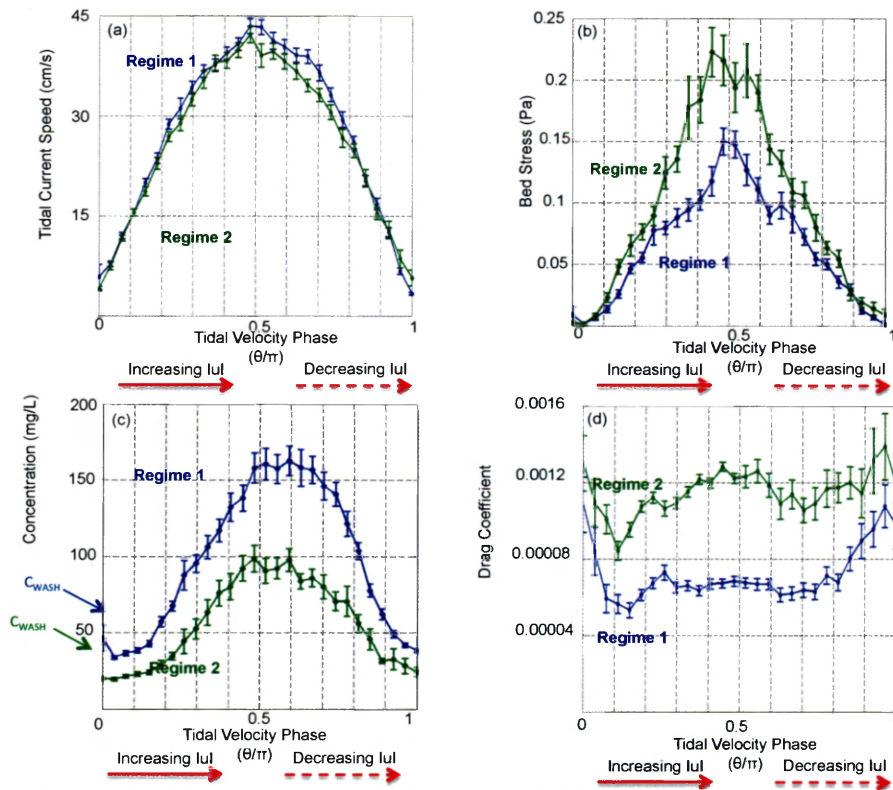


Figure 2.7: ADV measured current speed (a), bed stress (b), suspended sediment concentration (c), and drag coefficient (d) for the top 20% of tidal cycles with the strongest bed stresses for Regime 1 (blue) and Regime 2 (green). Error bars denote ± 1 standard error. The “washload” concentrations (C_{WASH}) are defined as background level of suspended sediment that is still in suspension, even when $\tau_b \approx 0$

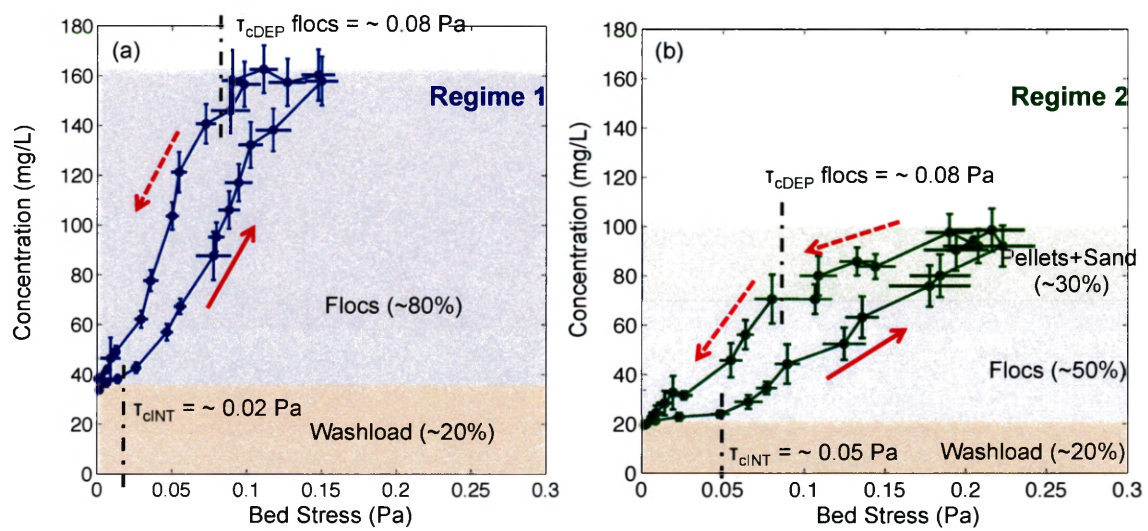


Figure 2.8: Hysteresis plots of c vs. τ_b for the top 20 % of tidal cycles with the strongest τ_b for Regime 1 (a) and Regime 2 (b).

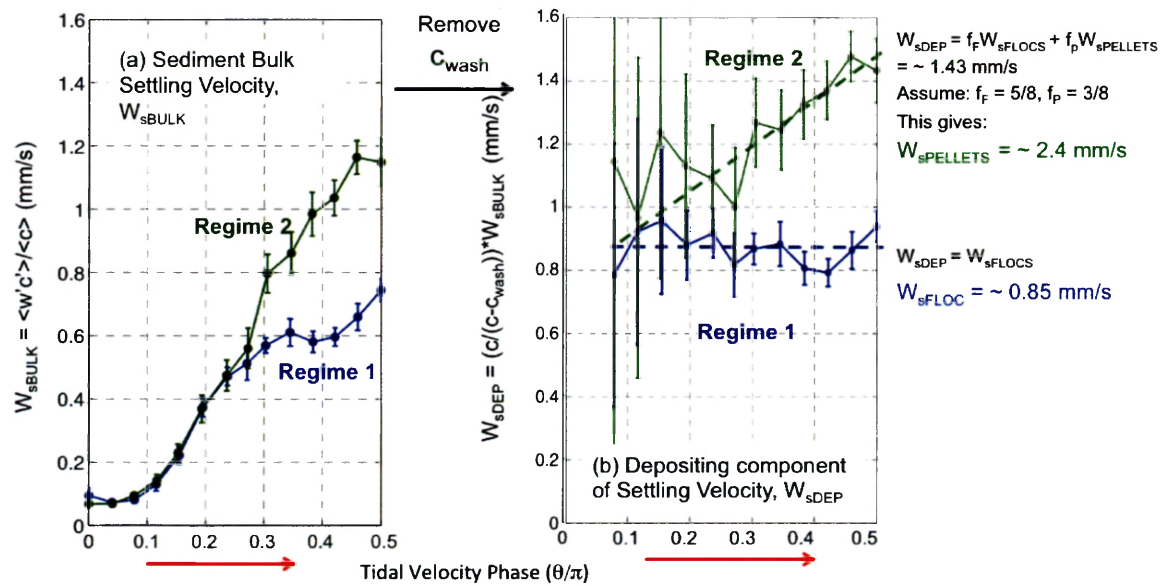


Figure 2.9: Bulk settling velocity (a) and the settling component of the settling velocity (b) during the increasing tidal velocity phase for the top 20% of tidal cycles with the highest bed stresses. Error bars denote +/- 1 standard error.

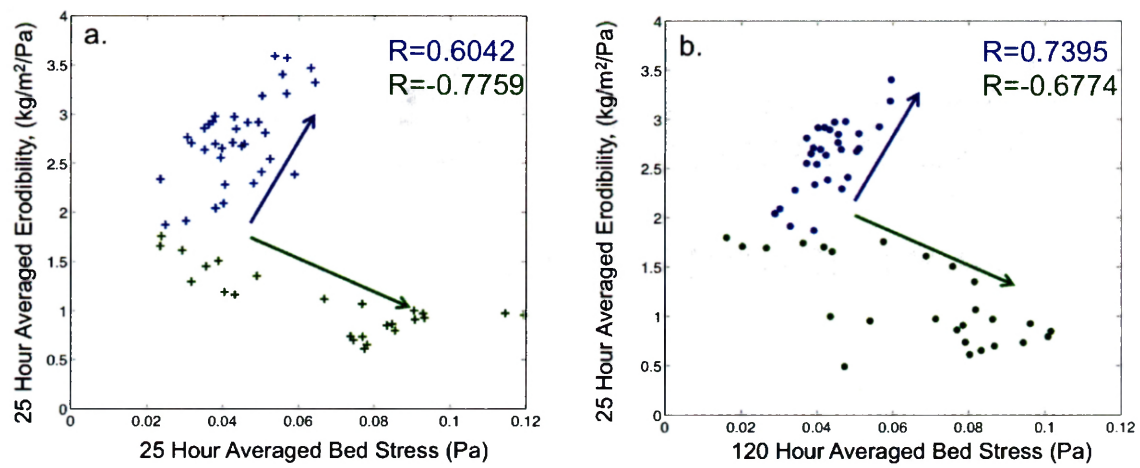


Figure 2.10: Daily averaged erodibility versus 25 hour averaged bed stress (a) and versus 120 averaged hour bed stress (b). Daily averaged erodibility during Regime 1 (blue) is better correlated to 120 hour averaged bed stress, while during Regime 2 daily averaged erodibility more strongly correlated to 25 hour averaged bed stress.

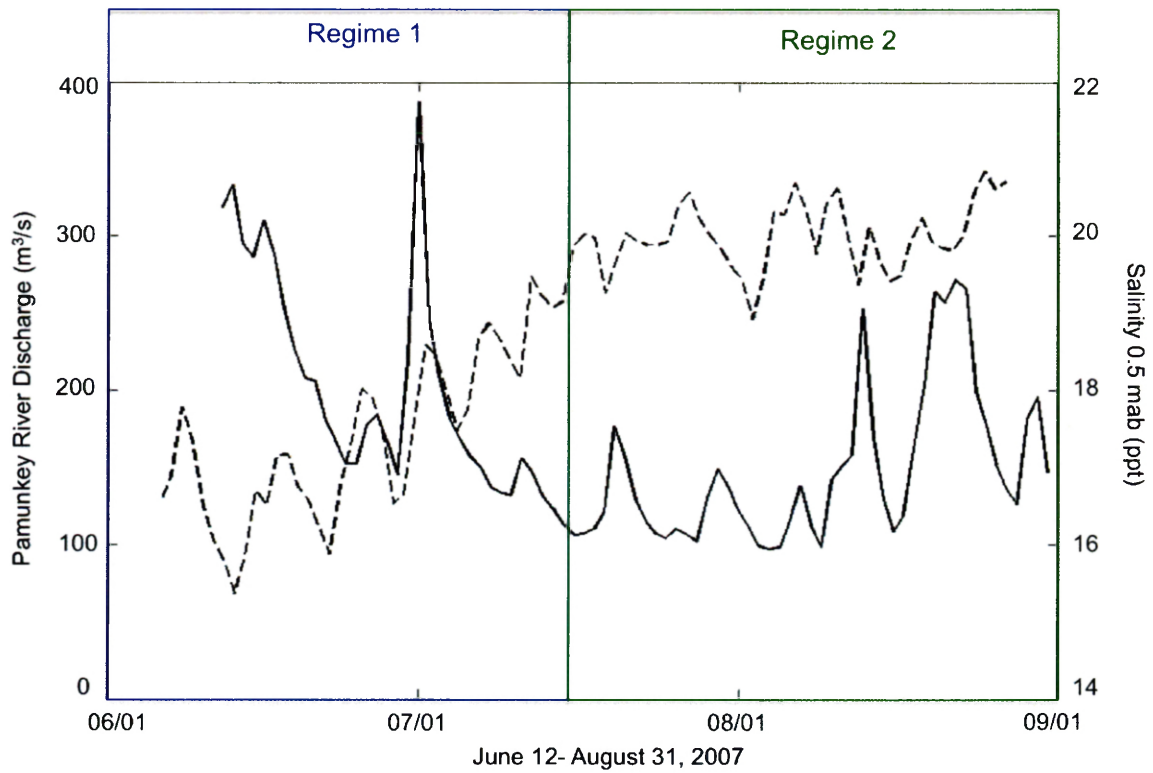


Figure 2.11: Pamunkey River Flow (solid black line) measured at Hanover, VA from USGS Water Data website at <http://waterdata.usgs.gov/nwis>. YSI measured salinity from (black solid line) from Chesapeake Bay National Estuarine Research Reserve (CBNEERS) continuous monitoring station. Salinity data was obtained from VECOS website, <http://www2.vims.edu/vecos>.

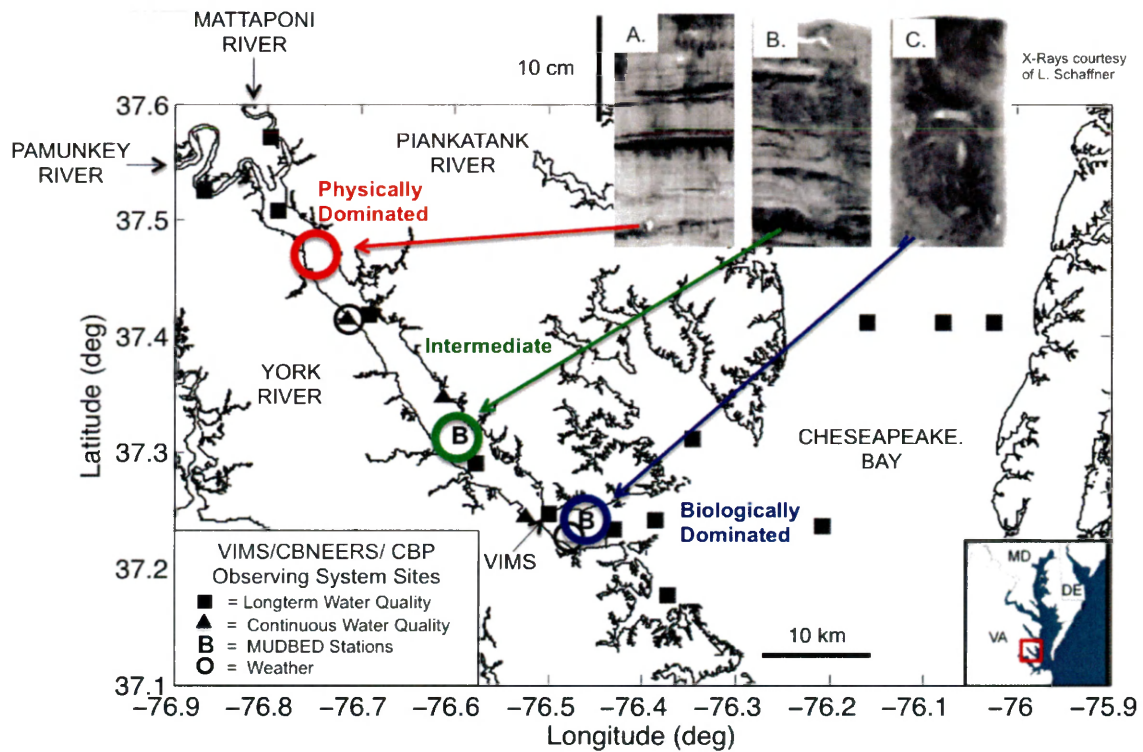


Figure 3.1: Map of York River estuary, Southeastern VA from Cartwright et al., 2009. The location of the MUDBED Intermediate Site is in green. X-radiographs for the upper (a), middle (b), and lower (c) estuary are courtesy of L. Schaffner.

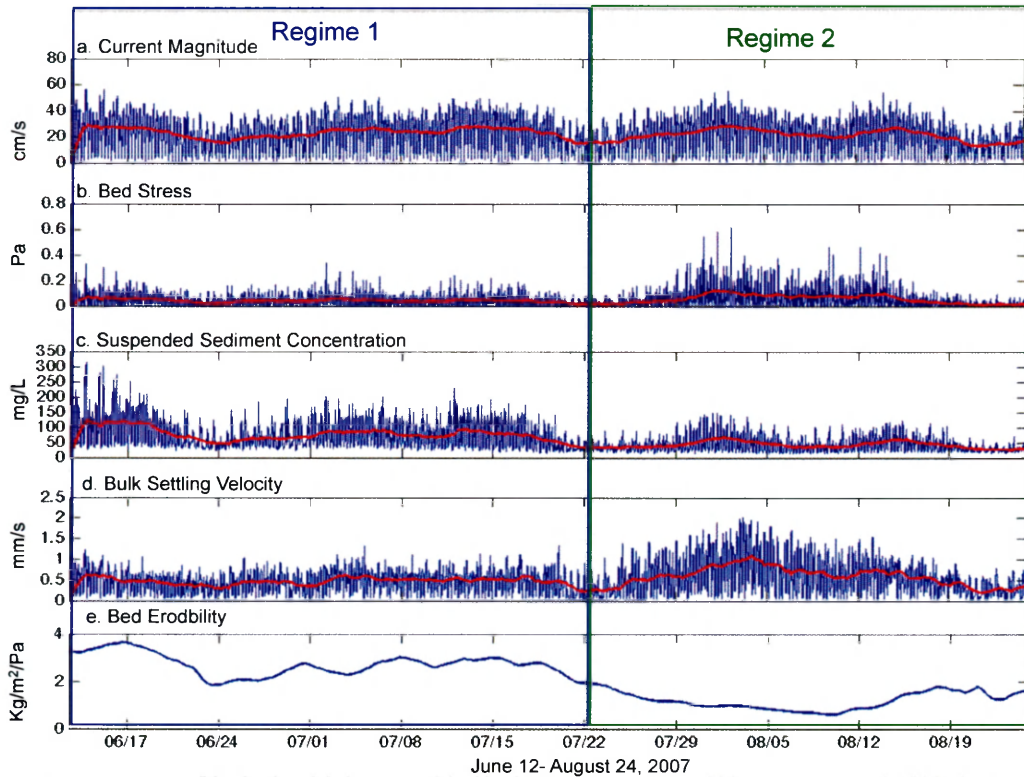


Figure 3.2: Instantaneous (blue line) and daily averaged (red line) ADV measurements of bulk settling velocity (a), bed erodibility (b), bed stress (c), suspended sediment concentration (d), and drag coefficient (e) from the summer of 2007. The two regimes defined in Chapter 2 are marked out in blue (Regime 1) and green (Regime 2).

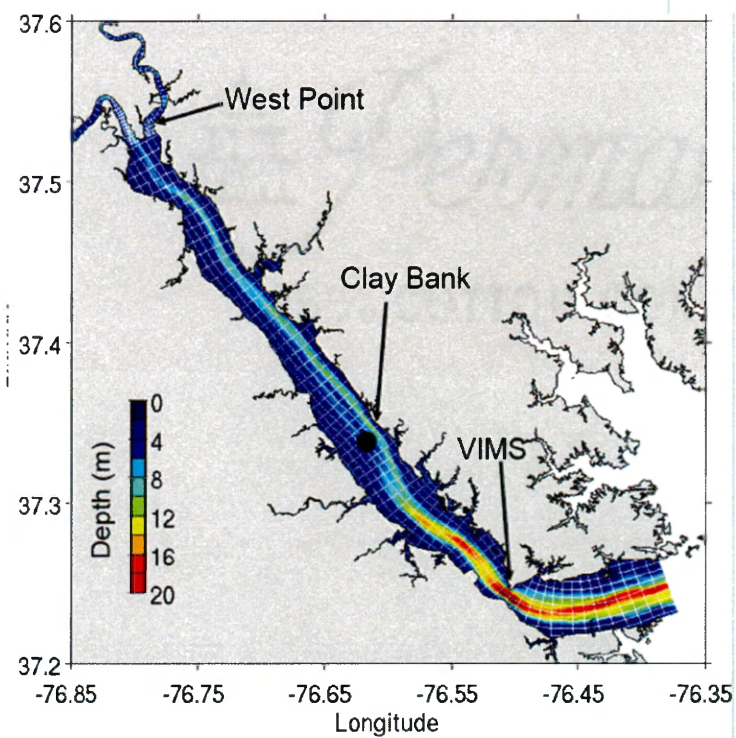


Figure 3.3: The York River Estuary Cohesive Bed Hydrodynamic ROMS Model grid (Rinehimer, 2008). Each square represents five model grid cells. The black circle represents the relative location of the MUDBED Intermediate Site.

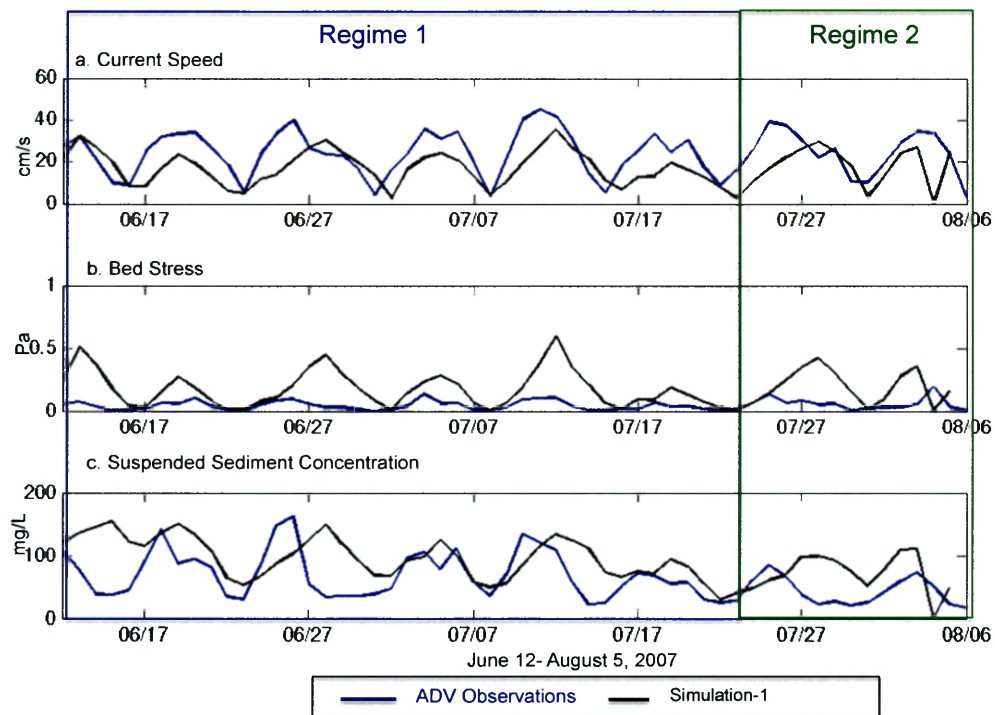


Figure 3.4: Tidally averaged ADV measurements (black line) and results from Simulation-1 (blue line) of current speed (a), bed stress (b), and suspended sediment concentration (c) from the summer of 2007. The two sediment Regimes are in the blue (Regime 1) and green (Regime 2) box.

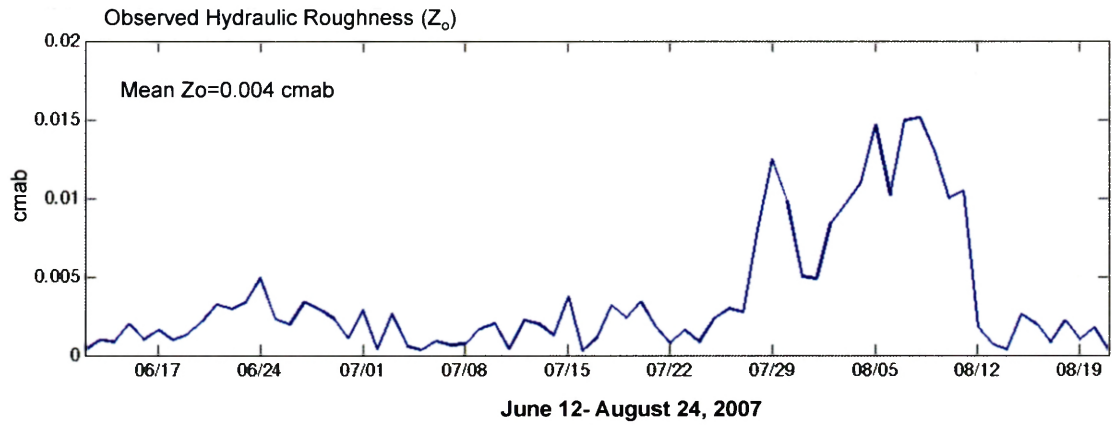


Figure 3.5: Tidally averaged hydraulic roughness (Z_o) during the observation period at the Intermediate site, estimated by the ADV assuming the law of the wall. Observations show a mean $Z_o=0.004$ centimeters above the bed.

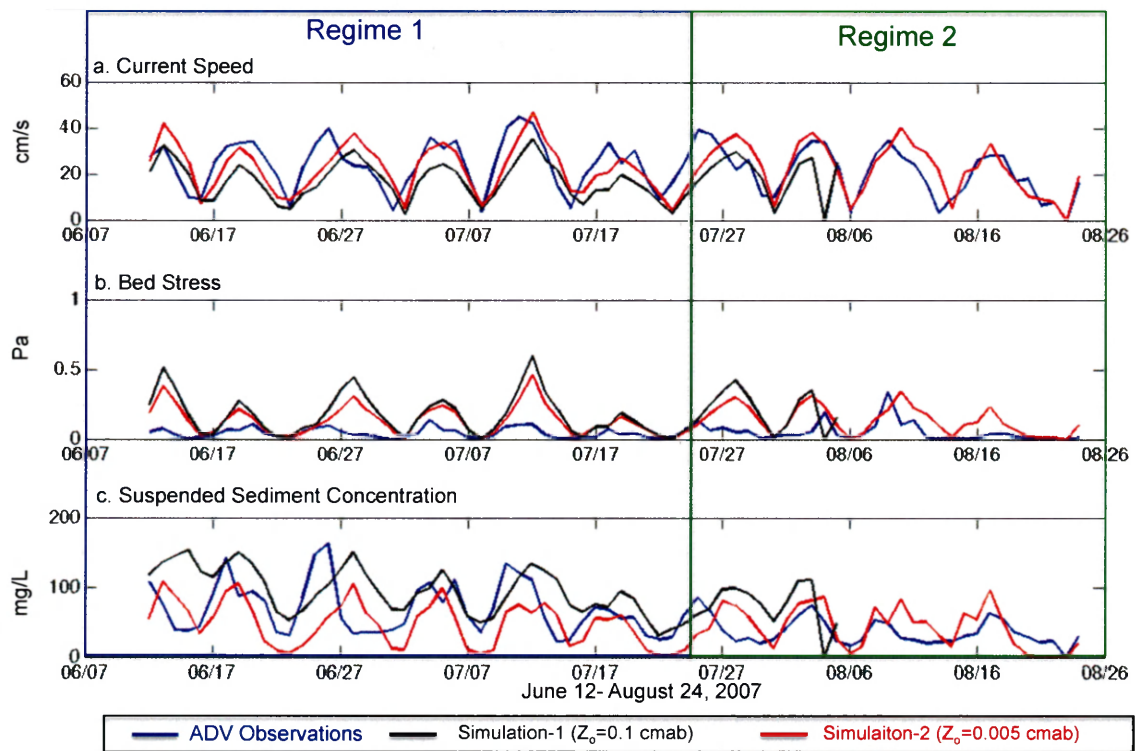


Figure 3.6: Tidally averaged ADV measurements (blue line), Simulation-1 (black line), and Simulation-2 (red line) of current speed (a), bed stress (b), and suspended sediment concentration (c) from the summer of 2007. The two sediment Regimes are within the blue box (Regime 1) and green box (Regime 2).

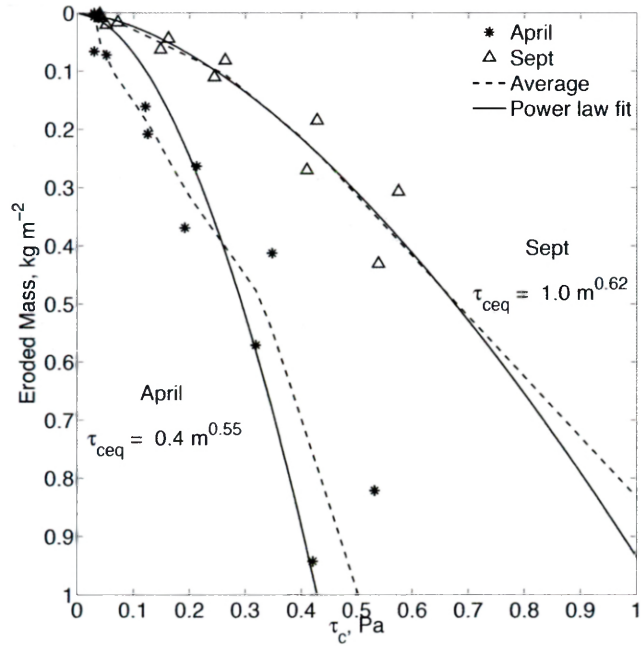


Figure 3.7: Critical stress profiles estimated using the Coummunity Sediment Transport Modeling System's (CSTMS) cohesive bed model (Rhinehimer, 2008), and measured from cores during two sampling period (April and September) using a Dual Process Gust Microcosm (Dickhudt et al., 2008). The symbols are the data points from Dickhudt et al., 2008 and the lines are the model average and power law fit to the data points (Rhinehimer, 2008). τ_{ceq} was defined in the model by the power law fit. The power law fit from September ($\tau_{ceq}=1.0m^{0.62}$) was used in Simulation-1 and Simulation-2, while the power law fit from April ($\tau_{ceq}=0.4m^{0.55}$) was used for Simulation-3.

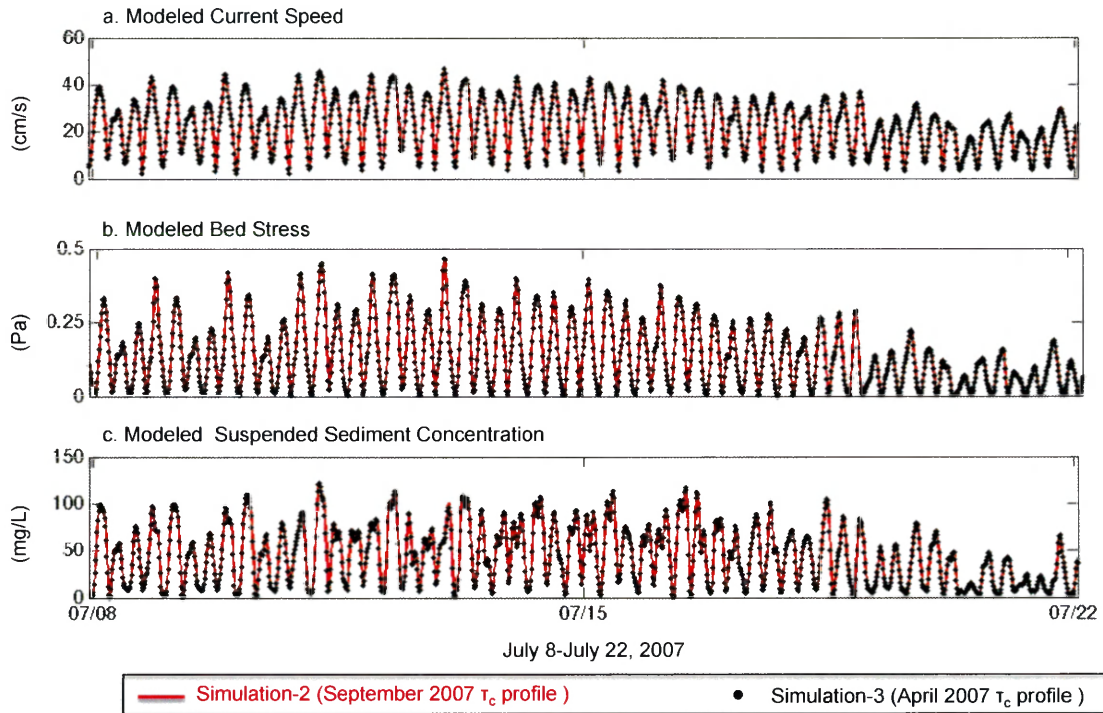


Figure 3.8: Current speed (a), bed stress (b) and suspended sediment concentration (c) for a two week period determined by Simulation-2 (black) and Simulation -3 (red). Model results were very similar between the two simulations.

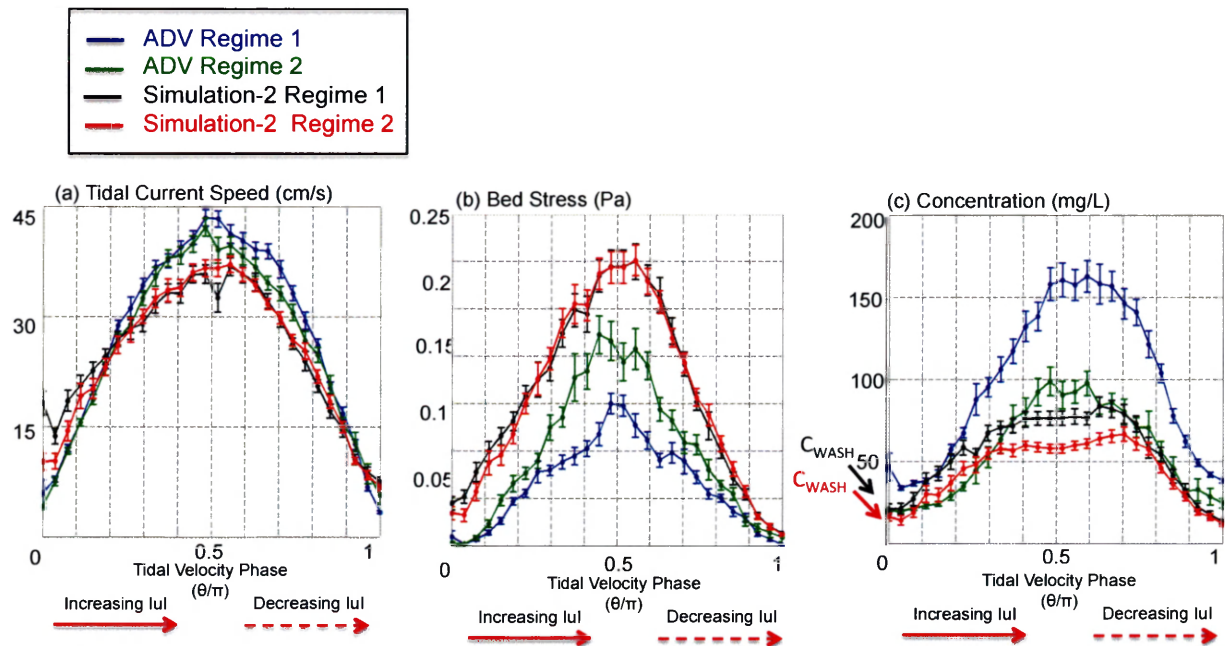


Figure 3.9: Comparison of tidal analysis of current speed (a), bed stress (b), and concentration (c) between ADV observations collected during Regime 1 (blue) and Regime 2 (green) and Simulation-2 results during Regime 1 (black) and Regime 2 (red).

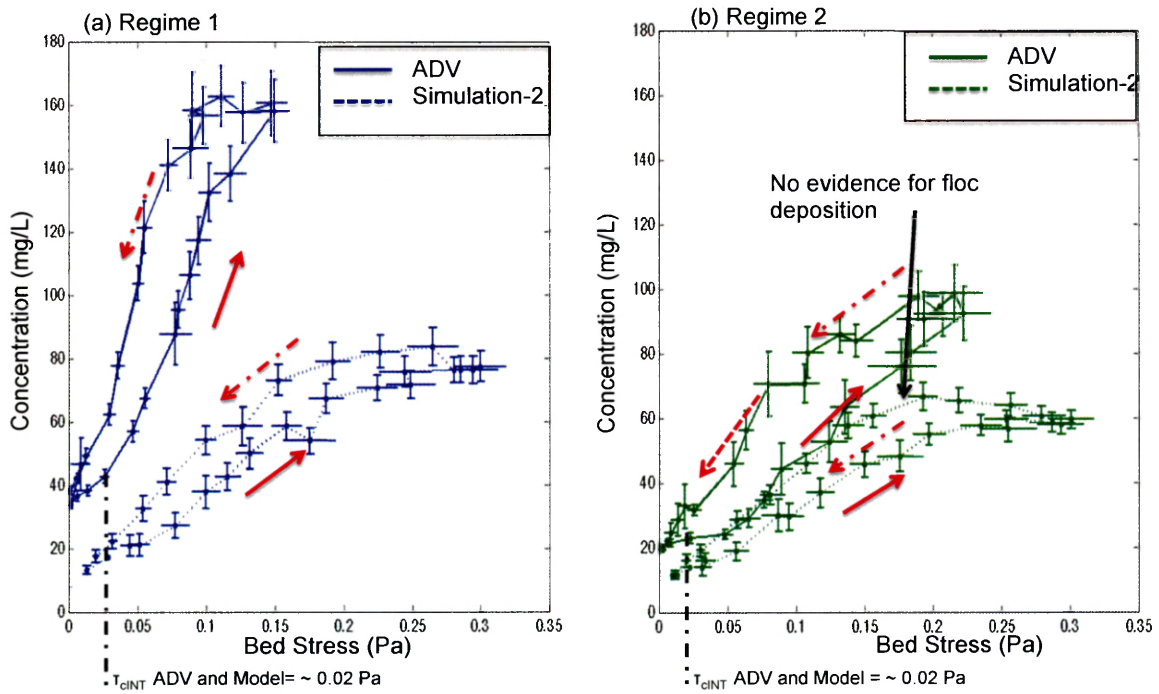
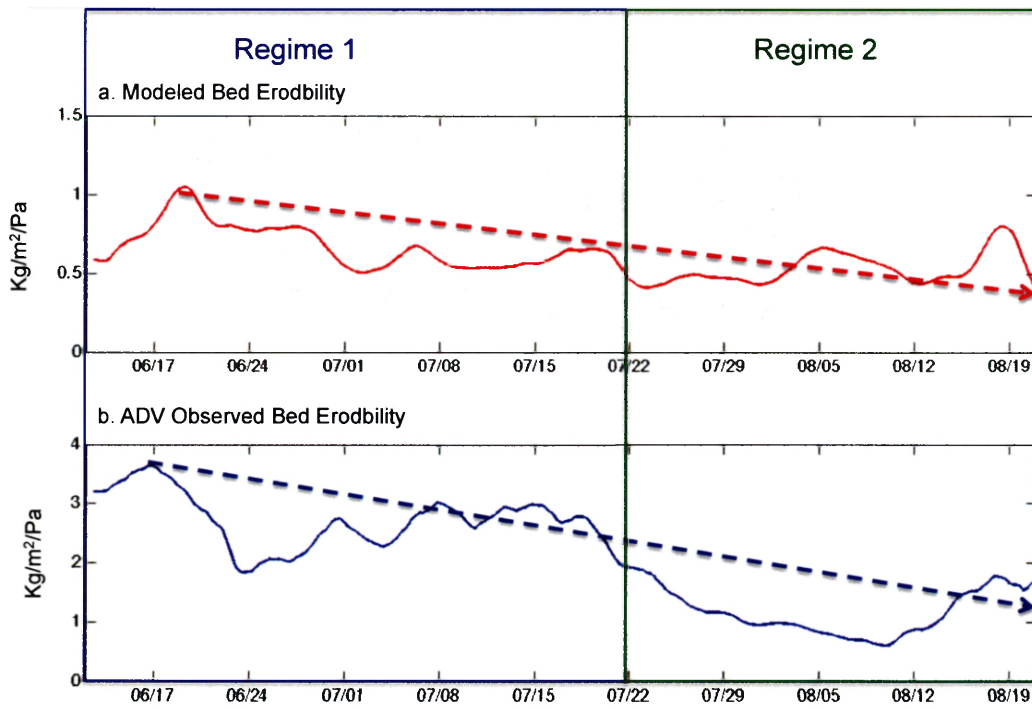


Figure 3.10: Hysteresis plots of concentration versus bed stress measured by the ADV (solid line) and estimated by Simulation-2 (dashed line) for the top 20% of tidal cycles with the strongest bed stress for Regime 1 (a) and Regime 2 (b). Note the similar bed stresses during both regimes estimated by Simulation-2.



June 12- August 24, 2007

Figure 3.11: Bed erodibility estimated by Simulation-2 (a) and by the ADV (b). Arrow trend lines indicate that both methods show bed erodibility decreasing throughout the study period.

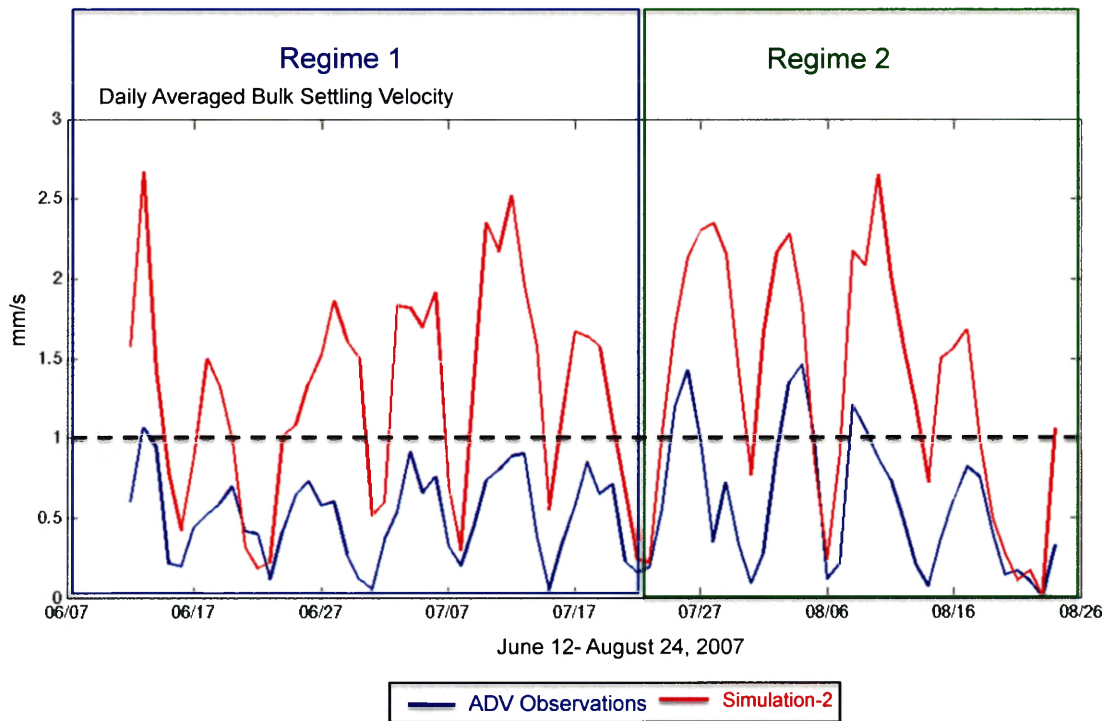


Figure 3.12: Tidally averaged bulk settling velocity (W_s) estimated by Simulation-2 (red) and by the ADV (blue). The black line corresponds to $W_s = 1$ mm/s.

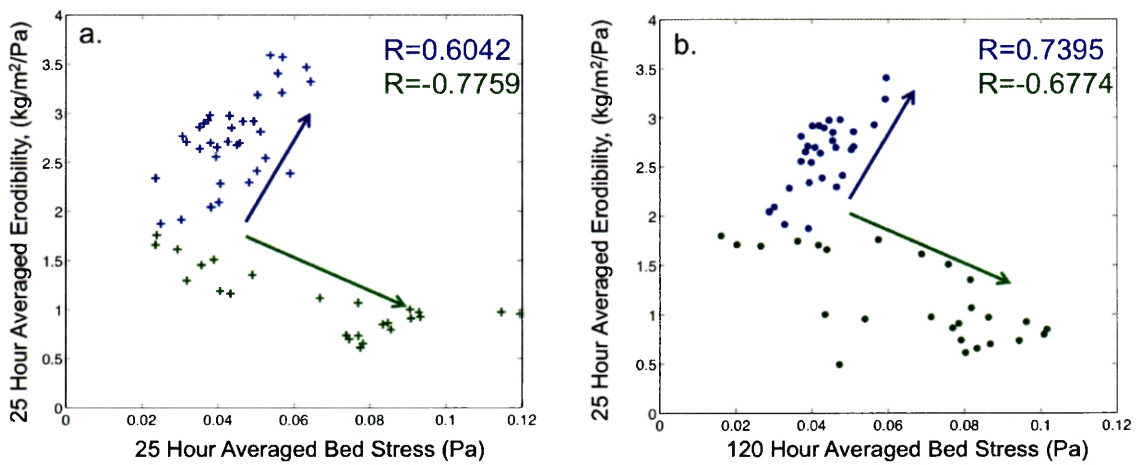


Figure 3.13: 25-hour averaged bed erodibility versus either 25 hour (a) or 120-hour bed stress (b). Daily averaged erodibility during Regime 1 (blue) is better correlated to 120 hour averaged bed stress, while during Regime 2 daily averaged erodibility more strongly correlated to 25 hour averaged bed stress.

ocean_york_mud_4c.in

```
!  
! ROMS/TOMS Standard Input parameters.  
!  
!svn $Id: ocean_york_mud.in 1499 2008-04-29 21:18:51Z jprinehimer $  
!===== Herman  
G. Arango ===  
! Copyright (c) 2002-2007 The ROMS/TOMS Group  
! Licensed under a MIT/X style license  
! See License_ROMS.txt  
!=====
```

```
!  
! Input parameters can be entered in ANY order, provided that the parameter !  
! KEYWORD (usually, upper case) is typed correctly followed by "=" or "==" !  
! symbols. Any comment lines are allowed and must begin with an exclamation !  
! mark (!) in column one. Comments may appear to the right of a parameter !  
! specification to improve documentation. All comments will ignored during !  
! reading. Blank lines are also allowed and ignored. Continuation lines in !  
! a parameter specification are allowed and must be preceded by a backslash !  
! (\). In some instances, more than one value is required for a parameter. !  
! If fewer values are provided, the last value is assigned for the entire !  
! parameter array. The multiplication symbol (*), without blank spaces in !  
! between, is allowed for a parameter specification. For example, in a two !  
! grids nested application:  
!  
! AKT_BAK == 2*1.0d-6 2*5.0d-6 ! m2/s !  
!  
! indicates that the first two entries of array AKT_BAK, in fortran column- !  
! major order, will have the same value of "1.0d-6" for grid 1, whereas the !  
! next two entries will have the same value of "5.0d-6" for grid 2. !  
!  
! In multiple levels of nesting and/or multiple connected domains step-ups, !  
! "Ngrids" entries are expected for some of these parameters. In such case, !  
! the order of the entries for a parameter is extremely important. It must !  
! follow the same order (1:Ngrids) as in the state variable declaration. The !  
! USER may follow the above guidelines for specifying his/her values. These !  
! parameters are marked by "==" plural symbol after the KEYWORD. !  
!  
!=====
```

```
!
```

! Application title.

TITLE = York River Cohesive Estuary

! C-preprocessing Flag.

MyAppCPP = YORK_MUD

! Input variable information file name. This file needs to be processed
! first so all information arrays can be initialized properly.

VARNAME = ../Include/varinfo.dat

! Grid dimension parameters. See notes below in the Glossary for how to set
! these parameters correctly.

Lm == 90 ! Number of I-direction INTERIOR RHO-points
Mm == 352 ! Number of J-direction INTERIOR RHO-points
N == 20 ! Number of vertical levels

Nbed = 20 ! Number of sediment bed layers

NAT = 2 ! Number of active tracers (usually, 2)
NPT = 0 ! Number of inactive passive tracers
NCS = 6 ! Number of cohesive (mud) sediment tracers
NNS = 0 ! Number of non-cohesive (sand) sediment tracers

! Domain decomposition parameters for serial, distributed-memory or
! shared-memory configurations used to determine tile horizontal range
! indices (Istr,Iend) and (Jstr,Jend), [1:Ngrids].

NtileI == 2 ! I-direction partition
NtileJ == 8 ! J-direction partition

! Time-Stepping parameters.

NTIMES == 470400
DT == 45.0d0
NDTFAST == 60

! Model iteration loops parameters.

ERstr = 1
ERend = 1
Nouter = 1

Ninner = 1
Nintervals = 1

! Number of eigenvalues (NEV) and eigenvectors (NCV) to compute for the
! Lanczos/Arnoldi problem in the Generalized Stability Theory (GST)
! analysis. NCV must be greater than NEV (see documentation below).

NEV = 2 ! Number of eigenvalues
NCV = 10 ! Number of eigenvectors

! Input/Output parameters.

NRREC == 0
LcycleRST == T
NRST == 80
NSTA == 20
NFLT == 1
NINFO == 10

! Output history, average, diagnostic files parameters.

LDEFOUT == T
NHIS == 80
NDEFHIS == 1920
NTSAVG == 1
NAVG == 1920
NDEF AVG == 0
NTSDIA == 1
NDIA == 1920
NDEFDIA == 0

! Output tangent linear and adjoint models parameters.

LcycleTLM == F
NTLM == 72
NDEF TLM == 0
LcycleADJ == F
NADJ == 72
NDEF ADJ == 0

! Output check pointing GST restart parameters.

LrstGST = F ! GST restart switch
MaxIterGST = 500 ! maximum number of iterations
NGST = 10 ! check pointing interval

! Relative accuracy of the Ritz values computed in the GST analysis.

Ritz_tol = 1.0d-15

! Harmonic/biharmonic horizontal diffusion of tracer: [1:NAT+NPT,Ngrids].

TNU2 == 0.1d0 0.1d0 0.1d0 0.1d0 ! m2/s
TNU4 == 2*0.0d0 ! m4/s

! Harmonic/biharmonic, horizontal viscosity coefficient: [Ngrids].

VISC2 == 0.1d0 ! m2/s
VISC4 == 0.0d0 ! m4/s

! Vertical mixing coefficients for active tracers: [1:NAT+NPT,Ngrids]

AKT_BAK == 1.0d-6 1.0d-6 ! m2/s

! Vertical mixing coefficient for momentum: [Ngrids].

AKV_BAK == 1.0d-5 ! m2/s

! Turbulent closure parameters.

AKK_BAK == 5.0d-6 ! m2/s
AKP_BAK == 5.0d-6 ! m2/s
TKENU2 == 0.0d0 ! m2/s
TKENU4 == 0.0d0 ! m4/s

! Generic length-scale turbulence closure parameters.

GLS_P == 3.0d0 ! K-epsilon
GLS_M == 1.5d0
GLS_N == -1.0d0
GLS_Kmin == 7.6d-6
GLS_Pmin == 1.0d-12

GLS_CMU0 == 0.5477d0
GLS_C1 == 1.44d0
GLS_C2 == 1.92d0
GLS_C3M == -0.4d0
GLS_C3P == 1.0d0
GLS_SIGK == 1.0d0
GLS_SIGP == 1.30d0

```
!   GLS_P == -1.0d0           ! k-omega
!   GLS_M == 0.5d0
!   GLS_N == -1.0d0
!   GLS_Kmin == 7.6d-6
!   GLS_Pmin == 1.0d-12
```

```
!   GLS_CMU0 == 0.5477d0
!   GLS_C1 == 0.555d0
!   GLS_C2 == 0.833d0
!   GLS_C3M == -0.6d0
!   GLS_C3P == 1.0d0
!   GLS_SIGK == 2.0d0
!   GLS_SIGP == 2.0d0
```

! Constants used in surface turbulent kinetic energy flux computation.

```
CHARNOK_ALPHA == 1400.0d0    ! Charnok surface roughness
ZOS_HSIG_ALPHA == 0.5d0      ! roughness from wave amplitude
SZ_ALPHA == 0.25d0          ! roughness from wave dissipation
CRGBAN_CW == 100.0d0        ! Craig and Banner wave breaking
```

! Constants used in momentum stress computation.

```
RDRG == 3.0d-04             ! m/s
RDRG2 == 3.0d-03            ! nondimensional
Zob == 5.0d-05              ! m
Zos == 5.0d-03              ! m
```

! Height (m) of atmospheric measurements for Bulk fluxes parameterization.

```
BLK_ZQ == 10.0d0           ! air humidity
BLK_ZT == 10.0d0           ! air temperature
BLK_ZW == 10.0d0           ! winds
```

! Minimum depth for wetting and drying.

```
DCRIT == 0.10d0            ! m
```

! Various parameters.

```
WTYPE == 1
LEVSFRC == 15
LEVBFRC == 1
```

! Vertical S-coordinates parameters, [1:Ngrids].

```
THETA_S == 3.0d0          ! 0 < THETA_S < 20
THETA_B == 1.0d0          ! 0 < THETA_B < 1
TCLINE == 2.0d0           ! m
```

! Mean Density and Brunt-Vaisala frequency.

```
RHO0 = 1028.0d0          ! kg/m3
BVF_BAK = 1.0d-5         ! 1/s2
```

! Time-stamp assigned for model initialization, reference time
! origin for tidal forcing, and model reference time for output
! NetCDF units attribute.

```
DSTART = 14101.0d0       ! days
TIDE_START = 0.0d0       ! days
TIME_REF = -2.0d0        ! yyymmdd.dd
```

! Nudging/relaxation time scales, inverse scales will be computed
! internally, [1:Ngrids].

```
TNUDG == 0.125d0        ! days
ZNUDG == 0.001d0        ! days
M2NUDG == 0.001d0       ! days
M3NUDG == 0.001d0       ! days
```

! Factor between passive (outflow) and active (inflow) open boundary
! conditions, [1:Ngrids]. If OBCFAC > 1, nudging on inflow is stronger
! than on outflow (recommended).

```
OBCFAC == 0.0d0         ! nondimensional
```

! Linear equation of State parameters:

```
R0 == 1027.0d0          ! kg/m3
T0 == 10.0d0            ! Celsius
S0 == 30.0d0            ! PSU
TCOEF == 1.7d-4         ! 1/Celsius
SCOEF == 7.6d-4         ! 1/PSU
```

! Slipperiness parameter: 1.0 (free slip) or -1.0 (no slip)

```
GAMMA2 == 1.0d0
```

! Starting (DstrS) and ending (DendS) day for adjoint sensitivity forcing.
! DstrS must be less or equal to DendS. If both values are zero, their
! values are reset internally to the full range of the adjoint integration.

DstrS == 0.0d0 ! starting day
DendS == 0.0d0 ! ending day

! Starting and ending vertical levels of the 3D adjoint state variables
! whose sensitivity is required.

KstrS == 1 ! starting level
KendS == 1 ! ending level

! Logical switches (TRUE/FALSE) to specify the adjoint state variables
! whose sensitivity is required.

Lstate(isFsur) == F ! free-surface
Lstate(isUbar) == F ! 2D U-momentum
Lstate(isVbar) == F ! 2D V-momentum
Lstate(isUvel) == F ! 3D U-momentum
Lstate(isVvel) == F ! 3D V-momentum

! Logical switches (TRUE/FALSE) to specify the adjoint state tracer
! variables whose sensitivity is required (NT values are expected).

Lstate(isTvar) == F F ! tracers

! Stochastic optimals time decorrelation scale (days) assumed for
! red noise processes.

SO_decay == 2.0d0 ! days

! Logical switches (TRUE/FALSE) to specify the state surface forcing
! variable whose stochastic optimals is required.

SOstate(isUstr) == T ! surface u-stress
SOstate(isVstr) == T ! surface v-stress

! Logical switches (TRUE/FALSE) to specify the surface tracer forcing
! variable whose stochastic optimals is required (NT values are expected).

SOstate(isTsur) == F F ! surface tracer flux

! Stochastic optimals surface forcing standard deviation for
! dimensionalization.

```

SO_sdev(isUstr) == 1.0d0      ! surface u-stress
SO_sdev(isVstr) == 1.0d0      ! surface v-stress
SO_sdev(isTsur) == 1.0d0 1.0d0 ! NT surface tracer flux

! Logical switches (TRUE/FALSE) to activate writing of fields into
! HISTORY output file.

Hout(idUvel) == T             ! 3D U-velocity
Hout(idVvel) == T             ! 3D V-velocity
Hout(idWvel) == T             ! 3D W-velocity
Hout(idOvel) == F             ! omega vertical velocity
Hout(idUbar) == T             ! 2D U-velocity
Hout(idVbar) == T             ! 2D V-velocity
Hout(idFsur) == T             ! free-surface
Hout(idBath) == F             ! time-dependent bathymetry

Hout(idTvar) == F T           ! temperature and salinity

Hout(idUsms) == F             ! surface U-stress
Hout(idVsms) == F             ! surface V-stress
Hout(idUbms) == T             ! bottom U-stress
Hout(idVbms) == T             ! bottom V-stress

Hout(idUbrs) == F             ! bottom U-current stress
Hout(idVbrs) == F             ! bottom V-current stress
Hout(idUbws) == F             ! bottom U-wave stress
Hout(idVbws) == F             ! bottom V-wave stress
Hout(idUbc) == F              ! bottom max wave-current U-stress
Hout(idVbc) == F              ! bottom max wave-current V-stress

Hout(idUbot) == F             ! bed wave orbital U-velocity
Hout(idVbot) == F             ! bed wave orbital V-velocity
Hout(idUbur) == F             ! bottom U-velocity above bed
Hout(idVbvr) == F             ! bottom V-velocity above bed

Hout(idW2xx) == F             ! 2D radiation stress, Sxx component
Hout(idW2xy) == F             ! 2D radiation stress, Sxy component
Hout(idW2yy) == F             ! 2D radiation stress, Syy component
Hout(idU2rs) == F             ! 2D radiation U-stress
Hout(idV2rs) == F             ! 2D radiation V-stress
Hout(idU2Sd) == F             ! 2D U-Stokes velocity
Hout(idV2Sd) == F             ! 2D V-Stokes velocity

Hout(idW3xx) == F             ! 3D radiation stress, Sxx component

```

Hout(idW3xy) == F ! 3D radiation stress, Sxy component
 Hout(idW3yy) == F ! 3D radiation stress, Syy component
 Hout(idW3zx) == F ! 3D radiation stress, Szx component
 Hout(idW3zy) == F ! 3D radiation stress, Szy component
 Hout(idU3rs) == F ! 3D U-radiation stress
 Hout(idV3rs) == F ! 3D V-radiation stress
 Hout(idU3Sd) == F ! 3D U-Stokes velocity
 Hout(idV3Sd) == F ! 3D V-Stokes velocity

Hout(idWamp) == F ! wave height
 Hout(idWlen) == F ! wave length
 Hout(idWdir) == F ! wave direction

Hout(idTsur) == F F ! surface net heat and salt flux
 Hout(idLhea) == F ! latent heat flux
 Hout(idShea) == F ! sensible heat flux
 Hout(idLrad) == F ! longwave radiation flux
 Hout(idSrad) == F ! shortwave radiation flux
 Hout(idevap) == F ! evaporation rate
 Hout(idrain) == F ! precipitation rate

Hout(idDano) == T ! density anomaly
 Hout(idVvis) == F ! vertical viscosity
 Hout(idTdif) == F ! vertical T-diffusion
 Hout(idSdif) == F ! vertical Salinity diffusion
 Hout(idHsbl) == F ! depth of surface boundary layer
 Hout(idHbbl) == F ! depth of bottom boundary layer
 Hout(idMtke) == T ! turbulent kinetic energy
 Hout(idMtls) == T ! turbulent length scale

! Logical switches (TRUE/FALSE) to activate writing of extra inert passive
 ! tracers other than biological and sediment tracers. An inert passive tracer
 ! is one that it is only advected and diffused. Other processes are ignored.
 ! These tracers include, for example, dyes, pollutants, oil spills, etc.
 ! NPT values are expected. However, these switches can be activated using
 ! compact parameter specification.

Hout(inert) == T ! inert passive tracers

! Logical switches (TRUE/FALSE) to activate writing of exposed sediment
 ! layer properties into HISTORY output file. Currently, MBOTP properties
 ! are expected for the bottom boundary layer and/or sediment models:

!
 ! Hout(idBott(isd50)), isd50 = 1 ! mean grain diameter
 ! Hout(idBott(idens)), idens = 2 ! mean grain density

```

! Hout(idBott(iwsed)), iwsed = 3      ! mean settling velocity
! Hout(idBott(itauc)), itauc = 4     ! critical erosion stress
! Hout(idBott(irlen)), irlen = 5     ! ripple length
! Hout(idBott(irhgt)), irhgt = 6     ! ripple height
! Hout(idBott(ibwav)), ibwav = 7     ! wave excursion amplitude
! Hout(idBott(izdef)), izdef = 8     ! default bottom roughness
! Hout(idBott(izapp)), izapp = 9     ! apparent bottom roughness
! Hout(idBott(izNik)), izNik = 10    ! Nikuradse bottom roughness
! Hout(idBott(izbio)), izbio = 11    ! biological bottom roughness
! Hout(idBott(izbfm)), izbfm = 12   ! bed form bottom roughness
! Hout(idBott(izbld)), izbld = 13    ! bed load bottom roughness
! Hout(idBott(izwbl)), izwbl = 14   ! wave bottom roughness
! Hout(idBott(iactv)), iactv = 15    ! active layer thickness
! Hout(idBott(ishgt)), ishgt = 16   ! saltation height
! Hout(idBott(idflux)), idflux = 17  ! erosion flux
! Hout(idBott(idnet)), idnet = 18    ! erosion or deposition
! Hout(idBott(idoff)), idoff = 19    ! tau critical offset
! Hout(idBott(idslp)), idslp = 20    ! tau critical slope
! Hout(idBott(idtim)), idtim = 21    ! erodibility time scale
! Hout(idBott(idbmx)), idbmx = 22    ! diffusivity db_max
! Hout(idBott(idbmm)), idbmm = 23    ! diffusivity db_m
! Hout(idBott(idbzs)), idbzs = 24    ! diffusivity db_zs
! Hout(idBott(idbzm)), idbzm = 25    ! diffusivity db_zm
! Hout(idBott(idbzp)), idbzp = 26    ! diffusivity db_zphi

```

```

!           1 1 1 1 1 1 1 1 1 2 2 2 2 2 2
!         1 2 3 4 5 6 7 8 9 0 1 2 3 4 5 6 7 8 9 0 1 2 3 4 5 6

```

```

Hout(idBott) == F F F F F F F F F F F F F T F T T F F F F F F F F

```

```

! Generic User parameters, [1:NUSER].
! Mean Amplitude, Spring-Neap Range, Pamunky, Mattaponi
  NUSER = 4
  USER = 0.3d0 0.1d0 42.0d0 25.0d0

```

```

! Input NetCDF file names, [1:Ngrids].

```

```

  GRDNAME == Data/Grid/grd_yorkmud.nc
  INiname == Data/Initial/ini_yorkmud_6seds4c.nc
  ITLNAME == ocean_itl.nc
  IRPNAME == ocean_irp.nc
  IADNAME == ocean_iad.nc
  CLMNAME == ocean_clm.nc

```



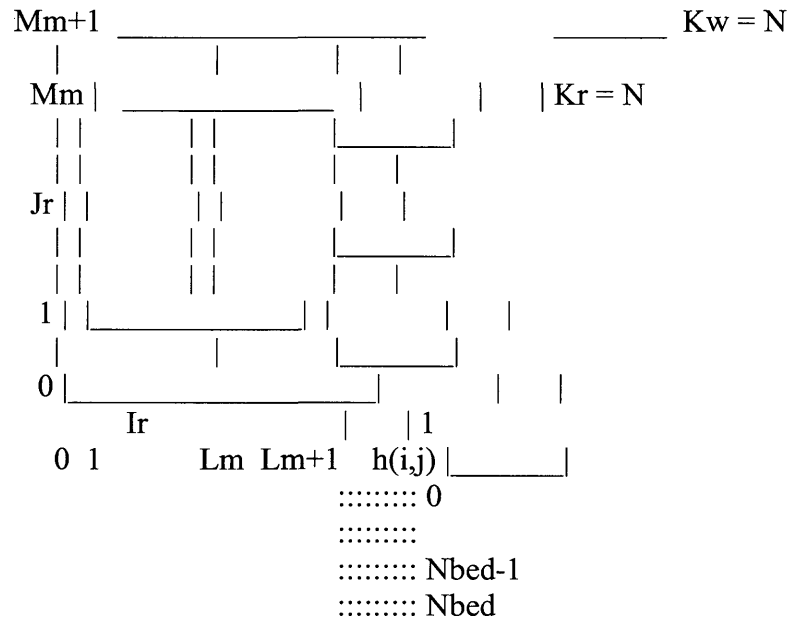
```

!
! GLOSSARY:
! =====
!
!-----
! Application tile (string with a maximum of eighty characters) and
! C-preprocessing flag.
!-----
!
! TITLE    Application title.
!
! MyAppCPP  Application C-preproceession option.
!
!-----
! Variable information file name (string with a maximum of eighty characters).
!-----
!
! VARNAME   Input/Output variable information file name. This file need to
!           be processed first so all information arrays and indices can be
!           initialized properly in "mod_ncparam.F".
!
!-----
! Grid dimension parameters.
!-----
!
! These parameters are very important since it determine the grid of the
! application to solve. They need to be read first in order to dynamically
! allocate all model variables.
!
! WARNING: It is trivial and posible to change these dimension parameters in
! ----- idealized applications via analytical expressions. However, in
! realistic applications any change to these parameters requires redoing all
! input NetCDF files.
!
! Lm        Number of INTERIOR grid RHO-points in the XI-direction for
!           each nested grid, [1:Ngrids]. If using NetCDF files as
!           input, Lm=xi_rho-2 where "xi_rho" is the NetCDF file
!           dimension of RHO-points. Recall that all RHO-point
!           variables have a computational I-range of [0:Lm+1].
!
! Mm        Number of INTERIOR grid RHO-points in the ETA-direction for
!           each nested grid, [1:Ngrids]. If using NetCDF files as
!           input, Mm=eta_rho-2 where "eta_rho" is the NetCDF file
!           dimension of RHO-points. Recall that all RHO-point
!           variables have a computational J-range of [0:Mm+1].

```

! N Number of vertical terrain-following levels at RHO-points, [1:Ngrids].

! Nbed Number of sediment bed layers, [1:Ngrids]. This parameter is only relevant if CPP option SEDIMENT is activated.



! NAT Number of active tracer type variables. Usually, NAT=2 for potential temperature and salinity.

! NPT Number of inert (dyes, age, etc) passive tracer type variables to advect and diffuse only. This parameter is only relevant if CPP option T_PASSIVE is activated.

! NCS Number of cohesive (mud) sediment tracer type variables. This parameter is only relevant if CPP option SEDIMENT is activated.

! NNS Number of non-cohesive (sand) sediment tracer type variables. This parameter is only relevant if CPP option SEDIMENT is activated.

The total of sediment tracers is $NST=NCS+NNS$. Notice that NST must be greater than zero ($NST>0$).

! Domain tile partition parameters.

```

!-----
!
! Model tile decomposition parameters for serial and parallel configurations
! which are used to determine tile horizontal range indices (Istr,Iend) and
! (Jstr,Jend). In some computers, it is advantageous to have tile partitions
! in serial applications.
!
! NtileI    Number of domain partitions in the I-direction (XI-coordinate).
!           It must be equal or greater than one.
!
! NtileJ    Number of domain partitions in the J-direction (ETA-coordinate).
!           It must be equal or greater than one.
!
! WARNING:  In shared-memory (OpenMP), the product of NtileI and NtileJ must
!           be a MULTIPLE of the number of parallel threads specified with
!           the OpenMP environmental variable OMP_NUM_THREADS.
!
!           In distributed-memory (MPI), the product of NtileI and NtileJ
!           must be EQUAL to the number of parallel nodes specified during
!           execution with the "mprun" or "mpirun" command.
!-----
! Time-Stepping parameters.
!-----
!
! NTIMES    Total number time-steps in current run.  If 3D configuration,
!           NTIMES is the total of baroclinic time-steps.  If only 2D
!           configuration, NTIMES is the total of barotropic time-steps.
!
! DT        Time-Step size in seconds.  If 3D configuration, DT is the
!           size of baroclinic time-step.  If only 2D configuration, DT
!           is the size of the barotropic time-step.
!
! NDTFAST   Number of barotropic time-steps between each baroclinic time
!           step.  If only 2D configuration, NDTFAST should be unity since
!           there is not need to splitting time-stepping.
!-----
! Model iteration loops parameters.
!-----
!
! ERstr     Starting ensemble run (perturbation or iteration) number.
!
! ERend     Ending  ensemble run (perturbation or iteration) number.
!

```

```

! Nouter   Maximum number of 4DVAR outer loop iterations.
!
! Ninner   Maximum number of 4DVAR inner loop iterations.
!
! Nintervals Number of time interval divisions for stochastic optimal
!           computations. It must be a multiple of NTIMES. The tangent
!           linear model (TLM) and the adjoint model (ADM) are integrated
!           forward and backward in different intervals. For example,
!           if Nintervals=3,
!
!           1           NTIMES/3       2*NTIMES/3       NTIMES
!           +.....+.....+.....+
!
! <===== (1)
!           <===== (2)
!                   <===== (3)
!
!           In the first iteration (1), the TLM is integrated forward from
!           1 to NTIMES and the ADM is integrated backward from NTIMES to 1.
!           In the second iteration (2), the TLM is integrated forward from
!           NTIMES/3 to NTIMES and the ADM is integrated backward from
!           NTIMES to NTIMES/3. And so on.
!
!-----
! Eigenproblem parameters.
!-----
!
! NEV      Number of eigenvalues to compute for the Lanczos/Arnoldi
!           problem. Notice that the model memory requirement increases
!           substantially as NEV increases. The GST requires NEV+1
!           copies of the model state vector. The memory requirements
!           are decreased in distributed-memory applications.
!
! NCV      Number of eigenvectors to compute for the Lanczos/Arnoldi
!           problem. NCV must be greater than NEV.
!
! At present, there is no a-priori analysis to guide the selection of NCV
! relative to NEV. The only formal requirement is that NCV > NEV. However
! in optimal perturbations, it is recommended to have NCV greater than or
! equal to 2*NEV. In Finite Time Eigenmodes (FTE) and Adjoint Finite Time
! Eigenmodes (AFTE) the requirement is to have NCV greater than or equal to
! 2*NEV+1.
!
! The efficiency of calculations depends critically on the combination of
! NEV and NCV. If NEV is large (greater than 10 say), you can use NCV=2*NEV+1

```

! but for NEV small (less than 6) it will be inefficient to use $NCV=2*NEV+1$.
! In complicated applications, you can start with $NEV=2$ and $NCV=10$. Otherwise,
! it will iterate for very long time.

!

! Input/Output parameters.

!

! NRREC Switch to indicate re-start from a previous solution. Use
! NRREC=0 for new solutions. In a re-start solution, NRREC
! is the time index of the re-start NetCDF file assigned for
! initialization. If NRREC is negative (said NRREC=-1), the
! model will re-start from the most recent time record. That
! is, the initialization record is assigned internally.
! Notice that it is also possible to re-start from a history
! or time-averaged NetCDF files. If a history file is used
! for re-start, it must contains all the necessary primitive
! variables at all levels.

!

! LcycleRST Logical switch (T/F) used to recycle time records in output
! re-start file. If TRUE, only the latest two re-start time
! records are maintained. If FALSE, all re-start fields are
! saved every NRST time-steps without recycling. The re-start
! fields are written at all levels in double precision.

!

! NRST Number of time-steps between writing of re-start fields.

!

! NSTA Number of time-steps between writing data into stations file.
! Station data is written at all levels.

!

! NFLT Number of time-steps between writing data into floats file.

!

! NINFO Number of time-steps between print of single line information
! to standard output. If also determines the interval between
! computation of global energy diagnostics.

!

! Output history and average files parameters.

!

! LDEFOUT Logical switch (T/F) used to create new output files when
! initializing from a re-start file, $abs(NRREC) > 0$. If TRUE
! and applicable, a new history, average, diagnostic and
! station files are created during the initialization stage.
! If FALSE and applicable, data is appended to an existing

! history, average, diagnostic and station files. See also
! parameters NDEFHIS, NDEFAVG and NDEFDIA below.
!
! NHIS Number of time-steps between writing fields into history file.
!
! NDEFHIS Number of time-steps between the creation of new history file.
! If NDEFHIS=0, the model will only process one history file.
! This feature is useful for long simulations when history files
! get too large; it creates a new file every NDEFHIS time-steps.
!
! NTSAVG Starting time-step for the accumulation of output time-averaged
! data.
!
! NAVG Number of time-steps between writing time-averaged data
! into averages file. Averaged data is written for all fields.
!
! NDEFAVG Number of time-steps between the creation of new average
! file. If NDEFAVG=0, the model will only process one average
! file. This feature is useful for long simulations when
! average files get too large; it creates a new file every
! NDEFAVG time-steps.
!
! NTSDIA Starting time-step for the accumulation of output time-averaged
! diagnostics data.
!
! NDIA Number of time-steps between writing time-averaged diagnostics
! data into diagnostics file. Averaged data is written for all
! fields.
!
! NDEFDIA Number of time-steps between the creation of new time-averaged
! diagnostics file. If NDEFDIA=0, the model will only process one
! diagnostics file. This feature is useful for long simulations
! when diagnostics files get too large; it creates a new file
! every NDEFDIA time-steps.
!
!-----
! Output tangent linear and adjoint model parameters.
!-----
!
! LcycleTLM Logical switch (T/F) used to recycle time records in output
! tangent linear file. If TRUE, only the latest two time
! records are maintained. If FALSE, all tangent linear fields
! are saved every NTLM time-steps without recycling.
!
! NTLM Number of time-steps between writing fields into tangent linear

! model file.
!
! NDEFTLM Number of time-steps between the creation of new tangent linear
! file. If NDEFTLM=0, the model will only process one tangent
! linear file. This feature is useful for long simulations when
! output NetCDF files get too large; it creates a new file every
! NDEFTLM time-steps.
!
! LcycleADJ Logical switch (T/F) used to recycle time records in output
! adjoint file. If TRUE, only the latest two time records are
! maintained. If FALSE, all tangent linear fields re saved
! every NADJ time-steps without recycling.
!
! NADJ Number of time-steps between writing fields into adjoint model
! file.
!
! NDEFADJ Number of time-steps between the creation of new adjoint file.
! If NDEFADJ=0, the model will only process one adjoint file.
! This feature is useful for long simulations when output NetCDF
! files get too large; it creates a new file every NDEFADJ
! time-steps.
!
!-----
! Generalized Stability Theory (GST) analysis parameters.
!-----
!
! LrstGST Logical switch (TRUE/FALSE) to restart GST analysis. If TRUE,
! the check pointing data is read in from the GST restart NetCDF
! file. If FALSE and applicable, the check pointing GST data is
! saved and overwritten every NGST iterations of the algorithm.
!
! MaxIterGST Maximum number of GST algorithm iterations.
!
! NGST Number of GST iterations between storing of check pointing
! data into NetCDF file. The restart data is always saved if
! MaxIterGST is reached without convergence. It is also saved
! when convergence is achieved. It is always a good idea to
! save the check pointing data at regular intervals so there
! is a mechanism to recover from an unexpected interruption
! in this very expensive computation. The check pointing data
! can be used also to recompute the Ritz vectors by changing
! some of the parameters, like convergence criteria (Ritz_tol)
! and number of Arnoldi iterations (iparam(3)).
!
! Ritz_tol Relative accuracy of the Ritz values computed in the GST

! analysis.

!-----

! Harmonic/Biharmonic horizontal diffusion for active tracers.

!-----

! TNU2 Lateral, harmonic, constant, mixing coefficient (m2/s) for
! active (NAT) and inert (NPT) tracer variables. If variable
! horizontal diffusion is activated, TNU2 is the mixing
! coefficient for the largest grid-cell in the domain.

! TNU4 Lateral, biharmonic, constant, mixing coefficient (m4/s) for
! active (NAT) and inert (NPT) tracer variables. If variable
! horizontal diffusion is activated, TNU4 is the mixing
! coefficient for the largest grid-cell in the domain.

!-----

! Harmonic/biharmonic horizontal viscosity coefficients.

!-----

! VISC2 Lateral, harmonic, constant, mixing coefficient (m2/s) for
! momentum. If variable horizontal viscosity is activated, UVNU2
! is the mixing coefficient for the largest grid-cell in the
! domain.

! VISC4 Lateral, biharmonic, constant mixing coefficient (m4/s) for
! momentum. If variable horizontal viscosity is activated, UVNU4
! is the mixing coefficient for the largest grid-cell in the
! domain.

!-----

! Vertical mixing coefficients for active tracers.

!-----

! AKT_BAK Background vertical mixing coefficient (m2/s) for active
! (NAT) and inert (NPT) tracer variables.

!-----

! Vertical mixing coefficient for momentum.

!-----

! AKV_BAK Background vertical mixing coefficient (m2/s) for momentum.

!-----

! Turbulent closure parameters.

```

!-----
!
! AKK_BAK   Background vertical mixing coefficient (m2/s) for turbulent
!           kinetic energy.
!
! AKP_BAK   Background vertical mixing coefficient (m2/s) for turbulent
!           generic statistical field, "psi".
!
! TKENU2    Lateral, harmonic, constant, mixing coefficient (m2/s) for
!           turbulent closure variables.
!
! TKENU4    Lateral, biharmonic, constant mixing coefficient (m4/s) for
!           turbulent closure variables.
!
!-----
! Generic length-scale turbulence closure parameters.
!-----
!
! GLS_P     Stability exponent (non-dimensional).
!
! GLS_M     Turbulent kinetic energy exponent (non-dimensional).
!
! GLS_N     Turbulent length scale exponent (non-dimensional).
!
! GLS_Kmin  Minimum value of specific turbulent kinetic energy
!
! GLS_Pmin  Minimum Value of dissipation.
!
! Closure independent constraint parameters (non-dimensional):
!
! GLS_CMU0  Stability coefficient.
!
! GLS_C1    Shear production coefficient.
!
! GLS_C2    Dissipation coefficient.
!
! GLS_C3M   Buoyancy production coefficient (minus).
!
! GLS_C3P   Buoyancy production coefficient (plus).
!
! GLS_SIGK  Constant Schmidt number (non-dimensional) for turbulent
!           kinetic energy diffusivity.
!
! GLS_SIGP  Constant Schmidt number (non-dimensional) for turbulent
!           generic statistical field, "psi".

```

```

!
! Suggested values for various parameterizations:
!
!      k-kl      k-epsilon  k-omega      gen
!
!      GLS_P = 0.d0      3.0d0      -1.0d0      2.0d0
!      GLS_M = 1.d0      1.5d0      0.5d0      1.0d0
!      GLS_N = 1.d0      -1.0d0      -1.0d0      -0.67d0
!      GLS_Kmin = 5.0d-6      7.6d-6      7.6d-6      1.0d-8
!      GLS_Pmin = 5.0d-6      1.0d-12      1.0d-12      1.0d-8
!
!      GLS_CMU0 = 0.5544d0      0.5477d0      0.5477d0      0.5544d0
!      GLS_C1 = 0.9d0      1.44d0      0.555d0      1.00d0
!      GLS_C2 = 0.52d0      1.92d0      0.833d0      1.22d0
!      GLS_C3M = 2.5d0      -0.4d0      -0.6d0      0.1d0
!      GLS_C3P = 1.0d0      1.0d0      1.0d0      1.0d0
!      GLS_SIGK = 1.96d0      1.0d0      2.0d0      0.8d0
!      GLS_SIGP = 1.96d0      1.30d0      2.0d0      1.07d0
!

```

```

-----
! Constants used in the various formulation of surface turbulent kinetic
! energy flux in the GLS.

```

```

-----
! CHARNOK_ALPHA  Charnok surface roughness,
!               Zos: (charnok_alpha * u_star**2) / g
!
! ZOS_HSIG_ALPHA  Roughness from wave amplitude,
!               Zos: zos_hsig_alpha * Hsig
!
! SZ_ALPHA       Surface flux from wave dissipation,
!               flux: dt * sz_alpha * Wave_dissip
!
! CRGBAN_CW      Surface flux due to Craig and Banner wave breaking,
!               flux: dt * crgban_cw * u_star**3
!

```

```

-----
! Constants used in the computation of momentum stress.

```

```

! RDRG          Linear bottom drag coefficient (m/s).
!
! RDRG2         Quadratic bottom drag coefficient.
!
! Zob           Bottom roughness (m).

```

! Zos Surface roughness (m).
!-----
! Height of atmospheric measurements for bulk fluxes parameterization.
!-----
! BLK_ZQ Height (m) of surface air humidity measurement. Usually,
! recorded at 10 m.
! BLK_ZT Height (m) of surface air temperature measurement. Usually,
! recorded at 2 or 10 m.
! BLK_ZW Height (m) of surface winds measurement. Usually, recorded
! at 10 m.
!-----
! Wetting and drying parameters.
!-----
! DCRIT Minimum depth (m) for wetting and drying.
!-----
! Jerlov Water type.
!-----
! WTYPE Jerlov water type: an integer value from 1 to 5.
!-----
! Body-force parameters. Used when CPP option BODYFORCE is activated.
!-----
! LEVSFRC Deepest level to apply surface momentum stress as a body-force.
! LEVBFRC Shallowest level to apply bottom momentum stress as a body-force.
!-----
! Vertical S-coordinates parameters.
!-----
! THETA_S S-coordinate surface control parameter, $[0 < \theta_s < 20]$.
! THETA_B S-coordinate bottom control parameter, $[0 < \theta_b < 1]$.
! TCLINE Width (m) of surface or bottom boundary layer in which

! higher vertical resolution is required during stretching.
!

! WARNING: Users need to experiment with these parameters. We
! have found out that the model goes unstable with
! high values of THETA_S. In steep and very tall
! topography, it is recommended to use THETA_S < 3.0.
!
!-----
! Mean Density and background Brunt-Vaisala frequency.
!-----
!
! RHO0 Mean density (Kg/m3) used when the Boussinesq approximation
! is inferred.
!
! BVF_BAK Background Brunt-Vaisala frequency squared (1/s2). Typical
! values for the ocean range (as a function of depth) from
! 1.0E-4 to 1.0E-6.
!
!-----
! Time Stamps.
!-----
!
! DSTART Time stamp assigned to model initialization (days). Usually
! a Calendar linear coordinate, like modified Julian Day. For
! Example:
!
! Julian Day = 1 for Nov 25, 0:0:0 4713 BCE
! modified Julian Day = 1 for May 24, 0:0:0 1968 CE GMT
!
! It is called truncated or modified Julian day because an offset
! of 2440000 needs to be added.
!
! TIDE_START Reference time origin for tidal forcing (days). This is the
! time used when processing input tidal model data. It is needed
! in routine "set_tides" to compute the correct phase lag with
! respect ROMS/TOMS initialization time.
!
! TIME_REF Reference time (yyyymmdd.f) used to compute relative time:
! elapsed time interval since reference-time. The "units"
! attribute takes the form "time-unit since reference-time".
! This parameter also provides information about the calendar
! used:
!
! If TIME_REF = -2, model time and DSTART are in modified Julian
! days units. The "units" attribute is:

```

!
!           'time-units since 1968-05-23 00:00:00 GMT'
!
!           If TIME_REF = -1, model time and DSTART are in a calendar
!           with 360 days in every year (30 days each month). The "units"
!           attribute is:
!
!           'time-units since 0000-01-01 00:00:00'
!
!           If TIME_REF = 0, model time and DSTART are in a common year
!           calendar with 365.25 days. The "units" attribute is:
!
!           'time-units since 0000-01-01 00:00:00'
!
!           If TIME_REF > 0, model time and DSTART are the elapsed time
!           units since specified reference time. For example,
!           TIME_REF=20020115.5 will yield the following attribute:
!
!           'time-units since 2002-01-15 12:00:00'
!
!-----
! Nudging/relaxation time scales, inverse scales will be computed internally.
!-----
!
! When passive/active open boundary conditions are activated, these nudging
! values correspond to the passive (outflow) nudging time scales.
!
! TNUDGD   Nudging time scale (days) for active tracer variables.
!           (1:NAT+NPT,1:Ngrids) values are expected.
!
! ZNUDGD   Nudging time scale (days) for free-surface.
!
! M2NUDGD  Nudging time scale (days) for 2D momentum.
!
! M3NUDGD  Nudging time scale (days) for 3D momentum.
!
! OBCFAC   Factor between passive (outflow) and active (inflow) open
!           boundary conditions. The nudging time scales for the
!           active (inflow) conditions are obtained by multiplying
!           the passive values by OBCFAC. If OBCFAC > 1, nudging on
!           inflow is stronger than on outflow (recommended).
!
!-----
! Linear equation of State parameters.
!-----

```

! Ignoring pressure, the linear equation of state is:

$$\rho(:,:,) = R0 - R0 * TCOEF * (t(:,:,:),itmp) - T0) + R0 * SCOEF * (t(:,:,:),isalt) - S0)$$

! Typical values: R0 = 1027.0 kg/m3
T0 = 10.0 Celsius
S0 = 35.0 PSU
TCOEF = 1.7d-4 1/Celsius
SCOEF = 7.6d-4 1/PSU

! R0 Background density value (Kg/m3) used in Linear Equation of State.

! T0 Background potential temperature (Celsius) constant.

! S0 Background salinity (PSU) constant.

! TCOEF Thermal expansion coefficient in Linear Equation of State.

! SCOEF Saline contraction coefficient in Linear Equation of State.

!-----
! Slipperiness parameter.
!-----

! GAMMA2 Slipperiness variable, either 1.0 (free slip) or -1.0 (no slip).

!-----
! Adjoint sensitivity parameters.
!-----

! DstrS Starting day for adjoint sensitivity forcing.

! DendS Ending day for adjoint sensitivity forcing.

! The adjoint forcing is applied at every time step according to desired state functional stored in the adjoint sensitivity NetCDF file. DstrS must be less or equal to DendS. If both values are zero, their values are reset internally to the full range of the adjoint integration.

! KstrS Starting vertical level of the 3D adjoint state variables whose sensitivity is required.

```

! KendsS   Ending vertical level of the 3D adjoint state variables whose
!           sensitivity is required.
!
! Lstate   Logical switches (TRUE/FALSE) to specify the adjoint state
!           variables whose sensitivity is required.
!
!           Lstate(isFsur): Free-surface
!           Lstate(isUbar): 2D U-momentum
!           Lstate(isVbar): 2D V-momentum
!           Lstate(isUvel): 3D U-momentum
!           Lstate(isVvel): 3D V-momentum
!           Lstate(isTvar): Traces (NT values expected)
!
!-----
! Stochastic optimals parameters.
!-----
!
! SO_decay Stochastic optimals time decorrelation scale (days) assumed
!           for red noise processes.
!
! SOstate  Logical switches (TRUE/FALSE) to specify the state surface
!           forcing variable whose stochastic optimals is required.
!
!           SOstate(isUstr): surface u-stress
!           SOstate(isVstr): surface v-stress
!           SOstate(isTsur): surface tracer flux (NT values expected)
!
! SO_sdev  Stochastic optimals surface forcing standard deviation for
!           dimensionalization.
!
!           SO_sdev(isUstr): surface u-stress
!           SO_sdev(isVstr): surface v-stress
!           SO_sdev(isTsur): surface tracer flux (NT values expected)
!
!-----
! Logical switches (T/F) to activate writing of fields into HISTORY file.
!-----
!
! Hout(idUvel) Write out 3D U-velocity component.
! Hout(idVvel) Write out 3D V-velocity component.
! Hout(idWvel) Write out 3D W-velocity component.
! Hout(idOvel) Write out 3D omega vertical velocity.
! Hout(idUbar) Write out 2D U-velocity component.
! Hout(idVbar) Write out 2D V-velocity component.
! Hout(idFsur) Write out free-surface.

```


! Hout(idBath) Write out time-dependent bathymetry.
 !
 ! Hout(idTvar) Write out active (NAT) tracers: temperature and salinity.
 !
 ! Hout(idUsms) Write out surface U-momentum stress.
 ! Hout(idVsms) Write out surface V-momentum stress.
 ! Hout(idUbms) Write out bottom U-momentum stress.
 ! Hout(idVbms) Write out bottom V-momentum stress.
 !
 ! Hout(idUbrs) Write out current-induced, U-momentum stress.
 ! Hout(idVbrs) Write out current-induced, V-momentum stress.
 ! Hout(idUbws) Write out wind-induced, bottom U-wave stress.
 ! Hout(idVbws) Write out wind-induced, bottom V-wave stress.
 ! Hout(idUbcS) Write out bottom maximum wave and current U-stress.
 ! Hout(idVbcS) Write out bottom maximum wave and current V-stress.
 !
 ! Hout(idUbot) Write out wind-induced, bed wave orbital U-velocity.
 ! Hout(idVbot) Write out wind-induced, bed wave orbital V-velocity.
 ! Hout(idUbur) Write out bottom U-velocity above bed.
 ! Hout(idVbvr) Write out bottom V-velocity above bed.
 !
 ! Hout(idW2xx) Write out 2D radiation stress, Sxx component.
 ! Hout(idW2xy) Write out 2D radiation stress, Sxy component.
 ! Hout(idW2yy) Write out 2D radiation stress, Syy component.
 ! Hout(idU2rs) Write out 2D U-radiation stress.
 ! Hout(idV2rs) Write out 2D V-radiation stress.
 ! Hout(idU2Sd) Write out 2D U-Stokes velocity.
 ! Hout(idV2Sd) Write out 2D V-Stokes velocity.
 !
 ! Hout(idW3xx) Write out 3D radiation stress, Sxx component.
 ! Hout(idW3xy) Write out 3D radiation stress, Sxy component.
 ! Hout(idW3yy) Write out 3D radiation stress, Syy component.
 ! Hout(idW3zx) Write out 3D radiation stress, Szx component.
 ! Hout(idW3zy) Write out 3D radiation stress, Szy component.
 ! Hout(idU3rs) Write out 3D U-radiation stress.
 ! Hout(idV3rs) Write out 3D V-radiation stress.
 ! Hout(idU3Sd) Write out 3D U-Stokes velocity.
 ! Hout(idV3Sd) Write out 3D V-Stokes velocity.
 !
 ! Hout(idWamp) Write out wave height.
 ! Hout(idWlen) Write out wave length.
 ! Hout(idWdir) Write out wave direction.
 !
 ! Hout(idTsur) Write out surface net heat and salt flux
 ! Hout(idLhea) Write out latent heat flux.

```

! Hout(idShea) Write out sensible heat flux.
! Hout(idLrad) Write out long-wave radiation flux.
! Hout(idSrad) Write out short-wave radiation flux.
! Hout(idevap) Write out evaporation rate.
! Hout(idrain) Write out precipitation rate.
!
! Hout(idDano) Write out density anomaly.
! Hout(idVvis) Write out vertical viscosity coefficient.
! Hout(idTdif) Write out vertical diffusion coefficient of temperature.
! Hout(idSdif) Write out vertical diffusion coefficient of salinity.
! Hout(idHsbl) Write out depth of oceanic surface boundary layer.
! Hout(idHbbl) Write out depth of oceanic bottom boundary layer.
! Hout(idMtke) Write out turbulent kinetic energy.
! Hout(idMtls) Write out turbulent kinetic energy times length scale.
!
! Hout(inert) Write out extra inert passive tracers.
!
! Hout(idBott) Write out exposed sediment layer properties, 1:MBOTP.
!
!-----
! Generic User parameters.
!-----
!
! NUSER    Number of User parameters to consider (integer).
! USER     Vector containing user parameters (real array). This array
!           is used with the SANITY_CHECK to test the correctness of
!           the tangent linear adjoint models. It contains information
!           of the model variable and grid point to perturb:
!
!           INT(user(1)): tangent state variable to perturb
!           INT(user(2)): adjoint state variable to perturb
!                   [isFsur=1] free-surface
!                   [isUbar=2] 2D U-momentum
!                   [isVbar=3] 2D V-momentum
!                   [isUvel=4] 3D U-momentum
!                   [isVvel=5] 3D V-momentum
!                   [isTvar=6] First tracer (temperature)
!                   [ ... ]
!                   [isTvar=?] Last tracer
!
!           INT(user(3)): I-index of tangent variable to perturb
!           INT(user(4)): I-index of adjoint variable to perturb
!           INT(user(5)): J-index of tangent variable to perturb
!           INT(user(6)): J-index of adjoint variable to perturb
!           INT(user(7)): K-index of tangent variable to perturb, if 3D

```

```

!           INT(user(8)): K-index of adjoint variable to perturb, if 3D
!
!           Set tangent and adjoint parameters to the same values
!           if perturbing and reporting the same variable.
!
!-----
! Input/output NetCDF file names (string with a maximum of eighty characters).
!-----
!
! GRDNAME   Input grid file name.
! ININAME   Input nonlinear initial conditions file name. It can be a
!           re-start file.
! IRPNAME   Input representer model initial conditions file name.
! ITLNAME   Input tangent linear model initial conditions file name.
! IADNAME   Input adjoint model initial conditions file name.
! FRCNAME   Input forcing fields file name.
! CLMNAME   Input climatology fields file name.
! BRYNAME   Input open boundary data file name.
! FWDNAME   Input forward solution fields file name.
! ADSNAME   Input adjoint sensitivity functional file name.
!
! GSTNAME   Output GST analysis re-start file name.
! RSTNAME   Output re-start file name.
! HISNAME   Output history file name.
! TLFNAME   Output impulse forcing for tangent linear (TLM and RPM) models.
! TLMNAME   Output tangent linear file name.
! ADJNAME   Output adjoint file name.
! AVGNAME   Output averages file name.

```

! DIANAME Output diagnostics file name.
! STANAME Output stations file name.
! FLTNAME Output floats file name.
!
!-----
! Input ASCII parameters file names.
!-----
!
! APARNAM Input assimilation parameters file name.
! SPOSNAM Input stations positions file name.
! FPOSNAM Input initial drifters positions file name.
! BPARNAM Input biological parameters file name.
! SPARNAM Input sediment transport parameters file name.
! USRNAME USER's input generic file name

sediment_york_mud_jun28.in

!
! ROMS/TOMS Cohesive and Non-cohesive Sediment Model Parameters.
!
!svn \$Id: sediment_york_mud.in 1499 2008-04-29 21:18:51Z jprinehimer \$
!===== Hernan

G. Arango ===
! Copyright (c) 2002-2007 The ROMS/TOMS Group !
! Licensed under a MIT/X style license !
! See License_ROMS.txt !
!=====

!
! Input parameters can be entered in ANY order, provided that the parameter !
! KEYWORD (usually, upper case) is typed correctly followed by "=" or "==" !
! symbols. Any comment lines are allowed and must begin with an exclamation !
! mark (!) in column one. Comments may appear to the right of a parameter !
! specification to improve documentation. All comments will ignored during !
! reading. Blank lines are also allowed and ignored. Continuation lines in !
! a parameter specification are allowed and must be preceded by a backslash !
! (\). In some instances, more than one value is required for a parameter. !
! If fewer values are provided, the last value is assigned for the entire !
! parameter array. The multiplication symbol (*), without blank spaces in !
! between, is allowed for a parameter specification. For example, in a two !
! grids nested application: !

!
! AKT_BAK == 2*1.0d-6 2*5.0d-6 ! m2/s !
!
! indicates that the first two entries of array AKT_BAK, in fortran column- !
! major order, will have the same value of "1.0d-6" for grid 1, whereas the !
! next two entries will have the same value of "5.0d-6" for grid 2. !
!

! In multiple levels of nesting and/or multiple connected domains step-ups, !
! "Ngrids" entries are expected for some of these parameters. In such case, !
! the order of the entries for a parameter is extremely important. It must !
! follow the same order (1:Ngrids) as in the state variable declaration. The !
! USER may follow the above guidelines for specifying his/her values. These !
! parameters are marked by "==" plural symbol after the KEYWORD. !

!
!=====

!
!-----
! Sediment model control switch.

```

!-----
! Switch is used to control sediment model computation within nested and/or
! multiple connected grids, [1:Ngrids].

  Lsediment == T

!-----
! General sediment bed model controls.
!-----

! Depositional bed layer thickness criteria to create a new layer (m). If
! deposition exceeds this value, then a new layer is created, [1:Ngrids].

  NEWLAYER_THICK == 0.2d-3
  NEWLAYER_MASS == 5.3d-2
  MINLAYER_THICK == 0.1d-3
! Bed load transport rate coefficient. [1:Ngrids].

  BEDLOAD_COEFF == 0.05d0

!-----
! Suspended Cohesive Sediment Parameters, [1:NCS,1:Ngrids] values expected.
!-----

! Median sediment grain diameter (mm).

  MUD_SD50 == 0.125d0 0.072d0 0.044d0 0.024d0 0.013d0 0.007d0

! Sediment concentration (kg/m3).

  MUD_CSED == 0.0d0 0.0d0 0.0d0 0.0d0 0.0d0 0.0d0

! Sediment grain density (kg/m3).

  MUD_SRHO == 2650.0d0 2650.0d0 2650.0d0 2650.0d0 2650.0d0 2650.0d0

! Particle settling velocity (mm/s).

  MUD_WSED == 3.2d0 1.6d0 0.8d0 0.4d0 0.2d0 0.1d0

! Surface erosion rate (m/(sec Pa)).

  MUD_ERATE == 0.3d-1 0.3d-1 0.3d-1 0.3d-1 0.3d-1 0.3d-1

```

! Critical shear for erosion and deposition (N/m2).

MUD_TAU_CE == 0.1d0 0.1d0 0.1d0 0.1d0 0.1d0 0.1d0
MUD_TAU_CD == 0.1d0 0.1d0 0.1d0 0.1d0 0.1d0 0.1d0

! Porosity (nondimensional: 0.0-1.0): Vwater/(Vwater+Vsed).

MUD_POROS == 0.9d0 0.9d0 0.9d0 0.9d0 0.9d0 0.9d0

! Minimum and maximum critical shear stress for erosion (N/m2)

MUD_TAUCR_MIN == 0.05d0
MUD_TAUCR_MAX == 1.0d0

! Equilibrium profile parameters

MUD_TAUCR_SLOPE == 1.601d0
MUD_TAUCR_OFF == -0.0665d0
MUD_TAUCR_CTIME == 86.4d3 !24 hrs !s
MUD_TAUCR_STIME == 43.2d5 !50 days

! Lateral, harmonic and biharmonic, constant, diffusion coefficient.

MUD_TNU2 == 0.1d0 0.1d0 0.1d0 0.1d0 0.1d0 0.1d0 ! m2/s
MUD_TNU4 == 0.0d0 0.0d0 0.0d0 0.0d0 0.0d0 0.0d0 ! m4/s

! Vertical diffusion coefficients.

MUD_AKT_BAK == 5.0d-6 5.0d-6 5.0d-6 5.0d-6 5.0d-6 5.0d-6 ! m2/s

! Nudging/relaxation time scales, inverse scales will be computed
! internally.

MUD_TNUDG == 0.0d0 0.0d0 0.0d0 0.0d0 0.0d0 0.0d0 ! days

! Morphological time scale factor (greater than or equal to 1.0). A
! value of 1.0 has no scale effect.

MUD_MORPH_FAC == 1.0d0 1.0d0 1.0d0 ! nondimensional

! Logical switch (TRUE/FALSE) to activate writing of cohesive sediment
! into HISTORY output file.

Hout(idmud) == T ! suspended concentration
Hout(iMfrac) == T ! bed layer fraction
Hout(iMmass) == T ! bed layer mass
Hout(iMUblld) == F ! bed load at U-points

Hout(iMVbld) == F ! bed load at V-points
Hout(ibtcr) == T ! bed critical stress

!-----
! Non-cohesive Sediment Parameters, [1:NNS,1:Ngrids] values expected.
!-----

! Median sediment grain diameter (mm).

SAND_SD50 == 1.0d0

! Sediment concentration (kg/m3).

SAND_CSED == 0.0d0

! Sediment grain density (kg/m3).

SAND_SRHO == 2650.0d0

! Particle settling velocity (mm/s).

SAND_WSED == 1.0d0

! Surface erosion rate (kg/m2/s).

SAND_ERATE == 5.0d-4

! Critical shear for erosion and deposition (N/m2).

SAND_TAU_CE == 0.1d0

SAND_TAU_CD == 0.1d0

! Porosity (nondimensional: 0.0-1.0): Vwater/(Vwater+Vsed).

SAND_POROS == 0.5d0

! Lateral, harmonic and biharmonic, constant, diffusion coefficient.

SAND_TNU2 == 0.0d0 ! m2/s

SAND_TNU4 == 0.0d0 ! m4/s

! Vertical diffusion coefficients.

SAND_AKT_BAK == 5.0d-6 ! m2/s

! Nudging/relaxation time scales, inverse scales will be computed
! internally.

SAND_TNUDG == 0.0d0 ! days

! Morphological time scale factor (greater than or equal to 1.0). A
! value of 1.0 has no scale effect.

SAND_MORPH_FAC == 1.0d0 1.0d0 1.0d0 ! nondimensional

! Logical switches (TRUE/FALSE) to activate writing of non-cohesive
! sediment into HISTORY output file.

Hout(idsand) == F ! suspended concentration
Hout(iSfrac) == F ! bed layer fraction
Hout(iSmass) == F ! bed layer mass
Hout(iSubld) == F ! bed load at U-points
Hout(iSVbld) == F ! bed load at V-points

!-----
! Bed layer and bottom sediment parameters, [1:Ngrids] values expected.
!-----

Hout(ithck) == T ! sediment layer thickness
Hout(iaged) == F ! sediment layer age
Hout(iporo) == T ! sediment layer porosity
Hout(idiff) == F ! biodiffusivity

!
! GLOSSARY:
! =====
!

!-----
! Sediment model control switch, [1:Ngrids].
!-----

!
! Lsediment Switch to control sediment model computation within nested
! and/or multiple connected grids. By default this switch
! is set to TRUE in "mod_scalars" for all grids. The USER
! has the option, for example, to compute sediment in just
! one of the nested grids. If so, this switch needs to be
! consistent with the dimension parameter NST in input
! script (ocean.in). In order to make the model more
! efficient in memory usage, NST(:) should be zero in
! such grids.

```

!
!-----
! General sediment bed model controls, [1:Ngrids] values are expected.
!-----
! NEWLAYER_THICK Depositional bed layer thickness criteria to create a new
!                 layer (m). If deposition exceeds this value, then a new
!                 layer is created.
!
! BEDLOAD_COEFF  Bed load transport rate coefficient.
!-----
! Suspended Cohesive Sediment KEYWORDS, [1:NCS,1:Ngrids] values expected.
!-----
! MUD_SD50      Median sediment grain diameter (mm).
!
! MUD_CSED      Sediment concentration (kg/m3). It may be used to initialize
!                 sediment fields using analytical expressions.
!
! MUD_SRHO      Sediment grain density (kg/m3).
!
! MUD_WSED      Particle settling velocity (mm/s).
!
! MUD_ERATE     Surface erosion rate (kg/m2/s).
!
! MUD_TAU_CE    Critical shear for erosion (N/m2).
!
! MUD_TAU_CD    Critical shear for deposition (N/m2).
!
! MUD_POROS     Porosity (nondimensional: 0.0-1.0):  $V_{water}/(V_{water}+V_{sed})$ .
!
! MUD_TNU2      Lateral, harmonic, constant, mixing coefficient (m2/s),
!                 TNU2(idsed(i)) with i=1:NCS. If variable horizontal
!                 diffusion is activated, TNU2 is the mixing coefficient
!                 for the largest grid-cell in the domain.
!
! MUD_TNU4      Lateral, biharmonic, constant, mixing coefficient (m4/s),
!                 TNU4(idsed(i)) with i=1:NCS. If variable horizontal
!                 diffusion is activated, TNU4 is the mixing coefficient
!                 for the largest grid-cell in the domain.
!
! MUD_AKT_BAK   Background vertical mixing coefficient (m2/s),
!                 AKT_BAK(idsed(i)) with i=1:NCS.
!
! MUD_TNUDG     Nudging time scale (days), TNUDG(idsed(i)) with i=1:NCS.

```

! Inverse scale will be computed internally.
! MUD_MORPH_FAC Morphological time scale factor (nondimensional; greater
! than or equal to 1.0). A value of 1.0 has no scale effect.
! Hout(idmud) Logical switches to activate writing of cohesive sediment
! concentration into HISTORY NetCDF file,
! HOUT(idTvar(idsed(i))) with i=1:NCS.
! Hout(iMfrac) Logical switches to activate writing of cohesive sediment
! class fraction composition of each bed layer into HISTORY
! NetCDF file, HOUT(idfrac(i)) with i=1,NCS.
! Hout(iMmass) Logical switches to activate writing of cohesive sediment
! mass of each bed layer into HISTORY NetCDF file,
! HOUT(idsed(i)) with i=1,NCS.
! Hout(iMUbld) Logical switches to activate writing of cohesive sediment
! bed load at U-points into HISTORY NetCDF file,
! HOUT(idsed(i)) with i=1,NCS.
! Hout(iMVbld) Logical switches to activate writing of cohesive sediment
! bed load at V-points into HISTORY NetCDF file,
! HOUT(idsed(i)) with i=1,NCS.

! Suspended Non-cohesive Sediment KEYWORDS, [1:NNS,1:Ngrids] values expected.

! SAND_SD50 Median sediment grain diameter (mm).
! SAND_CSED Sediment concentration (kg/m3). It may be used to initialize
! sediment fields using analytical expressions.
! SAND_SRHO Sediment grain density (kg/m3).
! SAND_WSED Particle settling velocity (mm/s).
! SAND_Erate Surface erosion rate (kg/m2/s).
! SAND_TAU_CE Critical shear for erosion (N/m2).
! SAND_TAU_CD Critical shear for deposition (N/m2).
! SAND_POROS Porosity (nondimensional: 0.0-1.0): $V_{water}/(V_{water}+V_{sed})$.

! SAND_TNU2 Lateral, harmonic, constant, mixing coefficient (m²/s),
! TNU2(idsed(i)) with i=NCS+1:NST. If variable horizontal
! diffusion is activated, TNU2 is the mixing coefficient
! for the largest grid-cell in the domain.
!

! SAND_TNU4 Lateral, biharmonic, constant, mixing coefficient (m⁴/s),
! TNU4(idsed(i)) with i=NCS+1:NST. If variable horizontal
! diffusion is activated, TNU4 is the mixing coefficient
! for the largest grid-cell in the domain.
!

! SAND_AKT_BAK Background vertical mixing coefficient (m²/s),
! AKT_BAK(idsed(i)) with i=NCS+1:NST.
!

! SAND_TNUDG Nudging time scale (days), TNUDG(idsed(i)) with i=NCS+1:NST.
! Inverse scale will be computed internally,
!

! SAND_MORPH_FAC Morphological time scale factor (nondimensional; greater
! than or equal to 1.0). A value of 1.0 has no scale effect.
!

! Hout(idsand) Logical switches to activate writing of non-cohesive
! sediment concentration into HISTORY NetCDF file,
! HOUT(idTvar(idsed(i))) with i=1:NCS+1,NST.
!

! Hout(iSfrac) Logical switches to activate writing of non-cohesive
! sediment class fraction composition of each bed layer
! into HISTORY NetCDF file, HOUT(idfrac(i)) with
! i=NCS+1,NST.
!

! Hout(iSmass) Logical switches to activate writing of non-cohesive
! sediment mass of each bed layer into HISTORY NetCDF file,
! HOUT(idsed(i)) with i=NCS+1,NST.
!

! Hout(iSUBld) Logical switches to activate writing of non-cohesive
! sediment bed load at U-points into HISTORY NetCDF file,
! HOUT(idsed(i)) with i=NCS+1,NST.
!

! Hout(iSVbld) Logical switches to activate writing of non-cohesive
! sediment bed load at V-points into HISTORY NetCDF file,
! HOUT(idsed(i)) with i=NCS+1,NST.
!

!-----
! Bed layer and bottom sediment KEYWORDS, [1:Ngrids] values expected.
!-----

! Hout(ithck) Sediment layer thickness.

!
! Hout(iaged) Sediment layer age.
!
! Hout(iporo) Sediment layer porosity
!
! Hout(idiff) Biodiffusivity at the bottom of each layer.

Literature Cited

Amos, C.L., Umgiesser, G., Ferrarin, C., Thompson, C.E.L., Whitehouse, R.J.S., Sutherland, T.F., Bergamasco, A., 2010. The erosion rates of cohesive sediments in Venice Lagoon, Italy. *Continental Shelf Research*. 30: 859-870

Amos, C.L., Bergamasco, A., Umgiesser, G., Cappuscci, S., Cloutier, D., DeNat, L., Flindt, M., Bonardi, M., Cristante, S., 2004. The stability of tidal flats in Venice Lagoon- the results of in-situ measurements using two benthic, annular flumes. *Journal of Marine Systems*. 51: 211-241

Anderson, T.J., Fredsoe, J., Pejrup, M., 2007. In situ estimation of erosion and deposition thresholds by Acoustic Doppler Velocimeter (ADV), *Estuarine, Coastal and Shelf Science* 75. 327-336.

Anderson T.J., Pejrup, M., 2002. Biological mediation of the settling velocity of bed material eroded from an intertidal mudflat, the Danish Wadden Sea, *Estuarine, Coastal and Shelf Science* 54, 737-745.

Anderson, T.J., 2001. Seasonal Variations in Erodibility of Two Temperate, Microtidal Mudflats. *Estuarine, Coastal, and Shelf Science*. 53:1-12.

Cartwright, G.M., Friedrichs, C.T., Sanford, L.P., 2011. In situ characterization of estuarine suspended sediment in the presence of muddy flocs and pellets. In: N.C. Kraus and J.D. Rosati (eds.), Coastal Sediments 2011, American Society of Civil Engineers, 14 p.

Cartwright, G. M., Friedrichs, C.T., Dickhudt, P.J., Gass, T., Farmer, F.H., 2009. Using the Acoustic Doppler Velocimeter (ADV) in the MUDBED Real-Time Observing System. Proceedings of Ocean Sciences 2009. Biloxi, MS, 26-29, 2009.

Dellapenna, T.M., Kuehl, S.A., Schaffner, L.C., 2003. Ephemeral deposition, seabed mixing and fine-scale strata formation in the York River estuary, Chesapeake Bay. Estuarine, Coastal and Shelf Science. 58: 621-643.

Dickhudt P.J., Friedrichs, C.T., Sanford, L.P., 2010. Mud matrix solids fraction and bed erodibility in the York River estuary, USA, and other muddy environments. Continental Shelf Research doi:10.1016/j.crs.2010.02.008.

Dickhudt P.J., Friedrichs, C.T., Schaffner, L.C., Sanford, L.P., 2009. Spatial and temporal variation in cohesive sediment erodibility in the York River estuary, eastern USA: A biologically influenced equilibrium modified by seasonal deposition. Marine Geology 267. 128-140.

Dickhudt, P.J., 2008. Controls on erodibility in a partially mixed estuary: York River, Virginia. M.S. Thesis, School of Marine Science, College of William & Mary, Gloucester Point, VA.

Drake, D.E., Eganhouse, R., McArthur, W., 2002. Physical and chemical effects of grain aggregates on the Palos Verdes margin, southern California. *Continental Shelf Research*. 22:967-986

Dyer, K.R., Manning, A.J., 1999. Observation of the size, settling velocity and effective density of flocs, and their fractal dimensions. *Journal of Sea Research*. 41: 87-95.

Dyer, K.R., Cornelisse, J., Dearnaley, M.P, Fennessy, M.J., Jones, S.E., Kappenberg, J, McCave, I.N., Pejrup, M., Puls, W., Van Leussen, W., Wolfstein, K., 1996. A comparison of in situ techniques for estuarine floc settling velocity measurements, *Journal of Sea Research* 36. 15-29.

Dyer, K.R., 1984. "Coastal and Estuarine Sediment Dynamics". Wiley Interscience, New York, 342 p.

Edelvang, K., Austen, I., 1997. The temporal variation of flocs and fecal pellets in a tidal channel. *Estuarine, Coastal and Shelf Science* 44. 361-367.

Friedrichs, C.T., 2009. York River physical oceanography and sediment transport. *Journal of Coastal Research: Special Issue 57 – The Chesapeake Bay NERRS in Virginia: A Profile of the York River Ecosystem [Moore & Reay]*: pp 17-22.

Friedrichs, C.T, Cartwright, G.M., Dickhudt, P.J., 2008. Quantifying benthic exchange of fine sediment via continuous, noninvasive, measurements of settling velocity and bed erodibility, *Oceanography: Special issue on coastal ocean processes observing technologies and models*. Vol. 21, No. 4.

Friedrichs, C.T., Wright, L.D., Hepworth, D.A., Kim, S.C., 2000. Bottom-boundary-layer processes associated with fine sediment accumulation in coastal seas and bays, *Continental Shelf Research* 20. 807-841.

Fugate, D.C., Friedrichs, C.T., 2003. Controls on suspended aggregate size in partially mixed estuaries. *Estuarine, Coastal, and Shelf Science*. 58:389-404

Fugate, D.C., Friedrichs, C.T., 2002. Determining concentration and fall velocity of estuarine particle populations using ADV, OBS, and LISST. *Continental Shelf Research*. 22:1867-1886.

Ha, Ho Kyung., Maa, Jerome P. -Y., 2010. Effects of suspended sediment concentration and turbulence on settling velocity of cohesive sediment. *Geosciences Journal*. 14: 163-171

Harris, C.K., P. Traykovski, and W.R. Geyer, 2005. Flood dispersal and deposition by near-bed gravitational sediment flows and oceanographic transport: a numerical modeling study of the Eel River shelf, northern California. *Journal of Geophysical Research*, 110 (C09025): doi:10.1029 / 2004JC002727.

Harris, C.K., Wiberg P.L., 1997. Approaches to quantifying long-term continental shelf sediment transport with an example from the Northern California STRESS mid-shelf site, *Continental Shelf Research* 17. 1389-1418.

Jolliff, J.K., Kindle, J.C., Shulman, I., Penta, B., Friedrichs, M. A.M., Helber, R., Arnon, R.A., 2009. Summary diagrams for coupled hydrodynamic-ecosystem model skill assessment, *Journal of Marine Systems*. Vol. 76, 64-82

Kemp, W.M., Boynton, W.R., Adolf, J.E., Boesch, D.F., Boicourt, W. C., Brush, G., Cornwell, J.C., Fisher, T.R., Gilbert, P.M, Hagy, J.D., Harding, L.W., Houde, E.D., Kimmel, D.G., Miller, W.D., Newell, R.I.E., Roman, M.R., Smith. E.M., Stevenson, J.C., 2005. Eutrophication of Chesapeake Bay: historical trends and ecological interactions, *Marine Ecology Progress Series* 303, 1-29.

Kim, S. -C., Friedrichs, C.T., Maa, J.P.-Y., Wright, L.D., 2000. Estimating bottom stress in tidal boundary layer from Acoustic Doppler Velocimeter data, *Journal of Hydraulic Engineering*. 399-406.

Kraatz, L.M., Friedrichs, C.T., Cartwright, G.M., Fall, K.A. Wilkerson, C.N., 2012. Relationships between erodibility and fine-grained sea bed properties on tidal to seasonal time-scales, York River Estuary, Virginia, USA, Physics of Estuaries and Coastal Seas, 16th International Biennial Conference, New York, NY. 12-16 August 2012.

Lin, J.L., Kuo, A. Y., 2001. Secondary turbidity maximum in a partially mixed microtidal estuary, Estuaries Vol. 24 No. 5. 707-720.

Maa, J.P.Y., Kwon, J.-I., 2007. Using ADV for cohesive sediment settling velocity measurements, Estuarine, Coastal and Shelf Science 73. 351-354.

Maa, J.P.Y., Kim, S.C., 2002. A Constant Erosion Rate Model for Fine Sediment in the York River, Virginia. Environmental Fluid Mechanics. 1: 345-360.

Maa, J.P.Y., Sanford, L., Halka, J.P., 1998. Sediment resuspension characteristics in Baltimore Harbor, Maryland. Marine Geology. 146: 137-145

Mackenzie, 2007. Causes underlying the historical decline in Eastern Oyster (*Crassostrea Virginica* Gmelin, 1791) Landings. Journal of Shellfish Research, Vol 26. No. 4 927-938

Miller, D.C, Muir, C.L., Hauser, O.A., 2002. Detrimental effects of sedimentation on marine benthos: what can be learned from natural processes and rates? *Ecological Engineering* 19: 211-232

Moore , K.A., 2009. Submerged Aquatic Vegetation of the York River. *Journal of Coastal Research* SI 57: 50-58

Orth, R.J., Moore, K.A., 1984. Distribution and Abundance of Submerged Aquatic Vegetation in Chesapeake Bay: An Historical Perspective. *Estuaries* Vol. 7 No. 4b: 531-540

Parchure, T.M. and Mehta, A. J. , 1985. Erosion of soft cohesive sediment deposits. *Journal of Hydraulic engineering*. Volume, 111 (10): 1308-1326.

Reay W., 2009. Water quality within the York River Estuary. *Journal of Coastal Research*. SI 57: 23-39

Rinehimer, J.P., C.K. Harris, C.R. Sherwood, and L.P. Sanford, 2008. Estimating cohesive sedi-ment erosion and consolidation in a muddy, tidally-dominated environment: model behavior and sensitivity. *Estuarine and Coastal Modeling*, Proceedings of the Tenth Conference, November 5-7, Newport RI. Spaulding, M.L., ed. 819-838.

Rinehimer, J.P., 2008. Sediment Transport and Erodibility in the York River Estuary: A Model Study. Master Thesis. School of Marine Science, College of William and Mary, Gloucester Point, VA.

Rodriguez-Calderón, C., 2010. Spatial and Temporal patterns in erosional and depositional processes: physical and biological controls in the York River, Chesapeake Bay, Virginia. M.S. Thesis, School of Marine Science, College of William & Mary, Gloucester Point, VA.

Sanford, L.P., 2008. Modeling a dynamically varying mixed sediment bed with erosion, deposition, bioturbation, consolidation, and armoring. *Computers & Geosciences*. 34: 1263-1283

Sanford, L.P., 2005. Uncertainties in Sediment Erodibility Estimates Due to a Lack of Standards for Experimental Protocols and Data Interpretation. *Integrated Environmental Assessment and Management*. Volume 2, Number 1. 29-34

Sanford, L.P., Maa, J.P., 2001. A unified erosion formulation for fine sediments. *Marine Geology* 179. 9-23.

Sanford, L.P., Chang, M.L., 1997. The bottom boundary condition for suspended sediment transport, *Journal of Coastal Research* SI 25: 3-17.

Sanford, L.P., Halka, J.P., 1993. Assessing the paradigm of mutually exclusive erosion and deposition of mud, with examples from upper Chesapeake Bay. *Marine Geology*. 114: 37-57.

Schaffner, L.C., Hinchey, E.K., Dellapenna, T.M., Friedrichs, C.T., Neubauer, M.E., Smith, M.E., Kuehl, S.A., 2001. Physical energy regimes, sea-bed dynamics and organism- sediment interactions along an estuarine gradient. In: Aller, J.Y., Woodin, S.A., Aller, R.C. (Eds.), *Organism–sediment Interactions*. University of South Carolina Press, Columbia, SC, pp. 159–179.

Scully, M.E., Friedrichs, C.T., Brubaker J.M., 2005. Control of estuarine stratification and mixing by wind-induced straining of the estuarine density field. *Estuaries*, 28, 321-326.

Scully M.E., Friedrichs, C.T., 2003. The influence of asymmetries in overlying stratification on near-bed turbulence and sediment suspension in a partially mixed estuary, *Ocean Dynamics* 53. 208-210.

Shchepetkin, A., and J.C. McWilliams, (1998), Quasi-monotone advection schemes based on explicit locally adaptive dissipation, *Monthly Weather Review*, 126, 1541-1580.

Shchepetkin, A.F., and J.C. McWilliams (2005), The regional oceanic modeling system (ROMS): a split-explicit, free-surface, topography-following-coordinate oceanic model, *Ocean Modelling*, 9, 4, 347-404.

Stevens A.W., Wheatcroft, R.A., Wiberg, P.L., 2007. Seabed properties and sediment erodibility along the western Adriatic margin, Italy, *Continental Shelf Research* 27. 400-416

Warner J.C., Sherwood, C.R., Signell, R.P., Harris, C.K., Arango, H.G., 2008. Development of a three-dimensional, regional, coupled wave, current, and sediment-transport model, *Computers & Geosciences* 34. 1284-1306.

Warner, J.C., Geyer, W.R., Lerczak, J.A., 2005. Numerical modeling of an estuary: A comprehensive skill assessment, *Journal of Geophysical Research*, Vol. 110.

Waycott, M., Duarte, C.M., Carruthers T. J.B., Orth, R.J., Dennison, W.C., Olyarnik, S., Calladine, A., Fourqurean, J.W., Heck, K.L. Jr., Hughes, A.R., Kendrick, G.A., Kenworthy, W.J., Short. F.T., Williams, S.L., 2009. Accelerating loss of seagrasses across the globe threatens coastal ecosystems. *PNAS*, Vol. 106, No. 30.

Winterwerp, J.C., 2006. Stratification effects by fine suspended sediment at low, medium, and very high concentrations, *Journal of Geophysical Research* Vol. 111.

Winterwerp, J.C., van Kesteren, W.G.M., 2005. Introduction to the physics of cohesive sediment in the marine environment. Elsevier.

Yang Z., Hamrick J.M., 2003. Variational inverse parameter estimation in a cohesive sediment transport model: an adjoint approach. *Journal Geophysical Research*. Volume 108, No. C2:3055

VITA

Kelsey Ann Fall

Born August 11, 1987 in Pittsburgh, Pennsylvania. Graduated from North Allegheny Senior High School in 2005. Earned B.S in Marine Science and Math (minor) from Coastal Carolina University in 2009. Entered M.S. program at College of William and Mary, School of Marine Science in 2009.